INSTITUTO CARLOS CHAGAS
MESTRADO EM BIOCIÊNCIAS E BIOTECNOLOGIA

RAFAEL FERNANDO CASTELLI

CARACTERIZAÇÃO DA PROTEÍNA NUCLEOLAR Nop16 NA FISIOLOGIA DO PATÓGENO *Cryptococcus gattii*

CURITIBA

2020

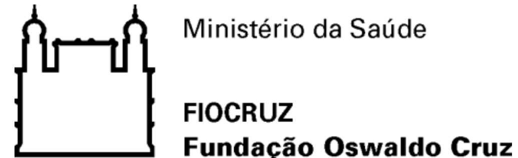

INSTITUTO CARLOS CHAGAS

Mestrado em Biociências e Biotecnologia

RAFAEL FERNANDO CASTELLI

CARACTERIZAÇÃO DA PROTEÍNA NUCLEOLAR Nop16 NA FISIOLOGIA DO PATÓGENO *Cryptococcus gattii*

Dissertação apresentada ao Instituto Carlos Chagas como parte dos requisitos para obtenção do título de Mestre em Biociências e Biotecnologia.

Orientador: Marcio Lourenço Rodrigues

CURITIBA

2020

Castelli, Rafael Fernando.

CARACTERIZAÇÃO DA PROTEÍNA NUCLEOLAR Nop16 NA FISIOLOGIA DO PATÓGENO *Cryptococcus gattii* / Rafael Fernando Castelli. - Curitiba, 2020.
94 f.

Dissertação (Mestrado) – Instituto Carlos Chagas, Pós-Graduação em Biociências e Biotecnologia, 2020.

Orientador: Marcio Lourenço Rodrigues.

Bibliografia: f. 53-63

1. Cryptococcus gattii. 2. Nop16. 3. Fisiologia celular. 4. patogenicidade . I. Título.

Elaborada pelo Sistema de Geração Automática de Ficha Catalográfica da Biblioteca de Manguinhos/ICICT com os dados fornecidos pelo(a) autor(a).

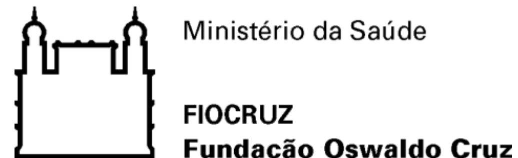

INSTITUTO CARLOS CHAGAS

Mestrado em Biociências e Biotecnologia

Termo de Aprovação

Autor: Rafael Fernando Castelli

Título: **CARACTERIZAÇÃO DA PROTEÍNA NUCLEOLAR Nop16 NA FISIOLOGIA DO PATÓGENO *Cryptococcus gattii***

Orientador: Marcio Lourenço Rodrigues

Instituição: Instituto Carlos Chagas

Examinadores:

Prof. Dra. Lívia Kmetzsch Rosa e Silva (Universidade Federal do Rio Grande do Sul)

Prof. Dra. Lysangela Ronalte Alves (Instituto Carlos Chagas)

Prof. Dra. Sheila Cristina Nardelli (Instituto Carlos Chagas)

Prof. Dra. Lia Carolina Almeida Soares de Medeiros Kuczera (Instituto Carlos Chagas)

Prof. Dr. Fabiano Borges Figueiredo (Instituto Carlos Chagas)

Data da aprovação: 13/07/2020

CURITIBA

2020

Esta dissertação, bem como todo o percurso que percorri para chegar até aqui, vêm acompanhado do nome de uma mulher incrível e batalhadora, sem a qual eu não estaria, sequer, nesse mundo. Nelci Maria Krein Castelli, a você, todo meu amor e agradecimento, mãe.

AGRADECIMENTOS

Ao instituo Carlos Chagas, à Fundação Oswaldo Cruz e ao Programa de Pós-Graduação em Biociências e Biotecnologia. As secretárias do programa Franciele Mendes e Raquel Keller, o trabalho de vocês faz da pós-graduação um ambiente mais acolhedor.

A minha família que sempre apoiou e respeitou minhas decisões, principalmente meu irmão Jacir, com certeza o maior entusiasta dos meus passos científicos.

Ao Felipe, por ficar ao meu lado, por ser meu apoio e por compreender que existem altos e baixos, fazendo com que os baixos sejam menos duradouros. Sortudo eu de ter descoberto que existem pessoas tão incríveis nesse mundo.

Meu orientador, Marcio Lourenço Rodrigues que desde o início mostrou-se um ser humano excepcional, por todos os momentos sérios e também os de descontração, meu muito obrigado.

Aos colegas do Laboratório de Regulação da Expressão Gênica, mais especialmente aos amigos que fiz dentro do grupo de pesquisa em fungos patogênicos: Amanda, Bianca, Diogo, Luisa e Vanessa. Carinho especial a Flavia Reis e Haroldo Oliveira aos quais devo, praticamente, tudo que aprendi nessa experiência, que me pegaram pela mão para ensinar e aplicar, que foram companheiros fora do laboratório e sempre estiveram dispostos a ajudar quando precisei, ter vocês por perto foi essencial para chegar até esse ponto. Muito obrigado, mesmo.

Às funcionárias da limpeza do instituto, por todas as risadas, abraços e cafés quentinhos, em especial a Dona Helena e a Rosangela, é muito bom ter gente boa assim por perto.

As “meninas da microscopia” por toda a paciência e dedicação pelo nosso trabalho, por todas as dicas, os aperfeiçoamentos, as técnicas ensinadas, as dúvidas sanadas bem longe do horário de expediente e sempre com atenção. Anny, Adriana, Bruna e Lia, muito obrigado por terem me ajudado a desenvolver o gosto pela microscopia.

Ao pessoal do Laboratório de Biologia Celular, por sempre me emprestarem um cantinho para o preparo das amostras, por ajudarem nas dúvidas, pelo material quando eu esquecia e pelas *playlists* mais aleatórias possíveis, que esses ambientes leves se propaguem nas instituições.

Ao Professor Dr. Leonardo Nimrichter da Universidade Federal do Rio de Janeiro pela colaboração nos experimentos.

Ao Professor Dr. Charley Staats pela construção das cepas mutantes, sem as quais este trabalho não poderia ter se desenvolvido.

A todos os técnicos de laboratório do Instituto Carlos Chagas, que sempre fizeram o nosso trabalho dentro dos laboratórios andar a passos mais largos, com grande dedicação e boa vontade, muito obrigado a vocês.

Aos membros da banca, por aceitarem prontamente o convite para participar desse trabalho e, mesmo com as adversidades que foram postas, não mediram esforços para essa colaboração. Lia, Lívia, Lysangela, Sheila e Fabiano.

RESUMO

Atualmente, estima-se que cerca de 300 milhões de pessoas sejam acometidas por doenças fúngicas anualmente em todo o globo. Espécies de *Aspergillus*, *Candida* e *Cryptococcus* são os principais causadores de micoses que afetam, em especial, indivíduos imunossuprimidos. Espécies de *C. neoformans* e *C. gattii* se destacam como agentes causadores da criptococose, uma micose sistêmica e invasiva que pode atingir o sistema nervoso central e, se não tratada rapidamente, pode levar à morte. Em estudos anteriores, nosso grupo sugeriu que o gene *NOP16* tem potencial para representar um alvo para agentes antifúngicos. Nesse estudo, buscamos entender o papel de Nop16 na fisiologia de *C. gattii* através da caracterização dos efeitos da deleção do gene *NOP16* nas características fenotípicas e patogênicas de *C. gattii*. Análises por microscopia óptica, de fluorescência, eletrônica de varredura e de transmissão, combinadas com ensaios sorológicos e de interação com fagócitos, demonstraram que a deleção do gene acarreta sutis alterações no tamanho da cápsula polissacarídica, na taxa de fagocitose e na secreção de GXM. Entretanto, o estudo de vesículas extracelulares (EVs) por microscopia eletrônica de transmissão e por rastreamento de nanopartículas revelou que mutantes deficientes na expressão do gene *NOP16* tiveram capacidade reduzida de produzir EVs. Esse fenótipo foi acompanhado de uma reduzida capacidade de levar à morte larvas de *Galleria mellonella*. Esses resultados indicam que Nop16 é um elemento importante na fisiologia e na patogênese de *C. gattii*.

Palavras-chave: *Cryptococcus gattii*; Nop16; fisiologia celular; patogenicidade.

ABSTRACT

It is currently estimated that approximately 300 million people are annually affected by fungal diseases across the globe. Species of *Aspergillus*, *Candida* and *Cryptococcus* are the main causes of mycoses that particularly affect immunosuppressed individuals. Species of *C. neoformans* and *C. gattii* are the causative agents of cryptococcosis, a systemic and invasive mycosis that can reach the central nervous system and, if not treated immediately, can lead to death. In previous studies, we suggested that the *NOP16* gene has the potential to represent a target for antifungal agents. In this study, we wanted to understand the role of Nop16 in the physiology of *C. gattii* through the characterization of the effects of the deletion of the *NOP16* gene on the phenotypic and pathogenic traits of *C. gattii*. Combined analyses of optical, fluorescence, scanning and transmission electron microscopy, in association with serological tests and interaction with phagocytes revealed that deletion of the gene causes subtle changes in the size of the polysaccharide capsule, the rate of phagocytosis and the secretion of GXM. However, the study of extracellular vesicles (EVs) by transmission electron microscopy combined with nanoparticle tracking analysis revealed that mutants deficient in *NOP16* expression had a reduced ability to produce EVs. This phenotype was accompanied by a reduced ability to kill larvae of *Galleria mellonella*. These results indicate that Nop16 is an important element in the physiology and pathogenesis of *C. gattii*.

Key-words: *Cryptococcus gattii*; EVs; *NOP16;* cellular physiology; pathogenicity.

LISTA DE FIGURAS

Figura 1: Incidência anual de criptococose por país 17
Figura 2: Mecanismos de infecção de *C. neoformans* e *C. gattii* no hospedeiro humano 18
Figura 3: Estrutura da cápsula polissacarídica de *Cryptococcus* spp. 21
Figura 4: Representação esquemática de uma EV de *Cryptococcus* spp.................22
Figura 5: Esquema da placa de 96 poços utilizada para o ensaio de ELISA 30
Figura 6: Cinética de crescimento das células fúngicas de *C. gattii*..........................37
Figura 7: Concentração inibitória mínima do antifúngico anfotericina B....................38
Figura 8: Concentração inibitória mínima do antifúngico fluconazol..........................39
Figura 9: Análises microscópicas da célula fúngica de *C. gattii* evidenciada por contra-coloração com tinta nanquim...39
Figura 10: Análise quantitativa do tamanho da cápsula em *C. gattii*.........................40
Figura 11: Células de *C. gattii* observadas por microscopia de fluorescência 41
Figura 12: Microscopia eletrônica de varredura das células crescidas em meio YPD 42
Figura 13: Análise da secreção de glucuronoxilomanana em *C. gattii*......................43
Figura 14: Microscopia eletrônica de transmissão das células de *C. gattii* 43
Figura 15: Imagem representativa do ensaio de fagocitose para as cepas de *C. gattii* com macrófagos murinos RAW 264.7 44
Figura 16: Taxa de fagocitose das cepas de *C. gattii*...45
Figura 17: Microscopia eletrônica de transmissão das EVs 45
Figura 18: Análise de rastreamento de nanopartículas (NTA)..................................46
Figura 19: Quantificação de EVs produzidas em *C. gattii*. 46
Figura 20: Análise de virulência de *C. gattii* em modelo invertebrado *Galleria mellonella*. 47

LISTA DE ABREVIATURAS

CO_2	Dióxido de carbono
cels	Células
BSA	"*Bovine Serum Albumin"* Soro Albumina Bovina
DMEM	"*Dulbecco's Modified Eagle Medium*" Dulbecco's modificado com Eagle's
ELISA	"*Enzyme-Linked Immunosorbent Assay*" ensaio de imunoabsorção enzimática
EUCAST	"*European Committee on Antimicrobial Susceptibility Testing*"
EVs	"*Extracellular Vesicles*" vesículas extracelulares
FITC	"*Fluorescein Isothiocyanate*" Isotiocianato de Fluoresceína
GXM	Glucuronoxilomanana
mAb	"*Monoclonal Antibody*" anticorpo monoclonal
MET	Microscopia eletrônica de transmissão
MEV	Microscopia eletrônica de varredura
MOI	"*Multiplicity of Infection"* multiplicidade da infecção
MOPS	Ácido morfolinopropanosulfônico
NTA	"*Nanotracking Analysys*" análise de traço de nanopartículas
NOP	"*Nucleolar Protein*" proteína nucleolar
PBS	"*Phosphate Buffered Saline*" tampão fosfato-salino
pNPP	Paranitrofenilfosfatase
RPM	Rotações por minuto
RPMI	"*Roswell Park Memorial Institute"*
SFB	Soro Fetal Bovino
spp.	Espécies
TBS	"*Tris Buffered Saline*"
YPD	"*Yeast Peptone Dextrose"* meio de cultura de leveduras com peptona e dextrose

WGA “*Wheat Germ Agglutinin*”, Lectina do Germe de Trigo

SUMÁRIO

1. Introdução 12

2. Revisão Bibliográfica 14

2.1 *Cryptococcus* e criptococose 14

2.2 Fatores de virulência de *Cryptococcus* 19

2.3 Novos alvos em potencial para o desenvolvimento de fármacos anti-*Cryptococcus* 24

3. Objetivos 26

4. Materiais e Métodos 27

4.1 Cepas fúngicas e condições e cultivo 27

4.2 Curva de crescimento 27

4.3 Análises da cápsula polissacarídica 28

4.3.1 Nanquim e medidas da célula fúngica 28

4.3.2 Imunomarcação 28

4.4 Ensaio Imunoenzimático (*Enzyme Linked Immunosorbent Assay* - ELISA) 29

4.5 Isolamento de EVs 31

4.6 Análise de Nanopartículas (*Nanoparticle Tracking Analysys* - NTA) 32

4.7 Microscopia Eletrônica de Transmissão (MET) 32

4.7.1 Células fúngicas 32

4.7.2 Vesículas Extracelulares 33

4.8 Microscopia Eletrônica de Varredura (MEV) 34

4.9 Ensaio de fagocitose de *C. gattii* 35

4.10 Infecção de *Galleria mellonella* 35

4.11 Sensibilidade a antifúngicos 36

4.12 Análises estatísticas 37

5. Resultados 37

5.1 Cinética de Crescimento..37

5.2 Perfil de sensibilidade à antifúngicos..38

5.3 Análises da morfologia capsular de *Cryptococcus gattii*...............................39

5.3.1 Contra-coloração com Nanquim...39

5.3.2 Dimensões da cápsula polissacarídica..40

5.3.3 Imunomarcação..40

5.3.4 MEV...41

5.3.5 Secreção de GXM..42

5.4 Análise ultraestrutural de *C. gattii*..43

5.5 Análise da interação de *C. gattii* com macrófagos RAW 264.7 *in vitro*...........44

5.6 Caracterização das EVs..45

5.7 Potencial patogênico das cepas fúngicas..47

6. Discussão..47

7. Conclusões..52

8. Referências Bibliográficas..53

9. Produção científica durante o período da dissertação 64

1. Introdução

Estima-se que mais de um milhão de pessoas percam a vida anualmente em decorrência de doenças fúngicas (GAFFI, 2020). Essas doenças estão associadas a elevados índices de mortalidade e morbidade, principalmente em populações que vivem sob condições de restrição socioeconômica (MAZIARZ e PERFECT, 2016; ZARAGOZA, 2019). Os fungos são altamente diversos e podem ser encontrados nos mais variados ambientes. O reino Fungi conta com, aproximadamente, 1,5 milhão de espécies, sendo importante ressaltar que menos de 300 são consideradas patogênicas (de OLIVEIRA et al., 2020).

Algumas espécies do gênero *Cryptococcus* causam doenças fúngicas invasivas de alta letalidade. As doenças associadas ao gênero consistem de micoses sistêmicas que começam no sistema respiratório e podem atingir o sistema nervoso central, causando a meningite criptocócica. Essa é considerada a doença mais letal que acomete populações em condição de imunossupressão (DE AZAMBUJA *et al.*, 2018; PERFECT *et al.*, 2010). São estimados cerca de 220.000 casos anuais de meningite criptocócica, com maior incidência da doença em países da África Subsaariana (RAJASINGHAM *et al.*, 2017). A doença impacta também países de clima tropical, como é o caso do Brasil (RAJASINGHAM *et al.*, 2017).

As espécies patogênicas de *Cryptococcus* tradicionalmente consistem de *C. neoformans* e *C. gattii*. Ressalta-se, entretanto, que foi recentemente proposta a reclassificação dessas duas espécies em sete espécies distintas (FARRER *et al.*, 2019; KWON-CHUNG *et al.*, 2017). Nesse estudo, utilizaremos a classificação tradicional, defendida por grande parte da comunidade científica (KWON-CHUNG *et al.*, 2017). *C. gattii* e *C. neoformans* são leveduras encapsuladas, haploides amplamente distribuídas no ambiente (BIELSKA e MAY, 2016; RODRIGUES *et al.*, 1999; VOELZ *et al.*, 2010). *C. neoformans* tem distribuição irrestrita e *C. gattii* é mais frequente em regiões de clima temperado, tropical e subtropical (KIDD *et al.*, 2007; LOCKHART *et al.*, 2013; MAY *et al.*, 2016; RAJASINGHAM *et al.*, 2017). Ambas as espécies possuem a capacidade de causar a criptococose humana, mas *C. neoformans* apresenta predileção por pacientes com sistema imune comprometido, enquanto *C. gattii* é capaz de desenvolver a doença em pacientes com sistema imune inalterado (BIELSKA e MAY, 2016; PARK *et al.*, 2009; RIZZO *et al.*, 2018; RODRIGUES *et al.*, 1999; VOELZ *et al.*, 2010; ZAVALA e BADDLEY, 2020).

A capacidade das duas espécies de infectar o hospedeiro humano e causar a doença está relacionada a sua capacidade de produzir e secretar fatores de virulência que garantam sua sobrevivência no hospedeiro, através da modulação do sistema imune e de alterações morfofisiológicas no fungo (RODRIGUES *et al.*, 2007). O principal fator de virulência associado a *Cryptococcus* é a presença de uma cápsula polissacarídica (BIELSKA e MAY, 2016; RODRIGUES *et al.*, 1999). Essa cápsula é característica pela presença do polissacarídeo glucuronoxilomanana (GXM) que, além de ser a principal molécula que compõe a estrutura capsular, também interage com os mecanismos imunes do hospedeiro. Outros fatores de virulência incluem a capacidade de pigmentação e a produção de urease (FU *et al.*, 2018; RODRIGUES *et al.*, 1999). Todas essas estruturas exercem suas funções após transporte para a superfície ou para o ambiente extracelular através de vesículas extracelulares (EVs). As EVs atuam carreando enzimas, lipídeos, polissacarídeos, proteínas e outros componentes moduladores da resposta imune (RIZZO *et al.*, 2018). As EVs são estruturas naturalmente secretadas por todos os tipos celulares e em todos os reinos da vida (COELHO e CASADEVALL, 2019). São estruturas esféricas, delimitadas por uma bicamada de lipídeos com diâmetro variável entre 20 e 800 nm (COELHO e CASADEVALL, 2019; RODRIGUES *et al.*, 2008; RODRIGUES *et al.*, 2007).

O tratamento da criptococose é altamente problemático. O regime de tratamento baseia-se em terapias com alto custo monetário, baixa eficácia, acentuados efeitos colaterais, acesso dificultado à populações mais necessitadas e resistência de patógenos microbianos aos fármacos disponíveis (DE AZAMBUJA *et al.*, 2018; MAZIARZ e PERFECT, 2016; PERFECT *et al.*, 2010). Nesse cenário, o entendimento sobre moléculas fúngicas que permitam a identificação de novos alvos para fármacos é fundamental. Em estudo anterior, nosso grupo sugeriu que a proteína Nop16, possivelmente envolvida na biogênese de ribossomos, poderia ser um alvo para a ação de antifúngicos (JOFFE *et al.*, 2017). A seleção desta proteína foi possível em testes de resistência a antifúngicos numa coleção de mutantes gerados por incubação com *Agrobacterium tumefaciens*. Nesta coleção, o gene responsável por codificar tal proteína foi interrompido e a cepa resultante apresentou perfil de resistência ao anti-helmíntico mebendazol, inferindo assim que a Nop16 seria necessária para que esse fármaco exerça sua atividade antifúngica (JOFFE *et al.*, 2017).

O papel de Nop16 na fisiologia e na patogênese de *C. gattii* permanece desconhecido. Dessa forma, este projeto buscou a caracterização dos efeitos da

deleção de *NOP16* em *C. gattii*, sendo analisados aspectos morfológicos e fenotípicos das cepas mutantes em comparação à cepa parental. Os resultados obtidos indicaram que proteína pode influenciar os mecanismos de virulência da espécie, reforçando seu papel como possível alvo no desenvolvimento de moléculas anti-criptocócicas (RODRIGUES, 2016; RODRIGUES e ALBUQUERQUE, 2018).

2. Revisão Bibliográfica

2.1 *Cryptococcus* e criptococose

Existem em torno de 300 espécies de fungos consideradas patogênicas, dentro de um grupo de cerca de 1.5 milhão de espécies fúngicas que habitam diversos ambientes. Dentre os patógenos fúngicos, destacam-se espécies de *Candida*, *Aspergillus* e *Cryptococcus* como causadores de doenças de alta mortalidade (ZARAGOZA, 2019).

Cryptococcus é um gênero de fungos basidiomicetos composto por, ao menos, 100 espécies. São considerados organismos saprofíticos ambientais. A primeira descrição do gênero foi realizada em 1894, atribuída a organismos semelhantes a *Saccharomyces* spp., isolados da tíbia de uma paciente (LEVITZ, 1991; MAY *et al.*, 2016; NYAZIKA *et al.*, 2018; ZARAGOZA, 2019; ZAVALA e BADDLEY, 2020). Apesar de ter sido descrita como um patógeno humano ainda no século XIX, a espécie *C. neoformans* aumentou em importância no fim dos anos 1970 (KNOKE e SCHWESINGER, 1994; MAZIARZ e PERFECT, 2016). *C. gattii* foi reconhecido como um importante patógeno no final dos anos 1990 (GALANIS *et al.*, 2010; LOCKHART *et al.*, 2013). Finalmente, outras espécies do gênero podem, minoritariamente, causar doenças humanas, com raros casos reportados para as espécies *C. albidus* e *C. laurenttii* (ZAVALA e BADDLEY, 2020).

A importância da criptococose aumentou em função do crescimento de doenças indutoras de imunossupressão, principalmente a AIDS (Síndrome da Imunodeficiência Adquirida). Além disso, outras situações ligadas a imunossupressão, como quimioterapias e preparação para transplantes de órgãos (MAY *et al.*, 2016; NYAZIKA *et al.*, 2018; RAMAN SHARMA, 2010; RODRIGUES *et al.*, 1999; STEENBERGEN e CASADEVALL, 2003), facilitam a instalação da doença. Dessa forma, *C. neoformans* e espécies correlatas passaram a ser reconhecidos como patógenos de grande importância, principalmente em populações imunologicamente

vulneráveis (MAZIARZ e PERFECT, 2016). Mesmo com o advento das terapias antirretrovirais (ART) o número de casos e de mortes associados a criptococose permanecem altos, sendo a busca por novas abordagens terapêuticas de grande valia para o tratamento dessa micose (MAZIARZ e PERFECT, 2016; ZARAGOZA, 2019).

Os principais patógenos do gênero, *C. neoformans* e *C. gattii,* apresentam particularidades que os diferenciam, como distribuição geográfica, nichos ambientais, status imunológico de seus hospedeiros e manifestações clínicas (HAGEN *et al.*, 2010; MAZIARZ e PERFECT, 2016). *C. neoformans* e *C. gattii* são leveduras haploides esféricas, encapsuladas, que atingem diâmetro que varia entre 5 e 10 µm. As leveduras se dividem por brotamento, eventos de reprodução sexuada podem ocorrer no ambiente ou por indução em laboratório (STEENBERGEN e CASADEVALL, 2003). É característica a presença de uma cápsula polissacarídica que pode variar de tamanho entre diferentes isolados (BIELSKA e MAY, 2016; RODRIGUES *et al.*, 1999; VOELZ *et al.*, 2010). As espécies também podem ser distinguidas de acordo com a diversidade antigênica associada a diferenças estruturais em sua cápsula polissacarídica (BIELSKA e MAY, 2016; ZAVALA e BADDLEY, 2020).

A espécie *C. neoformans* apresenta distribuição global e é encontrada geralmente associada a excretas de aves, sendo considerada a principal espécie patogênica do gênero (LEVITZ, 1991; MAY *et al.*, 2016; ZAVALA e BADDLEY, 2020). *C. gattii* já foi reconhecida como uma espécie endêmica de regiões tropicais e subtropicais, sendo facilmente encontrada em associação com o solo, cascas de eucaliptos ou árvores nativas de regiões endêmicas (KIDD *et al.*, 2007; LOCKHART *et al.*, 2013; MAY *et al.*, 2016). Dois importantes surtos destacaram *C. gattii* no cenário mundial em regiões de clima temperado, sendo um na Ilha de Vancouver no Canadá em 1999, onde é encontrada a maior população contaminada pela espécie, e outro na região do Noroeste Pacífico dos Estados Unidos da América (BYRNES e MARR, 2011; GALANIS *et al.*, 2010; KIDD *et al.*, 2007; LOCKHART *et al.*, 2013).

Recentemente, foi proposto que as espécies *C. neoformans* e *C. gattii* sejam reclassificadas (HAGEN *et al.*, 2015). A espécie *C. neoformans* foi dividida em *C. neoformans* (tipos moleculares VNI, VNII e VNB, anteriormente *C. neoformans* var. *grubii*) e *C. deneoformans* (VNIV, anteriormente *C. neoformans* var. *neoformans*). Foi proposto também que a espécie *C. gattii* seja subdividida em *C. gattii* (tipo molecular

VGI), *C. deuterogattii* (tipo molecular VGII), *C. bacillisporus* (tipo molecular VGIII), *C. tetragatttii* (tipo molecular VGIV) e *C. decagattii* (tipo molecular VGIV) (HAGEN *et al.*, 2015; KWON-CHUNG *et al.*, 2017; ZAVALA e BADDLEY, 2020). Em *C. gattii*, os tipos moleculares VGII e VGIII são mais facilmente encontrados como causadores de doença nas Américas, enquanto que infecções causadas pelo tipo molecular VGIV ocorrem quase que exclusivamente na África. O tipo molecular VGI é predominante na Europa, Austrália e Ásia (CAMPBELL *et al.*, 2005; CHATURVEDI *et al.*, 2005; HAGEN *et al.*, 2010; KIDD *et al.*, 2004; LOCKHART *et al.*, 2013; TRILLES *et al.*, 2008). Nesse estudo, utilizaremos a classificação tradicional em *C. neoformans* e *C. gattii*, defendida por grande parte da comunidade científica (KWON-CHUNG *et al.*, 2017).

A criptococose é a terceira doença fúngica invasiva mais comum, tratando-se de uma micose sistêmica associada a altas taxas de mortalidade e morbidade. A doença tem diferentes apresentações clínicas, podendo ser assintomática, crônica ou aguda, apresentando sua forma mais severa como uma meningite (DE AZAMBUJA *et al.*, 2018; MAZIARZ e PERFECT, 2016; PERFECT *et al.*, 2010; VOELZ *et al.*, 2010). A incidência anual de criptococose é estimada em 223.000 pacientes, com 181.000 mortes ao redor do globo (RAJASINGHAM *et al.*, 2017). A maior parte dos casos relatados de criptococose encontra-se entre pacientes imunocomprometidos, principalmente em decorrência da AIDS, sendo essa condição considerada o maior fator de risco para o desenvolvimento da doença. A criptococose é responsável pela morte de 15% da população com AIDS anualmente em todo o globo (DE AZAMBUJA *et al.*, 2018; NYAZIKA *et al.*, 2018; SLOAN e PARRIS, 2014).

Além de fatores associados ao estado humoral do paciente, podem ser encontradas diferenças numéricas no perfil da doença quando comparadas diferentes regiões geográficas e étnicas (figura 1). Por exemplo, os índices de criptococose na Austrália giram em torno de 6,6 casos a cada 1 milhão de habitantes, em províncias da África do Sul, esse número é estimado em 15,6 casos a cada 100 mil habitantes (FANG *et al.*, 2015; FIRACATIVE *et al.*, 2018). Mesmo com o advento das terapias antirretrovirais, que diminuíram drasticamente o número de complicações decorrentes da criptococose, os índices relacionados a doença ainda permanecem altos nos países em desenvolvimento e subdesenvolvidos. Países como Brasil, Colômbia, México e Argentina figuram como os países de maior incidência da meningite criptocócica na América Latina (DE AZAMBUJA *et al.*, 2018; FANG *et al.*, 2015; FIRACATIVE *et al.*, 2018; RAJASINGHAM *et al.*, 2017).

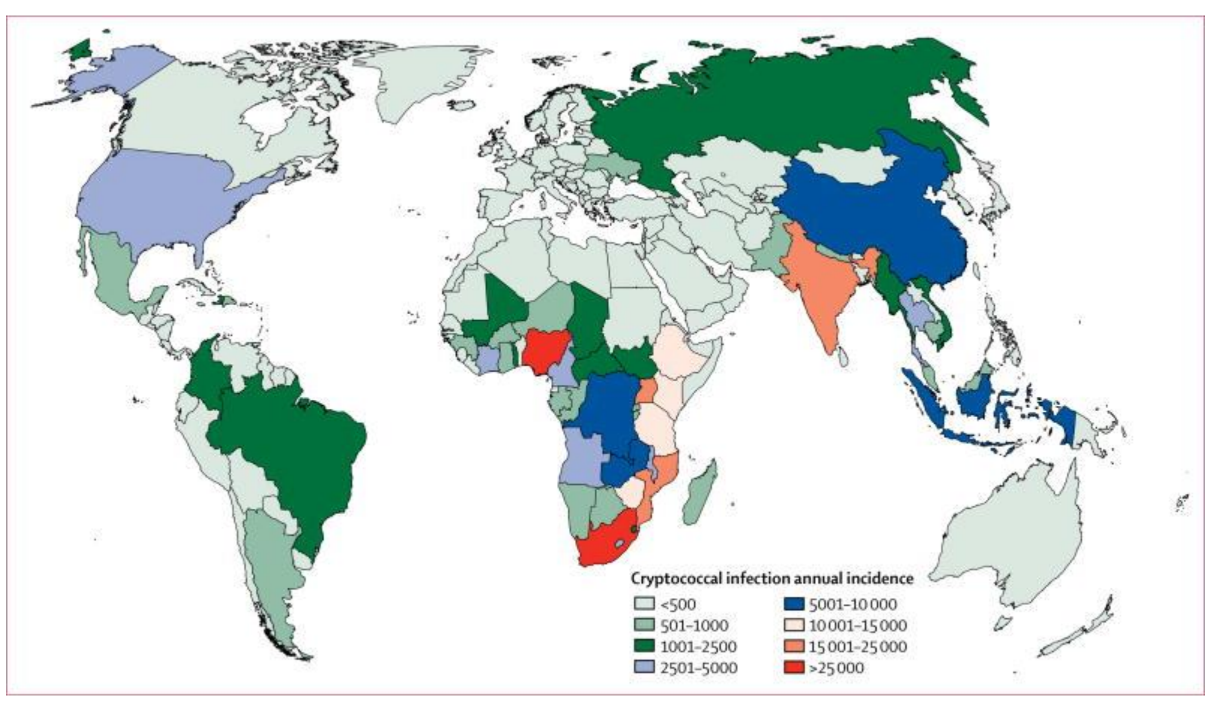

Figura 1: Incidência anual de criptococose por país. Fonte: Rajasingham *et al.*, 2017.

A infecção por *Cryptococcus* se dá, inicialmente, pela inalação de leveduras hipocapsulares ou basidiósporos, formas consideradas como propágulos infecciosos (figura 2) (BIELSKA e MAY, 2016; RODRIGUES *et al.*, 1999). Essas formas apresentam tamanho ideal para atingirem os alvéolos pulmonares no hospedeiro e interagir com os macrófagos nesse sitio anatômico (de OLIVEIRA et al., 2020). Após a exposição aos fungos, indivíduos imunocompetentes, geralmente, são capazes de controlar o patógeno e evitar a instauração da doença. Contudo, em hospedeiros com debilidades no sistema imune, o patógeno é capaz de se espalhar pelo organismo e causar dano a vários tecidos e órgãos (MURTHY e SUNDARAM, 2014; RAUCHWAY *et al.*, 2010) de OLIVEIRA et al., 2020). O quadro sintomático da criptococose é composto por febre, perda de peso, fadiga, tosse, dores torácicas, dores de cabeça, vômito e rigidez na nuca (BIELSKA e MAY, 2016; BROUWER *et al.*, 2007).

Dentre os sítios anatômicos afetados pela criptococose, os pulmões e o sistema nervoso central (SNC) apresentam as formas mais típicas da doença (figura 2). Nos pulmões, observa-se a formação de criptococomas e grânulos inflamatórios. Em caso de disseminação para o sistema nervoso central, a meningite, forma mais severa da doença, está associada a criptococomas cerebrais (GALANIS *et al.*, 2010; MAZIARZ e PERFECT, 2016; PERFECT *et al.*, 2010; ZAVALA e BADDLEY, 2020). A criptococose pulmonar tende a ser assintomática ou leve, produzindo sintomas semelhantes aos observados em outras doenças respiratórias. O quadro de meningite

pode levar a morte do hospedeiro, se não tratado rapidamente (VOELZ *et al.*, 2010). Como já mencionado, *C. neoformans* causa doença preferencialmente em indivíduos imunocomprometidos, com propensão a infectar o sistema nervoso central do hospedeiro. *C. gattii* tem capacidade de causar a patologia em indivíduos imunocompetentes, tendendo a instaurar-se nos pulmões do hospedeiro com elevados índices de mortalidade (BIELSKA e MAY, 2016; BROUWER *et al.*, 2007; MAY *et al.*, 2016; RODRIGUES *et al.*, 1999; RODRIGUES *et al.*, 2007; VOELZ *et al.*, 2010). Ressalta-se que o diagnóstico da criptococose é preciso e de baixo custo, sendo baseado na detecção de antígeno capsular circulante (ZAVALA e BADDLEY, 2020).

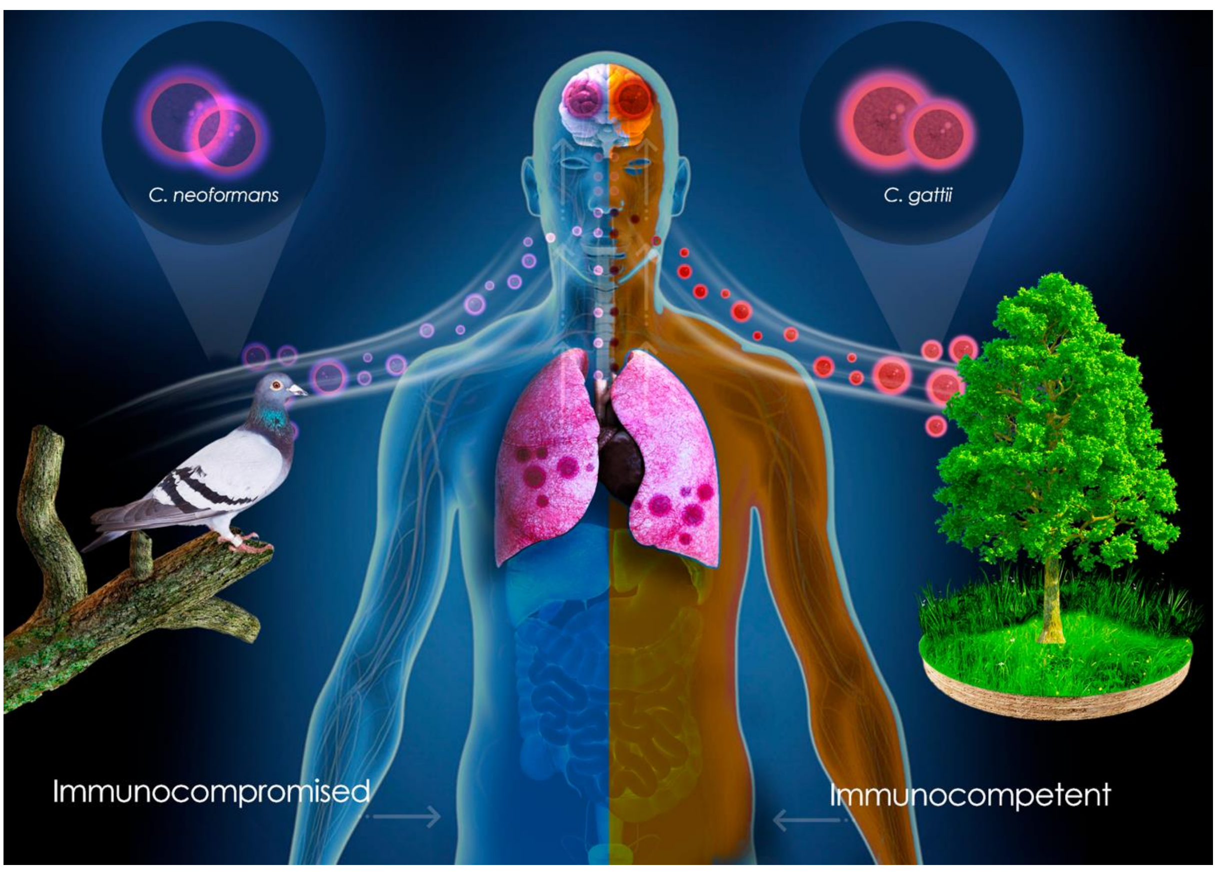

Figura 2: Mecanismos de infecção de *C. neoformans* e *C. gattii* no hospedeiro humano. É apontado o potencial de cada espécie de acordo com o nicho ambiental e o estado imunológico do hospedeiro. Fonte: de Oliveira *et al.*, 2020.

O tratamento da criptococose apresenta problemas relacionados à similaridade entre as células fúngicas e de mamíferos, o que aumenta a toxicidade dos fármacos ao hospedeiro, alto custo e espectro limitado de ação dos fármacos, que em geral possuem baixa biodisponibilidade (DENNING e BROMLEY, 2015; PERFECT, 2017). O tratamento padrão da doença é composto por três etapas: uma terapia de indução (administração de anfotericina B e 5-fluocitosina por 2 semanas), consolidação

(fluconazol por 8 semanas) e manutenção (fluconazol até a reversão do quadro adverso) (DROMER *et al.*, 2008; PERFECT *et al.*, 2010; RAUCHWAY *et al.*, 2010). A anfotericina B, além de tóxica para o hospedeiro mamífero, tem baixa disponibilidade em países em desenvolvimento (OSTERMANN *et al.*, 2014; PERFECT *et al.*, 2010). Na forma lipossomal, é menos tóxica para os pacientes, mas apresenta custo que pode atingir 500.000 reais por paciente no Brasil e apenas a formulação convencional é disponibilizada pelo sistema público de saúde (BORBA *et al.*, 2018).

2.2 Fatores de virulência de *Cryptococcus*

Protozoários de vida livre são organismos que podem ser encontrados nos mais diversos ambientes, como solo, ar, reservatórios de água doce e salgada, dentre outros (GONCALVES *et al.*, 2019). Organismos como amebas e nematoides apresentam alta atividade fagocítica no ambiente e, como consequência desse hábito, vários microrganismos são observados em cenário de endossimbiose com esses protozoários (GONCALVES *et al.*, 2019; MALLIARIS *et al.*, 2004). Essa associação garantiu a esses microrganismos o desenvolvimento da capacidade de explorar as amebas como nichos de replicação, garantindo a sua própria sobrevivência, com mecanismos similares aos utilizados para sobreviver em hospedeiros mamíferos (BONVICINI *et al.*, 2004; GONCALVES *et al.*, 2019).

Acanthamoeba castellanii é uma ameba de vida livre que pode ser infectada por diversas espécies de patógenos intracelulares (BONVICINI *et al.*, 2004). Vários estudos sugerem que a interação de fungos ambientais com organismos ameboides exerce pressão seletiva sobre os fungos, que resulta no desenvolvimento da capacidade de sobrevivência (ALBUQUERQUE *et al.*, 2019; CASADEVALL *et al.*, 2019; GONCALVES *et al.*, 2019). Considerando que patógenos fúngicos de distribuição ambiental não necessitam de hospedeiros animais para completar seu ciclo de vida, acredita-se que a interação entre predadores ambientais e patógenos fúngicos poderia explicar a origem dos mecanismos de virulência, favorecendo a virulência em hospedeiros mamíferos (MALLIARIS *et al.*, 2004; STEENBERGEN e CASADEVALL, 2003).

Para sobreviver no hospedeiro e escapar dos mecanismos de defesa do mesmo, as espécies de *Cryptococcus* expressam diversos fatores de virulência fundamentais para a sobrevivência do fungo (RODRIGUES *et al.*, 1999; RODRIGUES *et al.*, 2008;

ZARAGOZA, 2019). Para se instalar no hospedeiro humano, as células de *Cryptococcus* devem ser inicialmente capazes de se adaptar a temperatura do organismo de 36-37 ºC (BIELSKA e MAY, 2016; RODRIGUES *et al.*, 1999; ZARAGOZA, 2019), o que permitirá ao fungo a posterior defesa contra os mecanismos de imunidade. Nesse sentido, a síntese de melanina pode proteger o fungo contra a ação de radicais livres e outros fatores oxidantes produzidos por fagócitos (MEDNICK *et al.*, 2005; RODRIGUES *et al.*, 1999; ROSAS *et al.*, 2002). As espécies de *Cryptococcus* são capazes de produzir melanina a partir de compostos difenólicos produzidos pelo hospedeiro, como adrenalina e dopamina, e depositar o pigmento na parte interna da parede celular (CAMACHO *et al.*, 2019). Esse processo é catalisado pela enzima lacase e culmina com a resistência do fungo a mecanismos de imunidade e a fármacos antifúngicos (CAMACHO *et al.*, 2019; MEDNICK *et al.*, 2005; RODRIGUES *et al.*, 1999; ROSAS *et al.*, 2002). De fato, cepas de *Cryptococcus* mutadas em sua capacidade de expressar lacase tem virulência atenuada (RODRIGUES *et al.*, 1999).

Nos pulmões, as células fúngicas tem sua primeira interação com o sistema imune do hospedeiro, devendo ser capazes de resistir aos macrófagos presentes nos alvéolos pulmonares (RODRIGUES *et al.*, 1999). Uma vez fagocitado e presente no fagolisossomo, *Cryptococcus* se utiliza de estratégias para garantir sua sobrevivência, como a urease, capaz de modificar o pH do fagolisossomo para faixas onde a sobrevivência das células fúngicas não seja afetada. Essa modulação é realizada através da conversão enzimática da ureia em amônia, resultando no aumento do pH dentro do fagolisossomo (FEDER *et al.*, 2015; FU *et al.*, 2018). A defesa contra a fagocitose no pulmão pode se dar também no ambiente extracelular através de dois mecanismos importantes. Primeiro, no ambiente pulmonar as espécies de *Cryptococcus* podem passar por processos de transição morfológica que resultam na formação de leveduras gigantes denominadas células Titan, estruturas extremamente resistentes contra os mecanismos de imunidade (EVANS *et al.*, 2015; ZARAGOZA *et al.*, 2010). Segundo, a defesa anti-fagocítica pode ser mediada pelas estruturas capsulares, conforme discutido a seguir.

A cápsula polissacarídica é tida como fator determinante na interação com o sistema imune do hospedeiro e para virulência do patógeno. A cápsula consiste de uma rede de polissacarídeos hidratados e negativamente carregados ligados à parede celular de *Cryptococcus* spp. (figura 3) (BIELSKA e MAY, 2016; RODRIGUES *et al.*,

1999). As dimensões capsulares são reguladas em cada sítio anatômico infectado por *C. neoformans* (BIELSKA e MAY, 2016), o que determina o perfil de susceptibilidade do fungo à ação antimicrobiana de macrófagos.

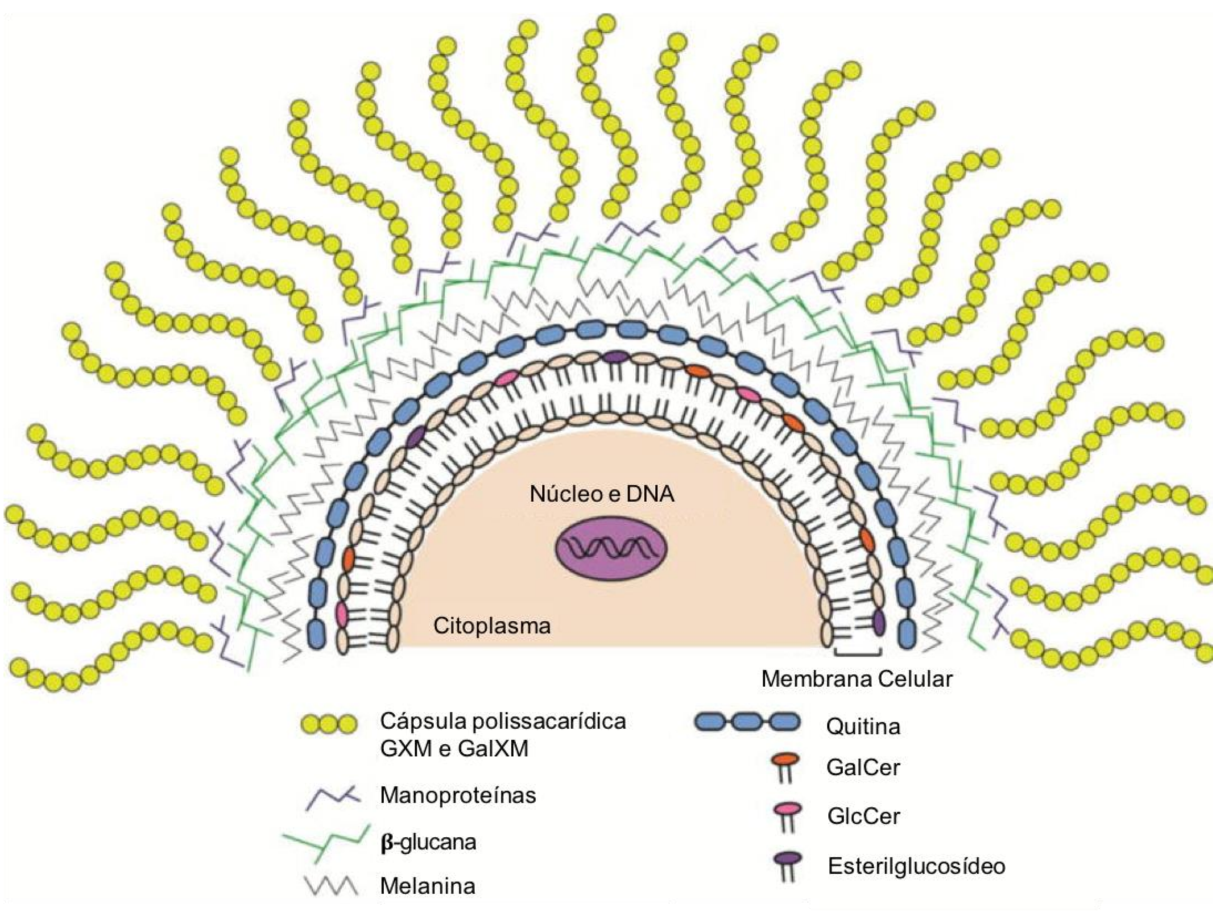

Figura 3: Estrutura da cápsula polissacarídica de *Cryptococcus* spp. Adaptado de: Caballero Van Dyke e Wormley Jr (2018).

Os componentes capsulares são produzidos no interior da célula, no complexo de Golgi, e liberados para o espaço extracelular através de EVs (BIELSKA e MAY, 2016; FELDMESSER *et al.*, 2001; GARCIA-RIVERA *et al.*, 2004; JANBON, 2004; YONEDA e DOERING, 2006). O principal constituinte capsular é a glucuronoxilomanana (GXM), um polissacarídeo de alto peso que consiste de unidades de manoses conectadas por ligações alfa1,3 com substituições de ácido glucurônico e xilose em ligações beta1,2 ou beta1,4 (RODRIGUES *et al.*, 1999). Os componentes minoritários são a glucuronoxilomanogalactana (GXMGal) e manoproteínas (figura 3) (BIELSKA e MAY, 2016; RODRIGUES *et al.*, 1999). As estruturas capsulares são altamente variáveis em decorrência das substituições de xilose e ácido glucurônico (RODRIGUES *et al.*, 1999), o que acarreta em alta diversidade sorológica.

As primeiras observações da cápsula polissacarídica como importante fator de virulência foram realizadas por Bulmer e colaboradores (1968) em estudo com diversas cepas de *C. neoformans* acapsulares, que se mostraram avirulentas em modelo animal (BULMER e SANS, 1968; RODRIGUES *et al.*, 1999). Em centenas de estudos posteriores, foi demonstrado que a cápsula tem diversas atividades imunomodulatórias que impactam diretamente a fisiopatologia da criptococose (FELDMESSER e CASADEVALL, 1998; RODRIGUES *et al.*, 1999).

Como já mencionado, as espécies de *Cryptococcus* também são capazes de produzir e secretar EVs (RODRIGUES *et al.*, 2007). Essas estruturas funcionam como carreadores de importantes fatores de virulência, incluindo a GXM (figura 4). Outros componentes carreados por vesículas incluem enzimas (lacase, urease, superóxido dismutase), lipídeos, pigmentos, proteínas, toxinas, ácidos nucleicos, antioxidantes e outros componentes possivelmente associados com virulência (COELHO e CASADEVALL, 2019; HERKERT *et al.*, 2019; RODRIGUES *et al.*, 2008; RODRIGUES *et al.*, 2007). Recentemente, foi descrito que as EVs possuem importante papel em mecanismos de comunicação intercelular (BIELSKA *et al.*, 2018; COELHO e CASADEVALL, 2019). Em outros modelos fúngicos, as EVs são ainda associadas com a resistência a fármacos antifúngicos e formação de biofilmes (BIELSKA *et al.*, 2018; YOON *et al.*, 2014; ZARNOWSKI *et al.*, 2018).

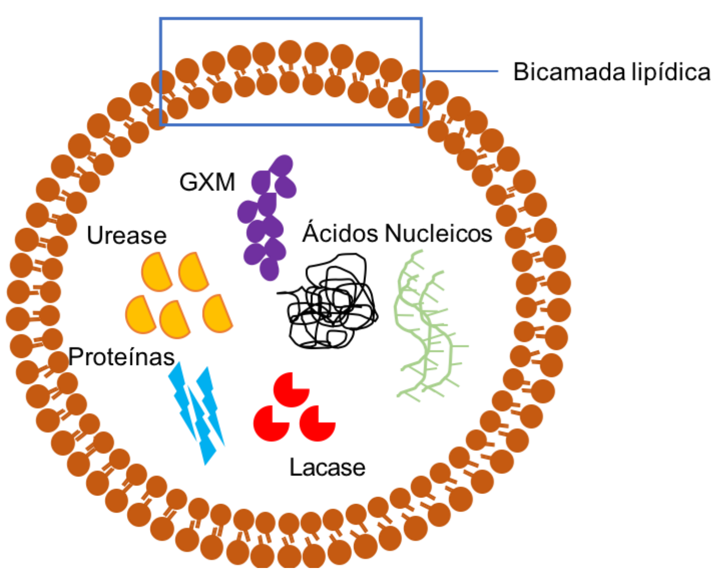

Figura 4: Representação esquemática de uma EV de *Cryptococcus* spp. São ilustrados os principais componentes exportados através de vesículas.

Para saída dos pulmões e colonização do sistema nervoso central, alguns elementos produzidos por *Cryptococcus* são essenciais. Por exemplo, a enzima

urease parece ter papel fundamental na passagem das células criptocócicas pela barreira endotelial para promover a invasão do SNC. Essa disseminação parece ocorrer através de microcapilares, consistindo de um importante mecanismo facilitador para invasão do SNC (FEDER *et al.*, 2015; OLSZEWSKI *et al.*, 2004; SHI *et al.*, 2010; SINGH *et al.*, 2013). O uso de inibidores da enzima reduz a disseminação fúngica para o cérebro (SINGH *et al.*, 2013). Com o emprego de camundongos como modelo de estudo, foi observado que a enzima é capaz regular a polarização da resposta imune do hospedeiro (OSTERHOLZER *et al.*, 2009; SINGH *et al.*, 2013). É importante ressaltar que a enzima não aparenta ter papel fundamental na sobrevivência do fungo quando alojado no SNC. Nesse sítio anatômico, a enzima lacase parece ser um fator relacionado à sobrevivência fúngica (MEDNICK *et al.*, 2005; OLSZEWSKI *et al.*, 2004).

A fosfolipase B1 (Plb1) pertence a uma classe de enzimas que promovem a degradação de fosfolipídios (COX *et al.*, 2001). Sua produção por *Cryptococcus* é essencial na disseminação para o SNC do hospedeiro (CHAYAKULKEEREE *et al.*, 2011; COX *et al.*, 2001). A degradação de fosfolipídios resultaria na desestabilização de membranas, causando lise celular e consequente aumento de capacidade invasiva, além do escape de células fagocíticas (COX *et al.*, 2001). Cepas deficientes na expressão de Plb1 tem diminuição no escape de macrófagos por vias não líticas (CHAYAKULKEEREE *et al.*, 2011; COELHO *et al.*, 2014). Ainda, Cox *et al.* (2001) demonstraram que cepas fúngicas nas quais foi deletado o gene responsável pela expressão Plb1 apresentam fenótipo hipovirulento e menor invasão do SNC, reforçando o papel da enzima na disseminação extrapulmonar em *Cryptococcus* (COX *et al.*, 2001).

Os fatores de virulência produzidos pelas espécies de *Cryptococcus* são fundamentais para a produção de dano no hospedeiro mamífero, mas também podem atuar no ambiente (STEENBERGEN e CASADEVALL, 2003). Por exemplo, a presença da cápsula polissacarídica é de grande importância para evitar a dessecação das células criptocócicas e a ingestão por organismos de vida livre no ambiente (LITTMAN e BOROK, 1968; STEENBERGEN *et al.*, 2001). A melanização protege o fungo contra a radiação ultravioleta (NOSANCHUK *et al.*, 1999). A alta concentração de ureia na excreta de pombos sugere a necessidade da urease na conversão de ureia em amônia e nitrogênio, modulando o pH local (STEENBERGEN e CASADEVALL, 2003).

2.3 Novos alvos em potencial para o desenvolvimento de fármacos anti-*Cryptococcus*

A busca por novos alvos e novas terapias anti-criptocócicas vêm sendo objeto de estudo de diversas pesquisas ao longo dos últimos anos, com várias possibilidades tendo sido identificadas. Destacam-se a busca de mecanismos que influenciam a patogênese de *Cryptococcus* e reposicionamento de fármacos já disponíveis e utilizados na clínica humana (COELHO e CASADEVALL, 2016; IANIRI e IDNURM, 2015; JUNG *et al.*, 2018; LEE *et al.*, 2020; MAYER e KRONSTAD, 2017; PIANALTO e ALSPAUGH, 2016; ROSSI *et al.*, 2020; SAMANTARAY *et al.*, 2016).

Buscando encontrar novas drogas com atividade anti-criptocócica, nosso grupo testou contra *C. neoformans* e *C. gattii* uma coleção de 727 compostos já aprovados para o uso clínico em outras enfermidades (JOFFE *et al.*, 2017). Dentre as moléculas ativas encontradas, derivados de benzimidazóis se destacaram por mostrar potente atividade antifúngica. O aprofundamento desses estudos com o mebendazol revelou atividade fungicida intra e extracelular, redução no tamanho da cápsula e atividade de inibição de biofilmes (JOFFE *et al.*, 2017). Este estudo identificou dois possíveis alvos celulares envolvidos no efeito antifúngico do mebendazol, a proteína escramblase, uma translocadora de lipídeos de membrana, e a proteína Nop16, possivelmente envolvida na biogênese ribossomal.

A identificação desses alvos se deu através da utilização de uma coleção de 7.000 mutantes de fenótipos variados, que foi gerada de forma aleatória através da transformação de *C. gattii* por *Agrobacterium tumefaciens.* Nesta coleção, cepas resistentes ao mebendazol foram selecionadas e através da técnica de PCR inversa foi possível identificar duas cepas com altas taxas de resistência ao fármaco. Uma delas apresentou interrupção no gene *AIM25* (escramblase) e uma segunda cepa teve interrompido o gene responsável por codificar a proteína Nop16 (JOFFE *et al.*, 2017).

Recentemente nosso grupo demonstrou que o fenbendazol é um eficaz agente anti-*Cryptococcus* (DE OLIVEIRA *et al.*, 2020). Ao contrário do mebendazol, o fenbendazol não depende de escramblase e Nop16 para exercer atividade antifúngica, atuando sobre a ß-tubulina (DE OLIVEIRA *et al.*, 2020). Esses estudos demonstram que existe grande diversidade de possíveis alvos antifúngicos nas células de *Cryptococcus,* justificando um aprofundamento desses estudos.

Até o momento, a função molecular de Nop16 em *Cryptococcus* ainda é desconhecida, mas sabe-se que em *Saccharomyces cerevisiae* a proteína é envolvida na produção da subunidade ribossomal 60S (HARNPICHARNCHAI *et al.*, 2001; JOFFE *et al.*, 2017). Foi sugerido que a interrupção do gene *NOP16* afeta a exportação de GXM para o meio extracelular e na cinética de produção de melanina, importantes fatores de virulência (JOFFE *et al.*, 2017). Entretanto, esses estudos foram realizados com mutantes gerados por transformação aleatória por *A. tumefaciens*, sendo necessária a confirmação e aprofundamento desses fenótipos por deleções dirigidas do gene *NOP16*.

Dado o possível envolvimento de Nop16 com importantes fatores de virulência em *Cryptococcus* (JOFFE *et al.*, 2017), a proteína em questão pode se revelar um alvo promissor para o desenvolvimento de antifúngicos. Esses estudos, entretanto, requerem a melhor caracterização dos papeis fisiológicos e patogênicos da Nop16.

3. Objetivos

Este estudo teve como objetivo geral analisar o efeito da deleção do gene *NOP16* em vários aspectos da biologia do *C. gattii*.

Especificamente, os objetivos do estudo foram:

- Comparar em cepas selvagens e mutantes o crescimento a 37 ºC;
- Analisar o perfil de sensibilidade das cepas selvagem e mutantes a fármacos antifúngicos;
- Analisar a morfologia das cepas selvagem e mutantes através de técnicas de microscopia ótica, de fluorescência e eletrônica de varredura e transmissão;
- Avaliar o potencial de secreção de glucuronoxilomanana das cepas;
- Observar a capacidade das cepas de interagir com macrófagos;
- Isolar, quantificar e caracterizar as EVs, considerando quantidade, morfologia e dimensões, através de análises de rastreamento de nanopartículas e microscopia eletrônica de transmissão;
- Analisar o potencial patogênico das cepas selvagens e mutantes em modelo de hospedeiro invertebrado (*Galleria mellonella*).

4. Materiais e Métodos

4.1 Cepas fúngicas e condições e cultivo

As cepas utilizadas neste trabalho pertencem à espécie *C. gattii.* Foram utilizadas a cepa padrão R265 (selvagem, *wild type*) e também mutantes independentes construídos a partir da interrupção do gene *NOP16* na cepa parental R265, aqui denominados como *nop16Δ.1* e *nop16Δ.2.* A construção das cepas mutantes foi realizada pelo grupo de pesquisa coordenado pelo Professor Charley Staats, da Universidade Federal do Rio Grande do Sul (UFRGS) (JOFFE *et al.*, 2017). Os mutantes foram gerados de acordo com a metodologia descrita por Joffe *et al.* (2017) e transferidos para nosso laboratório.

As cepas foram mantidas em placas de Sabouraud Ágar (extrato de levedura 1%, peptona 2%, dextrose 4% e ágar 1,5%), crescidas a 30 ºC por 24 horas e armazenadas a 4 ºC. 24 horas antes da realização dos experimentos as cepas foram repicadas para meio YPD líquido (extrato de levedura 1%, peptona 2% e dextrose 2%) e incubadas a 30º C por 24 horas com agitação de 200 rpm.

Em experimentos onde houve a necessidade da indução de cápsula, as células passaram por uma etapa extra de incubação em meio de indução de cápsula (Sabouraud 10% diluído em MOPS 50 mM pH 7,4) por 24 horas a 37 ºC e CO_2 5%. Para o ensaio de detecção de GXM por ELISA, as células cultivadas em meio YPD passaram por uma etapa adicional de incubação em RPMI, nas condições de 37 ºC, CO_2 5% durante 24 horas antes da coleta de sobrenadantes.

4.2 Curva de crescimento

Para acompanhar a cinética de crescimento de *C. gattii*, foram realizadas curvas de crescimento dos fungos em meio YPD ou Sabouraud a 37 ºC. Para tanto, as cepas tiveram sua densidade celular ajustada a 5×10^4 cels/ml e foram inoculadas em placas de 96 poços com meio YPD ou Sabouraud. As placas foram incubadas a 37ºC no em sistema SpectraMax PARADIGM (Molecular Devices) por 48 horas. Durante o período de incubação, a densidade óptica dos poços da placa foi tomada a cada 1 hora em comprimento de onda de 530 nm.

4.3 Análises da cápsula polissacarídica

4.3.1 Nanquim e medidas da célula fúngica

A técnica de contra-coloração com tinta Nanquim foi realizada para visualização em microscopia óptica da cápsula de *Cryptococcus* spp. Como a estrutura polissacarídica não é permeável ao nanquim, a contra-coloração gera alto contraste e permite evidenciar a estrutura capsular.

As células de *C. gattii* foram crescidas conforme o item 4.1 e passaram por etapa de indução da cápsula em meio contendo Sabouraud 10% em MOPS (ácido morfolinopropanosulfônico) 50 mM, pH 7.4 (ZARAGOZA e CASADEVALL, 2004) por 24 horas a 37 ºC e CO_2 5%. Após a indução da cápsula, as células foram recuperadas através de centrifugação a 3.000 x g, lavadas com PBS e fixadas em paraformaldeído 4%. A suspensão celular (3 µl) foi colocada sobre uma lâmina de vidro e suplementada com 2 µl de tinta Nanquim. A amostra foi finalmente recoberta por uma lamínula de vidro.

A lâmina preparada foi levada ao microscópio invertido (Leica DMi8) e observada sob aumento de 100 vezes em imersão para captura de imagens das células fúngicas. As imagens obtidas neste processo foram analisadas com o auxílio do software ImageJ (NIH) (SCHNEIDER *et al.*, 2012). Foram medidos diâmetro total da célula (compreendida por corpo celular + cápsula) e diâmetro celular. O tamanho da cápsula foi estimado pela diferença do diâmetro total da cápsula subtraído do diâmetro do corpo celular. Através da barra de escala inserida automaticamente nas imagens durante a captura das mesmas, o software foi calibrado para gerar medidas das estruturas analisadas.

4.3.2 Imunomarcação

As células criptocócicas cultivadas em YPD por 24 horas foram centrifugadas e o sedimento celular lavado com PBS para retirada do meio. As células foram transferidas para meio de indução de cápsula nas condições já descritas. As células foram então centrifugadas a 3.000 x g por 3 minutos e o sedimento celular lavado três vezes com PBS estéril. As células foram suspensas em 150 µl de solução fixadora (paraformaldeído a 4% em PBS) e incubadas em temperatura ambiente por 30 minutos. Após a fixação, a suspensão celular foi centrifugada novamente a 3.000 x g

durante 3 minutos. O sedimento celular foi submetido a três lavagens com PBS e o sedimento celular da última centrifugação foi bloqueado através da adição de 1 ml de tampão de bloqueio (BSA 1% em PBS), seguindo-se incubação durante uma hora 37 ºC. A suspensão foi centrifugada nas condições descritas neste protocolo, o sobrenadante foi descartado e ao sedimento celular foram adicionados 150 μl de calcofluor 25 μM, seguindo-se incubação durante 30 minutos a 37 ºC. Em seguida, foram realizadas 3 lavagens com PBS e ao sedimento foram adicionados 120 μl do anticorpo anti-GXM 18B7 (doado pelo Dr. Arturo Casadevall, Johns Hopkins University, Baltimore, USA) na concentração de 10 μg/ml diluído em tampão de bloqueio, para posterior incubação durante uma hora a 37 ºC. As células foram lavadas três vezes com PBS e suspensas em 120 μl do anticorpo secundário (anticorpo de cabra contra imunoglobulina de camundongo) conjugado com Alexa 546, diluído em tampão de bloqueio 1:1.500. As células foram incubadas por 1 hora no escuro e temperatura ambiente. Após a incubação com anticorpo secundário, as células passaram por nova bateria de lavagem com PBS. As células foram ainda marcadas com WGA (*wheat germ agglutinin*), que permite evidenciar oligômeros de quitina na parede celular (FONSECA *et al.*, 2009). Esta etapa foi realizada pela suspensão do sedimento celular lavado em 600 μl de WGA na concentração de 5 μg/ml, seguindo-se incubação por 30 minutos a 37 ºC. As células foram lavadas com PBS e o sedimento foi mantido em suspensão com PBS. As células foram analisadas no microscópio invertido de fluorescência DMi8 (Leica Microsystems).

4.4 Ensaio Imunoenzimático (*Enzyme Linked Immunosorbent Assay* - ELISA)

O ensaio de ELISA foi realizado para detectar glucuronoxilomanana (GXM) livre no sobrenadante de cultura. Para o ensaio de ELISA, as células crescidas em YPD foram lavadas e a densidade celular foi ajustada para 5 x 10^4 cels/ml. As células foram incubadas em meio RPMI (HyClone 1640 medium) durante 24 horas a 37 ºC em atmosfera de CO_2 5% para induzir o crescimento capsular.

Após a indução de cápsula por 24 horas, as suspensões foram transferidas para tubos de fundo cônico de 5 ml. Os tubos foram centrifugados a 3.000 x g durante três minutos para separação do sedimento celular do sobrenadante. O sobrenadante dessa centrifugação foi transferido para uma placa de 96 poços de fundo cônico, que foi posteriormente centrifugada durante 5 minutos a 3.500 x g para retirada de possíveis *debris*. O sobrenadante recolhido desta última etapa foi armazenado em

tubos de 1 ml, para a detecção da GXM. As amostras recolhidas foram diluídas 20 vezes em meio RPMI em volume final de 200 μl. Os ensaios de ELISA foram realizados em placas de poliestireno com 96 poços (Corning). Primeiramente, os poços das placas foram sensibilizados com os sobrenadantes ou com GXM purificada. Na fileira A foram adicionados 75 μl do padrão de GXM diluído em PBS a 5 μg/ml nas colunas 1 e 2. Nas colunas seguintes (3-8) os poços foram sensibilizados com os sobrenadantes recolhidos a serem testados, em duplicatas, conforme o esquema abaixo:

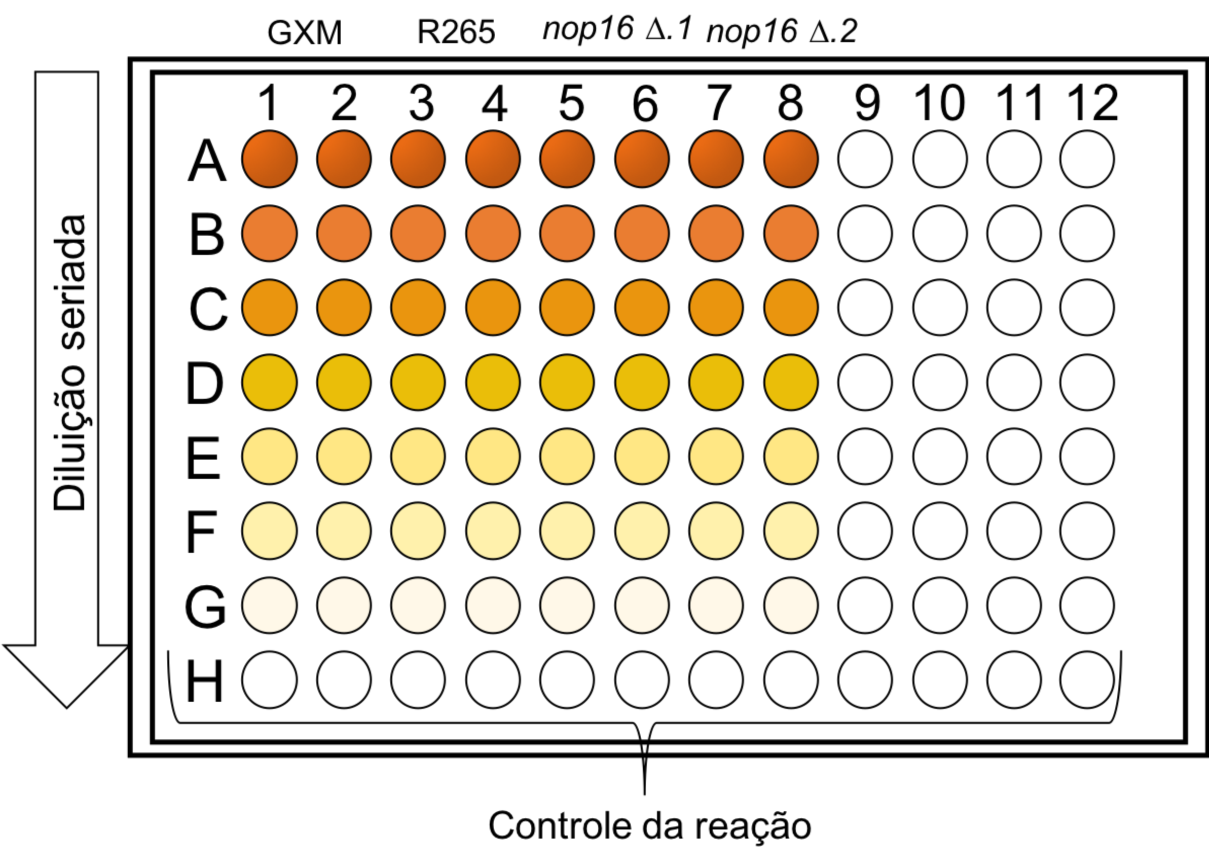

Figura 5: Esquema da placa de 96 poços utilizada para o ensaio de ELISA. A ilustração demonstra a direção da diluição das amostras e também a distribuição de cada amostra na placa. A fileira H é o controle da reação.

As fileiras B-G foram preenchidas com 50 μl de PBS e as amostras e controles foram então diluídos em série na proporção 1:3 em PBS entre as fileiras B-G. A fileira H foi acrescida apenas de PBS e utilizada como controle negativo do experimento. O volume final utilizado para a sensibilização dos poços foi de 50 μl.

A seguir, a placa foi incubada a 37 ºC durante 1 hora. Após a incubação, o conteúdo dos poços foi descartado e os poços lavados 3 vezes com 200 μl de PBS.

Após as lavagens, foi realizada a etapa de bloqueio, adicionando-se 200 μl por poço de tampão de bloqueio (BSA 1% em PBS), seguindo-se incubação por 1 hora a 37 ºC. Após o bloqueio, o conteúdo das placas foi descartado e em cada poço foram adicionados 50 μl do anticorpo primário anti-GXM 18B7 na concentração de 1 μg/ml em tampão de bloqueio. Os sistemas foram incubados por 1 hora a 37 ºC. Após a incubação os poços foram novamente lavados com 200 μl de PBS por 3 vezes. Após as lavagens, foram adicionados 50 μl por poço do anticorpo secundário (anticorpo de cabra contra imunoglobulina de camundongo) conjugado à fosfatase alcalina na concentração de 2 μg /ml. As placas foram incubadas por mais 1 hora nas condições apontadas acima. O conteúdo solúvel das placas foi descartado e os poços foram lavadas 3 vezes com 200 μl de tampão fosfatase alcalina (TBS, Tris 50 mM Ph 7,6, NaCl 150 mM em H_2O). Após as lavagens, a cada poço foram adicionados 50 μl de paranitrofenilfosfato (pNPP) na concentração de 1 mg/ml em TBS. A revelação das placas foi feita em temperatura ambiente ou em estufa a 30 ºC, com posterior leitura da absorbância a 405 nm no leitor de microplacas SpectraMax PARADIGM (Molecular Devices).

4.5 Isolamento de EVs

O isolamento das EVs produzidas por mutantes e células selvagens de *C. gattii* seguiu o protocolo desenvolvido por Reis *et al.* (2019) em meio sólido. Culturas fúngicas crescidas conforme o item 4.1 tiveram as densidades celulares determinadas em câmara de Neubauer e ajustadas para 3,5 x 10^7 cels/ml. Alíquotas de 300 μl de cada inóculo foram espalhadas com uma alça de Drigalski em placas de Petri contendo 25 ml de YPD sólido. Foram utilizadas 3 placas por cepa. As placas foram incubadas a 30 ºC por 24 horas para atingir confluência, e então as células fúngicas foram recuperadas através de raspagem com alça de inoculação e transferidas para um tubo de centrifugação, preenchido com 30 ml de PBS estéril. Foram então feitas centrifugações sequenciais dos tubos para remoção das células. Na primeira etapa de centrifugação, as amostras foram centrifugadas a 5.000 x g durante 15 minutos a 4 ºC. O sobrenadante da primeira etapa de centrifugação foi transferido para um tubo estéril. Estes tubos seguiram para uma segunda centrifugação a 15.000 x g por 15 minutos a 4 ºC, para que os *debris* celulares da solução fossem sedimentados. Após esta etapa o sobrenadante dos tubos foi transferido para tubos de 50 ml com fundo cônico, filtrados em membranas com poro de 0,45 μm para retirada de possíveis

restos celulares da amostra. As amostras foram então transferidas para tubos de ultracentrifugação e centrifugadas em ultracentrífuga (Hitachi) com velocidade de 100.000 x g por 1 hora e temperatura de 4 ºC. As EVs encontram-se sedimentadas e o sobrenadante dessa etapa foi descartado. As EVs foram suspensas em volume final de 300 μl de PBS e armazenadas em tubos de 1 ml a 4 ºC.

4.6 Análise de Nanopartículas (*Nanoparticle Tracking Analysys* - NTA)

A quantificação das EVs foi feita com a utilização do sistema de análise de nanopartículas LM10 acoplado a um laser em 488 nm, equipado com câmera e bomba de fluxo (Malvern Panalytical, Malvern, United Kingdom) e do software NTA 3.0 (Malvern Panalytical). A análise de nanopartículas é uma técnica utilizada para mensuração de tamanho e concentração das partículas através da utilização de dispersão da luz e iluminação das partículas através de um feixe de laser (SOUZA *et al.*, 2019).

As amostras recuperadas foram diluídas 200 vezes em PBS para atingir a diluição ideal de leitura (9 x 10^7 até 2,9 x 10^9 partículas/ml). As amostras foram inseridas em seringas de 1 ml acopladas a uma bomba de injeção em fluxo contínuo. Foram obtidos filmes das amostras passando pelo feixe de luz para posterior análise (três vídeos de 60 segundos por amostra, com nível da câmera a 15, ganho em 3). A viscosidade da amostra foi indicada como a mesma da água. Para análise de dados o ganho da câmera foi alterado para 10-15 e o limite de detecção usado foi 3 para todas as amostras.

4.7 Microscopia Eletrônica de Transmissão (MET)

A microscopia eletrônica de transmissão foi utilizada para visualização das ultraestruturas celulares de *C. gattii* e também das EVs. Para o detalhamento da preparação, a metodologia foi separada para as células fúngicas e para as EVs, por se tratarem de protocolos diferenciados.

4.7.1 Células fúngicas

A preparação das células fúngicas para visualização por MET foi realizada com as células obtidas conforme descrito no item 4.1. As células foram fixadas em paraformaldeído 4% e glutaraldeído 2,5% em tampão cacodilato 0,1 M, pH 7,2 por

uma hora em temperatura ambiente. As amostras fixadas passaram por 3 lavagens com o tampão cacodilato através de centrifugações a 5.000 x g por 2 minutos. O sedimento foi tratado com tetróxido de ósmio 1% e ferrocianeto potássio 1,6% 5 mM diluído em tampão cacodilato 0,1 M (na proporção de 1:1) e incubado por 1 hora a temperatura ambiente. As amostras foram então lavadas 3 vezes com tampão cacodilato e então foi iniciada a bateria de desidratação das amostras utilizando acetona. A bateria de desidratação foi realizada seguindo trocas do solvente na seguinte ordem: 30%, 50%, 70%, 90% e duas vezes com 100% acetona. As amostras tiveram contato com a acetona por 30 minutos em cada etapa. Logo após a última etapa de desidratação o sedimento celular foi coberto com resina EMbed 812 (EMS) diluída em acetona. A diluição inicial foi de 1 parte de resina para 2 partes de acetona 100% e essa proporção foi alterada com trocas diárias. No segundo dia, foi usada 1 parte de resina para 1 parte de acetona; no terceiro dia 2 partes de resina para 1 parte de acetona. No quarto dia foram feitas duas trocas com 100% de resina e a partir da segunda troca o sedimento celular coberto por resina foi incubado em estufa a 60 ºC por 48 horas, até a completa polimerização da resina. O bloco de resina polimerizada com a amostra foi então preparado com o auxílio de uma lâmina para a etapa de microtomia. Os cortes foram feitos utilizando um ultramicrótomo (Leica EM UC6) com espessura de 70-80 nm e montagem sobre grades microscópicas. A observação das amostras foi feita no microscópio JEOL 1400Plus com aceleração de 90 kV. A obtenção das imagens foi realizada através de uma câmera digital com CCD de 8 megapixels acoplada ao equipamento.

4.7.2 Vesículas Extracelulares

A visualização das EVs por microscopia eletrônica de transmissão foi realizada com o emprego da técnica de coloração negativa. As EVs que foram obtidas de meio sólido, conforme o protocolo de isolamento de vesículas, foram empregadas nesta metodologia, de acordo com a descrição seguinte.

As amostras foram homogeneizadas com um vórtex por dois minutos para desfazer possíveis agregados. Em uma placa de vidro recoberta com parafilme, foram adicionados 50 μl da suspensão de EVs e cada suspensão foi coberta com grades revestidas por Formvar, para adesão das EVs durante 60 minutos em temperatura ambiente. As grades foram então lavadas com 30 μl de PBS esterilizado. O excesso de tampão foi retirado pela aplicação de papel de filtro na parte inferior de cada grade.

Em sequência as EVs aderidas ao Formvar da grade foram fixadas com 30 μl de solução Karnowski por 10 minutos, lavadas 3 vezes com tampão cacodilato e por fim as amostras foram secas com papel filme pela lateral da grade. A contrastação das amostras foi feita utilizando solução de uranila 5% por 2 minutos. As grades foram lavadas uma vez com dH_2O, secas com papel filme e levadas ao metalizador (Leica EM ACE200), onde foram recobertas por partículas de carbono para posterior visualização no microscópio eletrônico de transmissão JEOL 1400Plus com aceleração do feixe a 90 kV.

4.8 Microscopia Eletrônica de Varredura (MEV)

A superfície das células fúngicas foi analisada por MEV. Para tal, as células de *C. gattii* crescidas em YPD foram centrifugadas a 3.000 x g e o sedimento celular lavado com PBS. A amostra foi fixada com glutaraldeído 2,5% em tampão cacodilato (cacodilato de sódio 0,1 M, pH 7,2). Lamínulas circulares (Knittel) foram lavadas com etanol 100% e sonicadas por 10 minutos. As lamínulas foram distribuídas em placa de 24 poços e revestidas com 150 µl de poli-L-lisina tipo I 0,01% (SigmaAldrich) para funcionalização. Os sistemas foram incubados durante 30 minutos e lavados 3 x com dH_2O para retirar o excesso de poli-L-lisina. Os sistemas foram levados a secura em temperatura ambiente. As células em fixador foram centrifugadas a 3.000 x g e lavadas com pós-fixador (sacarose 0,2 M, tampão cacodilato de sódio 0,1M, cloreto de magnésio 2 mM em dH_2O) por 3 vezes. As amostras lavadas foram aderidas sobre as lamínulas por 30 minutos em temperatura ambiente, sendo utilizado o volume de 150 µl para cada amostra. Logo após a adesão foi dado início a bateria de desidratação das amostras. A bateria foi realizada com soluções de etanol 30%, 50% e 70% por 5 minutos em cada concentração, seguiu-se para etanol 90% e duas passagens por etanol 100%, sendo estas três etapas com duração de 10 minutos cada.

As lamínulas com amostras fixadas e desidratadas foram acomodadas dentro de bases metálicas (*stubs*) submersas em etanol 100% e seguiram para o ponto crítico, onde toda a umidade da amostra foi retirada através de trocas consecutivas entre CO_2 líquido e etanol. Dentro da câmara de ponto crítico (Leica EM CPD300) os *stubs* foram submersos em etanol e a câmara foi preenchida com CO_2 líquido, sendo realizadas 10 trocas. Após o ponto crítico, as lamínulas seguiram para o metalizador (Leica EM ACE200) onde foram recobertas por partículas de ouro. A visualização das

amostras foi feita utilizando o microscópio JEOL JSM-6010 Plus/LA com aceleração de 5 kV.

4.9 Ensaio de fagocitose de *C. gattii*

Para os testes de fagocitose, a linhagem de macrófagos murinos RAW 264.7 foi utilizada e mantida em meio Dulbecco's modificado com Eagle's (DMEM) suplementado com soro fetal bovino 10% (SFB) a 37 °C em CO_2 5%. Na véspera do experimento, um inóculo de RAW 264.7 contendo 5 x 10^5 cels/ml foi preparado em DMEM suplementado com SFB 10%. 200 µl desse inóculo foram distribuídos por poço em placas de 96 poços, que foram incubadas a 37°C e CO_2 5% por 24 horas.

Para os experimentos de fagocitose as células fúngicas foram cultivadas conforme o item 4.1, e os inóculos então ajustados para a densidade de 1 x 10^6 cels/ml em YPD. Após o ajuste do inóculo, as células foram lavadas 1 vez com PBS e então incubadas com 0,5 mg/ml de FITC em PBS à temperatura ambiente por 15 minutos no escuro. As células foram lavadas três vezes com PBS e então os inóculos foram ajustados para 5 x 10^5 cels/ml em DMEM e opsonizados com 10 µg/ml do anticorpo 18B7. O processo de opsonização foi feito em incubação por 1 hora a 37 ºC em atmosfera de CO_2 5%. As células opsonizadas foram utilizadas para infectar os macrófagos previamente semeados em placas de 96 poços, utilizando-se o MOI (multiplicidade de infecção) de 1:1. Os sistemas foram incubados por 3 horas a 37 ºC em CO_2 5%. Após a incubação, os poços foram lavados 3 vezes com PBS para retirada das células não fagocitadas e a cada poço foi adicionado 200 µl de DMEM + SFB 10%. As placas foram então levadas ao equipamento Operetta high-content imaging system (PerkinElmer). O equipamento foi ajustado para temperatura de 37 ºC e atmosfera de CO_2 5% e programado para fotografar as células infectadas após a interação. As imagens foram obtidas nos canais Alexa 488 para detecção da fluorescência emitida pelo FITC, também utilizando campo claro. As imagens foram processadas utilizando os softwares Harmony high-content imaging and analysis software (PerkinElmer) e ImageJ (NIH). Os índices de fagocitose consistiram da porcentagem de células infectadas com o fungo em cada campo.

4.10 Infecção de *Galleria mellonella*

Para avaliar o potencial patogênico das cepas estudadas, o modelo animal alternativo de infecção em *Galleria mellonella,* consolidado para o estudo da

patogênese de *Cryptococcus* (MYLONAKIS *et al.*, 2005), foi utilizado. Larvas de *G. mellonella* pesando entre 0,10-0,15 g foram divididas em grupos de 15 animais em placas de petri e incubadas *overnight* a 37 ºC antes do experimento, para aclimatação. Também no dia anterior ao experimento, as diferentes cepas de *C. gattii* foram cultivadas conforme item 4.1.

No dia do experimento, inóculos de 1 x 10^8 cels/ml foram preparados em PBS, para cada uma das cepas a ser analisada. 10 µl desses inóculos, contendo 1 x 10^6 fungos, foram utilizados para infectar as larvas de *G. mellonella* utilizando seringa Hamilton na última propata dos animais. As placas foram então incubas a 37 ºC para acompanhamento da sobrevivência dos animais ao longo dos dias. Os grupos analisados foram: 1) animais infectados com a cepa *WT* R265; 2) animais infectados com a cepa mutante *nop16Δ.1*; 3) animais infectados com a cepa mutante *nop16Δ.2* e 4) grupo controle com inoculação apenas de PBS.

A mortalidade das larvas foi observada diariamente, sendo constatada pela falta de movimentos a partir da estimulação com uma pinça. Curvas de morte foram plotadas e análises estatísticas foram aplicadas sobre os dados obtidos (Mantel-Cox). Os resultados obtidos representam a porcentagem média de sobrevivência das larvas de todos os grupos mencionados.

4.11 Sensibilidade a antifúngicos

Para a determinação da concentração inibitória mínima (CIM) para anfotericina B (AmB, Sigma) e fluconazol (FLZ, Sigma) contra cada cepa, foi realizado o teste de sensibilidade antifúngica seguindo o protocolo EUCAST (Método de referência E.Def 7.3.1) (ARENDRUP *et al.*, 2016). De acordo com o protocolo, as placas de sensibilidade antifúngica foram preparadas com uma faixa de concentrações de AmB de 16 a 0,03 µg/ml e de FLZ de 64 a 0,12 µg/ml em RPMI (Gibco) 2x concentrado, suplementado com glicose 4%, tamponado a pH 7,0 com MOPS 165 mM (Sigma).

Para o experimento, os isolados de *C. gattii* R265 e mutantes *nop16Δ.1* e *nop16Δ.2* foram cultivados em placas de ágar Sabouraud por 48 h antes do experimento e então uma suspensão de 5 x 10^5 cels/ml foi preparada em dH_20. 100 µL dos inóculos preparados foram utilizados para inocular as placas de antifúngico, que após a inoculação atingem as concentrações desejadas em RPMI suplementado

com 2% de glicose. Após serem inoculadas, as placas foram incubadas a 35 °C sem agitação por 48 horas. Em seguida, mediu-se a DO a 530 nm e definiu-se a CIM como a concentração antifúngica capaz de inibir 90% (para AmB) e 50% (para FLZ) do crescimento, em comparação com o poço controle sem antifúngico. As cepas *Candida parapsilosis* (ATCC 22019) e *Candida krusei* (ATCC 6258) foram utilizadas como controle de qualidade nos experimentos, conforme preconizado pelo EUCAST.

4.12 Análises estatísticas

As análises estatísticas foram realizadas com a utilização do software GraphPadPrism software 7.0 (GraphPad Software, Inc. La Jolla, USA). A análise empregada nos experimentos foi o *one-way* Anova com pós teste de Tukey, exceto para o ensaio de sobrevivência com *Galleria mellonella,* onde foi utilizada a análise com Mantel-Cox. As diferenças encontradas foram consideradas significativas quando o valor de $p \leq 0,05$.

5. Resultados

5.1 Cinética de Crescimento

Para avaliar o perfil de crescimento das cepas fúngicas, as três cepas em estudo foram inoculadas em meio YPD ou Sabouraud e incubadas em temperatura de 37 ºC durante 48 horas. As análises foram feitas a partir da leitura da absorbância dos poços da placa a 530 nm, com leituras a cada 1 hora. A cinética do crescimento das células em cada um dos meios aqui citados é demonstrada na figura 6.

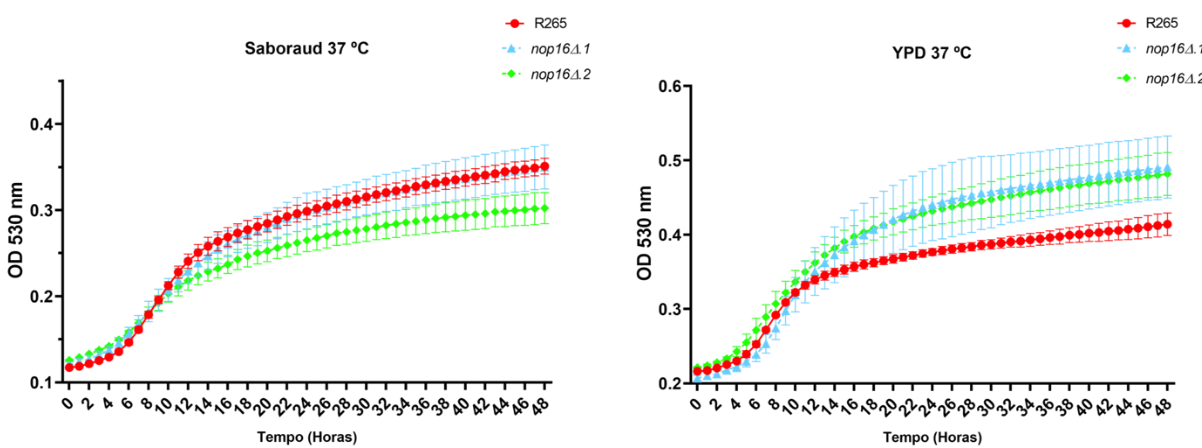

Figura 6: Cinética de crescimento das células fúngicas de *C. gattii* (R265, *nop16Δ.1* e *nop16Δ.2*) em meios de cultivo Sabouraud e YPD a 37 ºC durante 48 horas.

Apesar de tendências de crescimento ligeiramente inferior para a cepa R265 em meio YPD e da cepa *nop16Δ*.2 em meio Sabouraud, o perfil de crescimento das

cepas mutantes em geral se assemelhou a cinética de replicação da cepa parental R265. Em geral, o meio de cultivo YPD favoreceu o crescimento celular de todas as cepas de *C. gattii* que foram analisadas. Esses resultados nos permitiram excluir a hipótese de que outras eventuais alterações fenotípicas se dariam por conta de alterações na capacidade de replicação de cada cepa aqui estudada.

5.2 Perfil de sensibilidade à antifúngicos

Para avaliar se a deleção de *NOP16* modificaria a sensibilidade de *C. gattii* a antifúngicos, determinamos a concentração inibitória mínima (CIM) de células selvagens e mutantes para anfotericina B (AmB) e fluconazol (FLZ), seguindo protocolos preconizados pelo EUCAST. A determinação da CIM para ambos os fármacos é demonstrada nas figuras 7 e 8.

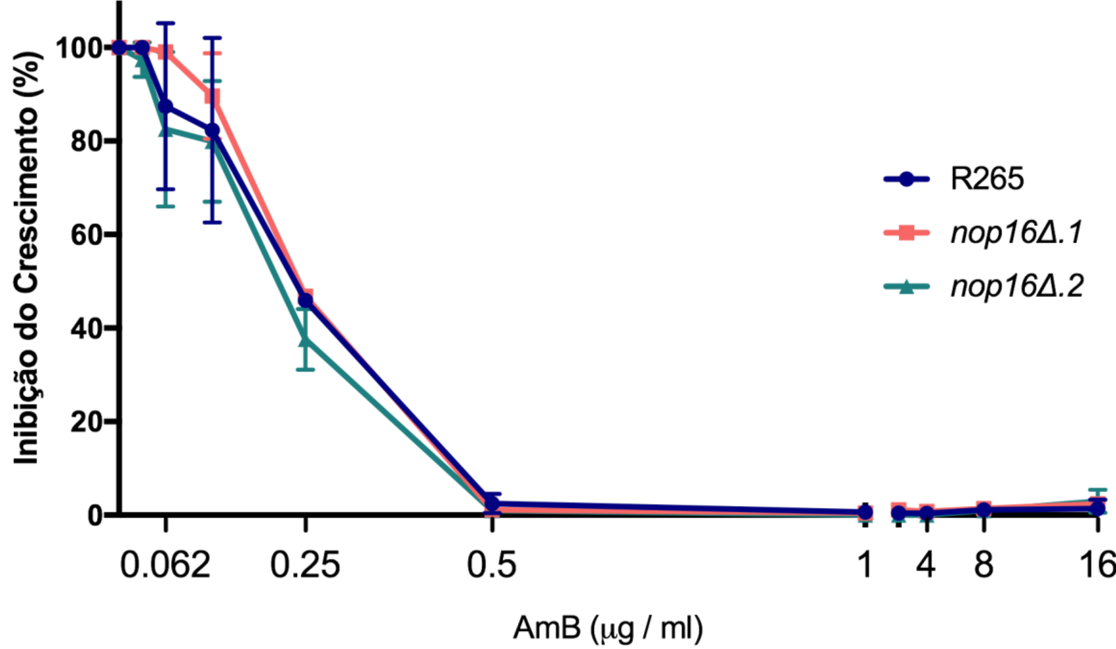

Figura 7: Concentração inibitória mínima do antifúngico anfotericina B para as diferentes cepas de *C. gattii* aqui estudadas. Foram testadas concentrações entre 0,03 e 16 μg/ml.

O perfil de sensibilidade das cepas para AmB foi similar. Considerando que para AmB a CIM é definida como a concentração de droga capaz de inibir 90% ou mais do crescimento fúngico, para todas as cepas o valor obtido correspondeu a 0,5 μg/ml. Para as cepas controle *Candida parapsilosis* e *Candida krusei* a CIM encontrada também foi de 0,5 μg/ml, concentração esperada de acordo com o protocolo preconizado pelo EUCAST.

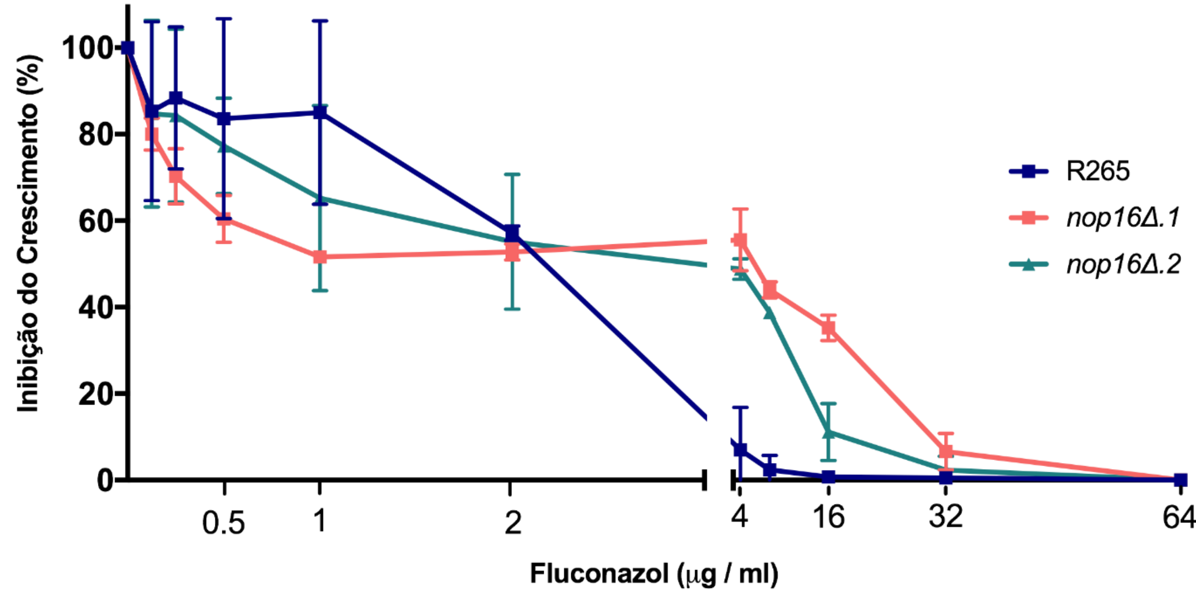

Figura 8: Concentração inibitória mínima do antifúngico fluconazol para as diferentes cepas de *C. gattii* aqui estudadas. Foram testadas concentrações entre 0,125 e 64 μg/ml.

Quando o FLZ foi testado, observamos que os mutantes de *NOP16* apresentaram menor sensibilidade ao antifúngico. A concentração de 2 μg/ml foi suficiente para inibir 50% do crescimento de todas as cepas. Porém, ao analisarmos a capacidade do fármaco de inibir mais de 90% do crescimento, observamos que os mutantes apresentaram CIM90 de 32 μg/ml, enquanto que para a cepa R265 esse valor foi de 4 μg/ml. Na cepa controle *C. parapsilosis* a CIM foi definida em 2 μg/ml, enquanto que para *C. krusei* a CIM encontrada foi de 64 μg/ml, conforme esperado pela preconização do EUCAST.

5.3 Análises da morfologia capsular de *Cryptococcus gattii*

5.3.1 Contra-coloração com Nanquim

Para avaliar se a deleção do gene *NOP16* afetou as dimensões da cápsula de *C. gattii*, avaliamos inicialmente os aspectos morfológicos das três cepas aqui estudadas em preparações com tinta Nanquim (Figura 9).

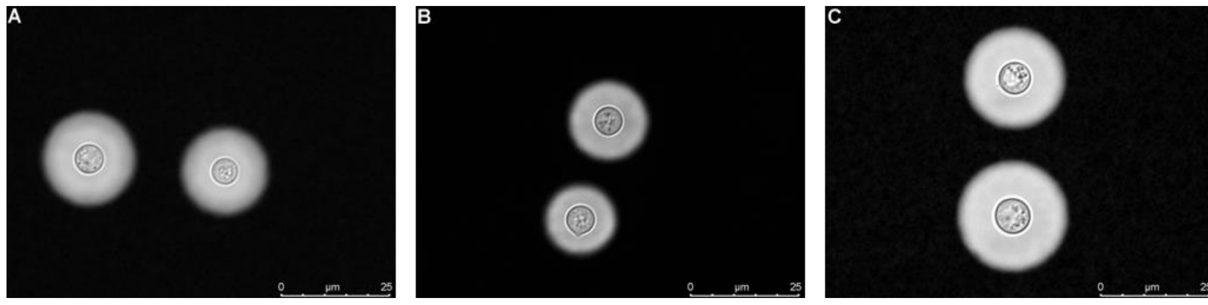

Figura 9: Análises microscópicas da célula fúngica de *C. gattii* evidenciada por contra-coloração com tinta nanquim a visualização do corpo celular e da cápsula polissacarídica. (A) R265, (B) *nop16Δ.1* e (C) *nop16Δ.2*. Barra 25 μm.

Em média, 100 células foram fotografadas e analisadas em relação ao tamanho das células. Tanto as células selvagens quanto as mutantes apresentaram as características típicas da cápsula criptocócica, com dimensões aparentemente similares.

5.3.2 Dimensões da cápsula polissacarídica

O impacto da deleção de *NOP16* nas dimensões capsulares foi medido em sistemas de indução da cápsula *in vitro*. A obtenção das medidas foi tomada através do software ImageJ (NIH). Os valores obtidos foram analisados estatisticamente e os resultados obtidos são apresentados na figura 10.

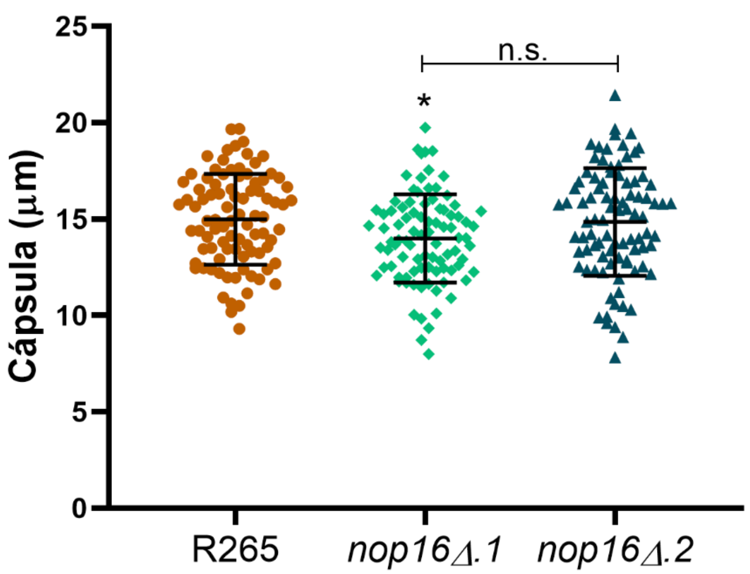

Figura 10: Análise quantitativa do tamanho da cápsula em *C. gattii*. * p < 0,05. n.s.: não significativo.

Em torno de 100 células, em 3 experimentos independentes, tiveram suas medidas tomadas para análise do tamanho capsular e os valores obtidos representam o resultado da subtração do diâmetro do corpo celular da medida total de diâmetro das leveduras, incluindo a cápsula. Nossos resultados demonstraram que as dimensões capsulares nas três cepas foram muito semelhantes, apesar da significância estatística obtida quando o mutante *nop16 Δ.1* foi comparado com a cepa parental R265 (figura 10).

5.3.3 Imunomarcação

Para avaliar se a deleção de *NOP16* resultou em alterações no perfil de reatividade sorológica da cápsula, as três cepas aqui estudadas foram marcadas com

o anticorpo anti-GXM 18B7. Nessa análise, também avaliamos o efeito da deleção de *NOP16* na arquitetura da parede celular, através da marcação das células com calcofluor e WGA. Esses resultados estão apresentados na figura 11.

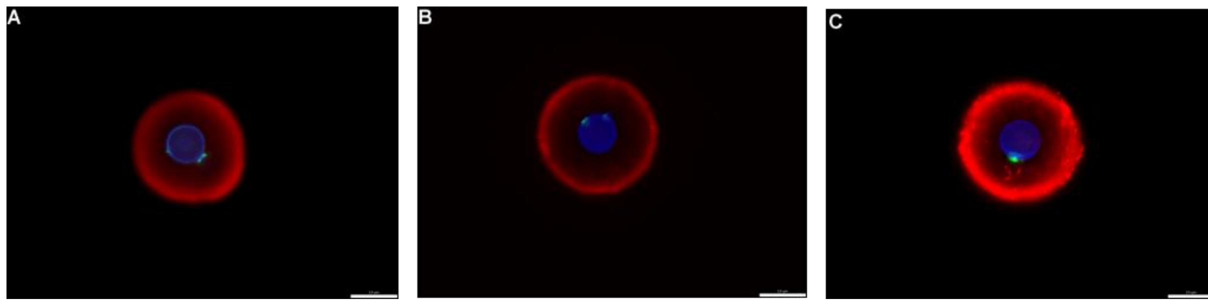

Figura 11: Células de *C. gattii* observadas por microscopia de fluorescência. Em vermelho a cápsula polissacarídica marcada com o mAb 18B7, em azul o corpo celular evidenciado pela ligação de calcofluor a quitina da parece celular. Os pontos em verde representam a marcação de quitooligômeros pela lectina WGA. (A) R265, (B) *nop16Δ.1* e (C) *nop16Δ.2*. Barra 10µm.

A visualização das estruturas celulares revelou perfis similares de reatividade sorológica com o mAb 18B7 e aspectos morfológicos normais da parede celular em todas as cepas. Dessa forma, a deleção de *NOP16* não pareceu acarretar em alterações na arquitetura da superfície celular em *C. gattii*.

5.3.4 MEV

Apesar das análises microscópicas em preparações contra-coradas ou preparadas para fluorescência não terem apontado alterações expressivas em células mutantes, aprofundamos a análise da arquitetura da superfície celular em *C. gattii* por MEV, uma vez que há precedentes na literatura demonstrando que certas alterações da cápsula são imperceptíveis por microscopia óptica (SILVA *et al.*, 2020). A observação das células, ilustradas na figura 12, entretanto, contradisse essa hipótese.

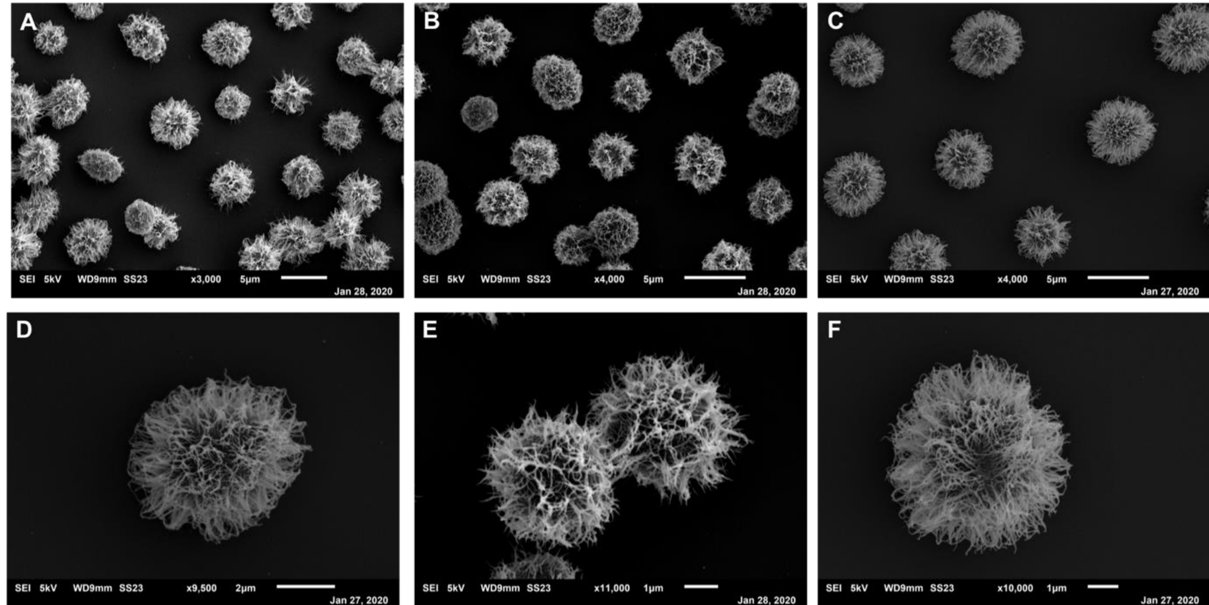

Figura 12: Microscopia eletrônica de varredura das células crescidas em meio YPD, sem indução de cápsula. (A, D) R265, (B, E) *nop16Δ.1* e (C, F) *nop16Δ.2*.

A morfologia geral das três cepas de *C. gattii* aqui avaliadas foi muito semelhante em todas as imagens obtidas para MEV. Para melhor visualização do padrão de distribuição morfológico, foram selecionadas imagens que mostram um conjunto de células (A-C) e também imagens em maior aumento, para uma visualização mais detalhada das células de *C. gattii* e dos mutantes aqui estudados (D-F). Tanto a distribuição das fibras polissacarídicas e do formato do corpo das células se mantiveram similares em todas as cepas. Esses resultados, associados às análises por microscopia óptica, nos levaram a concluir que a deleção do gene *NOP16* não acarretou em deformações de estruturas como a cápsula fúngica e a parede celular.

5.3.5 Secreção de GXM

A determinação da secreção de GXM em cada cepa fúngica foi realizada através do ensaio de ELISA com a utilização do anticorpo monoclonal anti-GXM 18B7. A quantificação da GXM é apresentada na figura 13.

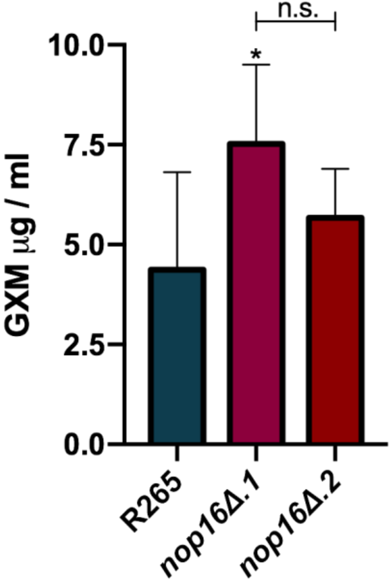

Figura 13: Análise da secreção de glucuronoxilomanana em *C. gattii*. *p < 0,05. n.s. não significativo.

Os resultados apresentados foram obtidos de três experimentos independentes, com valores analisados individualmente e posteriormente plotados no mesmo gráfico. Para as cepas mutantes, foi possível observar uma tendência no aumento da secreção de GXM, quando comparadas a cepa R265. Apesar dessa tendência, só foram observadas diferenças estatísticas quando a cepa parental R265 foi comparada com o mutante *nop16Δ.1.* Dessa forma, apesar da tendência de maior produção do polissacarídeo nas cepas mutantes, não podemos afirmar categoricamente que a deleção de *NOP16* resulta em produção aumentada de GXM em *C. gattii*.

5.4 Análise ultraestrutural de *C. gattii*

O efeito da deleção de *NOP16* sobre os aspectos ultraestruturais + intracelulares de *C. gattii* foi avaliado por microscopia eletrônica de transmissão de células fúngicas selvagens e mutantes. As imagens obtidas por essa técnica de microscopia encontram-se elencadas pela figura 14.

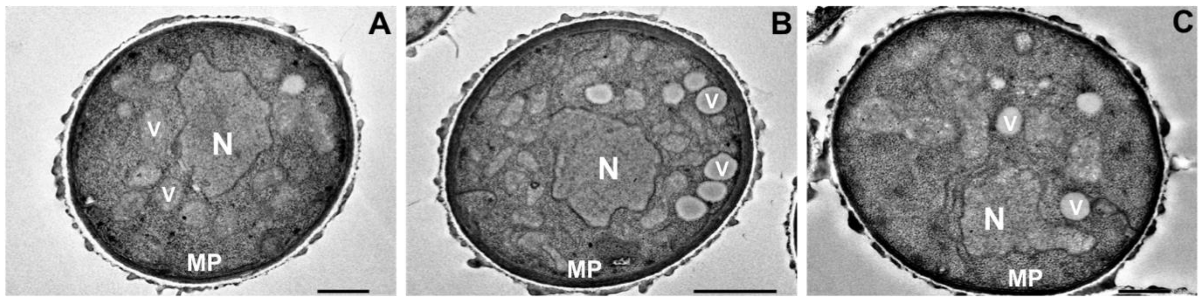

Figura 14: Microscopia eletrônica de transmissão das células de *C. gattii*. (A) R265, (B) *nop16Δ.1* e (C) *nop16Δ.2*. N: núcleo; MP: membrana plasmática; V: vacúolos. Barra 500 nm.

Nas imagens obtidas para as células selvagens de *C. gattii* e para ambos os mutantes *nop16Δ.1* e *nop16Δ.2,* foram observadas as estruturas celulares típicas de eucariotos, como núcleo, estruturas vacuolares e distribuição complexa de membranas intracelulares. Não houve evidência de alterações expressivas nos mutantes, em comparação com a cepa parental R265. Dessa forma, até esse ponto de nosso estudo, concluímos que a deleção de *NOP16* não acarretou em nenhum fenótipo evidente que caracterize alterações celulares expressivas.

5.5 Análise da interação de *C. gattii* com macrófagos RAW 264.7 *in vitro*

O potencial patogênico em *Cryptococcus* está diretamente ligado à capacidade de sobrevivência do fungo durante a interação com fagócitos. Dessa forma, avaliamos se a deleção de *NOP16* afetou o perfil de interação de *C. gattii* com macrófagos, como ilustrado na Figura 15.

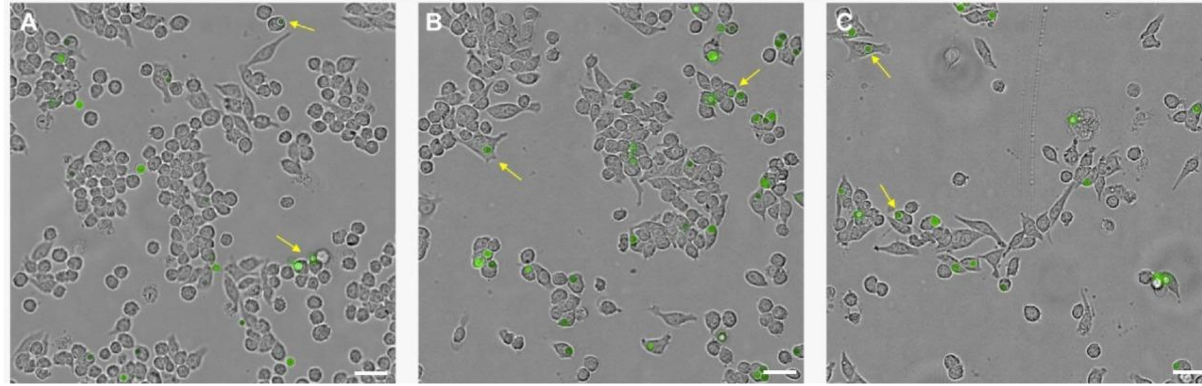

Figura 15: Imagem representativa do ensaio de fagocitose para as cepas de *C. gattii* (A) R265, (B) *nop16Δ.1* e (C) *nop16Δ.2* com macrófagos murinos RAW 264.7. Setas amarelas: eventos de fagocitose. Barra: 20 μm.

Observamos uma tendência de aumento na taxa de fagocitose para as cepas *nop16Δ.1* e *nop16Δ.2* com valores médios de 19,77% e 22,09%, A cepa parental R265 apresentou taxa média de fagocitose de 15,20% (figura 16).

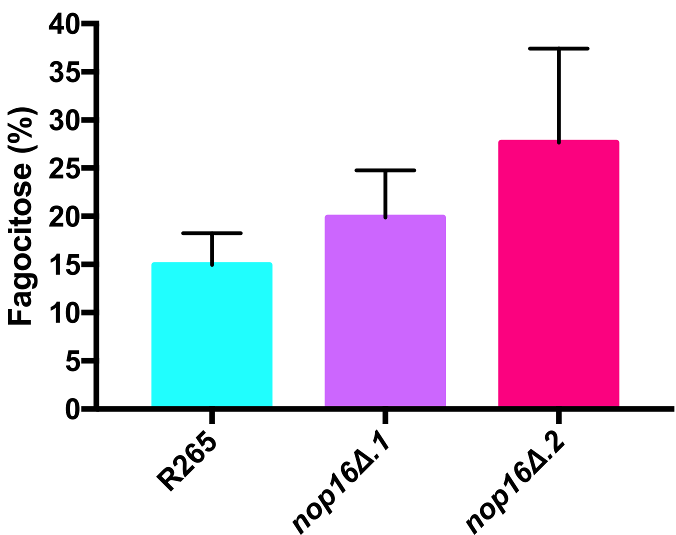

Figura 16: Taxa de fagocitose das cepas de *C. gattii* por macrófagos murinos RAW 264.7.

Apesar da tendência de aumento na taxa de fagocitose para as cepas mutantes, não obtivemos significância entre os sistemas comparados. Dessa forma, não foi possível determinar de forma acurada se a deleção de *NOP16* predispõe *C. gattii* a índices de fagocitose, de fato, aumentados.

5.6 Caracterização das EVs

A literatura recente demonstra que componentes celulares muito distintos podem afetar a liberação de EVs por fungos (SILVA *et al.*, 2019). Dessa forma, para avaliar se a deleção de *NOP16* afetou a população de EVs produzida por cada cepa, as amostras foram analisadas por duas técnicas independentes. Inicialmente, as EVs produzidas por cada cepa tiveram seus aspectos morfológicos analisados pela técnica de contrastação negativa, seguida de MET (figura 17).

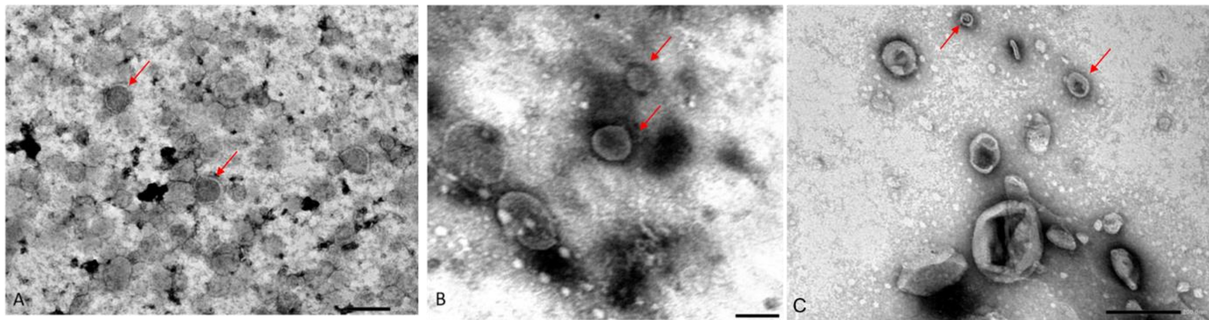

Figura 17: Microscopia eletrônica de transmissão das EVs (apontadas pelas setas vermelhas) produzidas pelas cepas (A) R265, (B) *nop16Δ.1* e (C) *nop16Δ.2.* As EVs foram preparadas para contrastação negativa com acetado de uranila. Barra 200 nm.

A presença de EVs foi confirmada em todas as cepas, sendo possível a visualização de estruturas esféricas com bicamada lipídica e tamanhos similares e em conformidade com as descrições de estruturas vesiculares.

A análise de nanopartículas (NTA) também foi realizada em amostras de EVs obtidas de meio sólido. O perfil de distribuição das EVs obtido na análise de NTA pode ser observado através da figura 18.

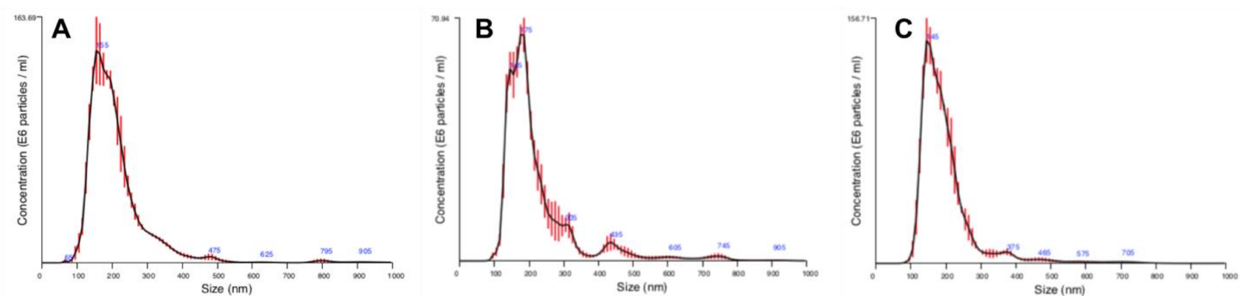

Figura 18: Análise de rastreamento de nanopartículas (NTA) de *C. gattii* recuperadas a partir do isolamento de EVs. (A) R265, (B) *nop16Δ.1* e (C) *nop16Δ.2.*

As análises de nanopartículas foram realizadas em três experimentos independentes. Em todas as cepas analisadas o perfil de distribuição das EVs foi semelhante, consistindo de uma população de vesículas concentrada na faixa de diâmetro correspondente a 200 nm. Em todos os sistemas, populações minoritárias com diâmetros entre 300 e 500 nm foram observadas.

A técnica de análise de nanopartículas também nos informa a concentração de partículas em cada amostra. Essa análise revelou diferenças importantes entre as cepas aqui estudadas, depois da normalização entre o número de EVs detectadas pelo número de células responsável pela produção de vesículas. Conforme demonstrado na Figura 19, a deleção de *NOP16* resultou em redução na produção de EVs por *C. gattii*.

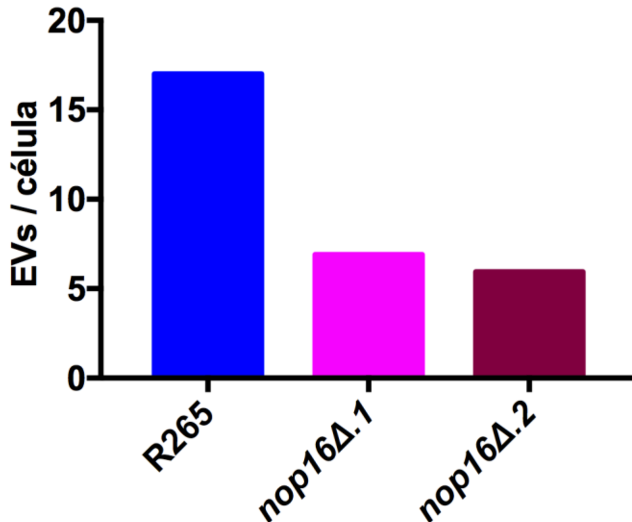

Figura 19: Quantificação de EVs produzidas em *C. gattii*.

5.7 Potencial patogênico das cepas fúngicas

A exportação de EVs vem sendo crescentemente relacionada com a virulência no gênero *Cryptococcus* (RODRIGUES e CASADEVALL, 2018; RODRIGUES *et al.*, 2008). Dada a redução no número de EVs produzidos pelos mutantes *nop16Δ.1* e *nop16Δ.2*, testamos se a produção reduzida de EVs poderia afetar o potencial patogênico de *C. gattii*. Essa análise foi feita através da utilização do modelo invertebrado com *G. mellonella* em colaboração com o grupo do Prof. Leonardo Nimrichter na UFRJ. As cepas fúngicas foram inoculadas no hospedeiro invertebrado e as larvas acompanhadas diariamente, conforme apresentado na figura 20.

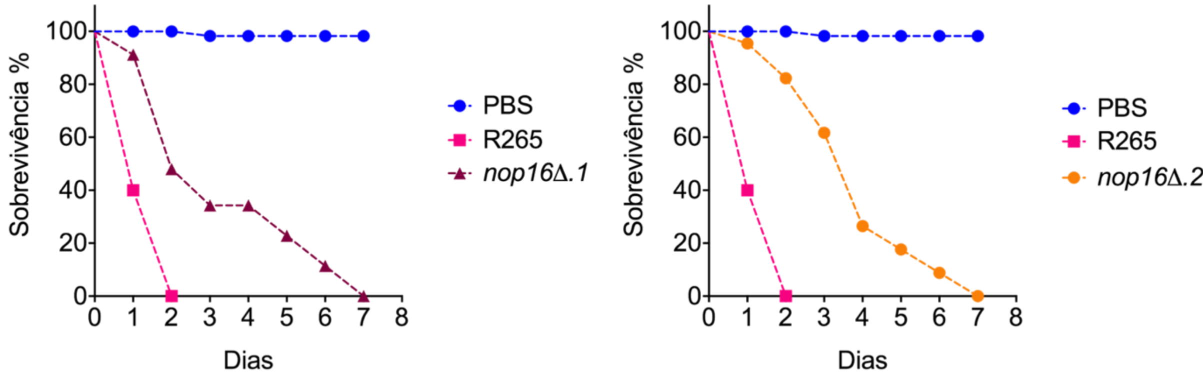

Figura 20: Análise de virulência de *C. gattii* (R265, *nop16Δ.1* e *nop16Δ.2*) em modelo invertebrado *Galleria mellonella*. Resultado representativo de dois experimentos independentes com resultados similares.

O perfil de sobrevivência das larvas, apresentado na figura 20, demonstra que nas cepas fúngicas com deleção do gene *NOP16* o perfil de virulência foi atenuado, em comparação à cepa selvagem R265. O grupo infectado com a cepa parental R265 teve 100% de morte em 48 horas após a infecção, enquanto as larvas que foram infectadas com os mutantes atingiram a mortalidade de 100% 7 dias após infecção. A análise estatística Mantel-Cox foi realizada para avaliar diferenças entre todos os grupos, gerando valor de $p < 0,0001$ em comparações entre sistemas infectados com células selvagens ou mutantes. Sendo assim, concluímos que a deleção de *NOP16* acarreta em um perfil hipovirulento na infecção causada pelas cepas *nop16Δ.1* e *nop16Δ.2,* quando comparadas a cepa selvagem de *C. gattii*.

6. Discussão

As funções da proteína nucleolar 16 (Nop16), alvo deste estudo, são pouquíssimo conhecidas em *Cryptococcus* spp. e em qualquer outro modelo biológico. Os dados disponíveis se resumem a cinco artigos científicos disponíveis na plataforma “PubMed” e a informações disponibilizadas no *Saccharomyces Genome*

Database (SGD). Nessa base, a proteína é descrita como um constituinte da unidade pré-ribossomal 66S com possível envolvimento com a biogênese da subunidade ribossomal 60S (HARNPICHARNCHAI *et al.*, 2001; HORSEY *et al.*, 2004). Um desses estudos, realizados por Horsey e colaboradores (2004) aponta que a proteína Nop16 interage com a proteína Rrp1, envolvida na biogênese de pré-rRnas em *S. cerevisiae* (HORSEY *et al.*, 2004). A proteína também estaria ligada, em mamíferos, ao crescimento de tumores mamários através do controle da biogênese ribossomal, sendo também responsável pela regulação de estrogênio (KUNDEL *et al.*, 2012; ZHANG *et al.*, 2014). Em ciliados, a Nop16 pode estar envolvida na coordenação de respostas celulares a fatores estressantes, além da expressão de proteínas ligadas ao encistamento (CHEN *et al.*, 2014). Em *Arabidopsis thaliana,* a Nop16 é capaz de interagir com a proteína GTS1, envolvida com o desenvolvimento e resposta a estressores (GACHOMO *et al.*, 2014). Este estudo também aponta o envolvimento de Nop16 na biogênese da subunidade ribossomal 60S (GACHOMO *et al.*, 2014). Ainda, Pratte e colaboradores (2013) sugeriram que a proteína Nop16 é integrante de um *cluster* de proteínas envolvidas no arranjo estrutural da subunidade 60S em eucariotos (PRATTE *et al.*, 2013).

Em *Cryptococcus,* nosso grupo sugeriu que a Nop16 poderia ser um alvo para ação de fármacos (JOFFE *et al.*, 2017). Neste estudo, buscou-se dentro de uma coleção de 7.569 mutantes de *C. gattii* geradas aleatoriamente cepas que apresentassem perfil de resistência ao mebendazol. Além da Nop16, a proteína Aim25, uma escramblase translocadora de lipídeos, se mostraram necessárias para a ação do mebendazol (JOFFE *et al.*, 2017). Os efeitos da deleção de *AIM25* em *C. gattii* foram recentemente caracterizados por nosso grupo (REIS *et al.*, 2019), mas o papel de Nop16 permaneceu desconhecido até o início do presente trabalho. Dessa forma, avaliamos em dois mutantes *nop16Δ* independentes parâmetros como arquitetura da superfície celular, sensibilidade a antifúngicos, ultraestrutura, produção de EVs, interação com macrófagos e virulência em modelo invertebrado *G. mellonella.*

Na grande maioria dos testes que realizamos, as cepas nas quais o gene *NOP16* foi deletado apresentaram fenótipos muito similares ao observado em células parentais. Por exemplo, o perfil de crescimento das células de *Cryptococcus* a 37 ºC não foi afetado pela ausência da proteína. Os mutantes também foram estudados através de técnicas microscópicas como MEV e MET. Mais uma vez, não foram observadas alterações no padrão morfológico de *C. gattii*.

A produção do polissacarídeo GXM e a montagem da cápsula em *Cryptococcus* spp. são tidos como importantes fatores de virulência, visto que a cápsula, formada majoritariamente por GXM, é considerada como o principal fator regulando a patogenicidade no gênero (CASADEVALL *et al.*, 2009; OLIVEIRA *et al.*, 2010; PIERINI e DOERING, 2001). As estruturas capsulares não apresentaram alterações morfológicas evidentes na ausência de *NOP16.* O perfil de reatividade sorológica com o anticorpo anti-GXM 18B7 também permaneceu inalterada, bem como a estrutura geral da parede celular. Entretanto, não podemos descartar alterações capsulares menos evidentes em nosso modelo. Por exemplo, nas cepas nas quais houve deleção do gene *NOP16,* houve tendência a uma ligeira redução nas dimensões capsulares, acompanhada de uma tendência a produção aumentada de GXM solúvel no sobrenadante de cultura. Ainda não podemos estimar o impacto biológico desses achados, mas nas cepas mutantes o índice de fagocitose também demonstrou uma sutil tendência ao aumento. *Cryptococcus* spp. tem capacidade de sobreviver e proliferar durante a interação com fagócitos e acredita-se que essa característica esteja ligada à exportação de diversos fatores de virulência para o meio extracelular (CASADEVALL *et al.*, 2009; RODRIGUES *et al.*, 2008). Possivelmente, estudos futuros de cinéticas de construção capsular, secreção de GXM e fagocitose em *C. gattii* revelarão a relação entre Nop16, formação da cápsula e susceptibilidade à ingestão por fagócitos hospedeiros. Nesse momento, ainda não podemos afirmar que essas são conexões com relevância biológica.

Apesar do potencial envolvimento em mecanismos de virulência, nossos resultados desencorajam o uso de Nop16 como um alvo para a ação de antifúngicos. Essa suposição se baseia na observação de que os mutantes sem a expressão de *NOP16* apresentaram tendência a serem mais resistentes ao fluconazol, fármaco de amplo uso terapêutico na criptococose. Esses dados podem sugerir que a eventual neutralização da Nop16 poderia prejudicar a eficiência das ferramentas terapêuticas atualmente disponíveis para o tratamento da doença. De forma similar, a deleção de *AIM25* resultou em cepas com cápsulas maiores e altos níveis de GXM (JOFFE *et al.*, 2017; REIS *et al.*, 2019), o que promoveria aumento de virulência. Esses resultados ilustram a complexidade do desenvolvimento de fármacos antifúngicos e apontam para a necessidade de abordagens cuidadosas e multidisciplinares para a caracterização de alvos celulares.

Vários fatores de virulência em *Cryptococcus* são exportados através de EVs, incluindo a GXM, urease, e lacase (RODRIGUES *et al.*, 2008). Diferentes cepas

apresentam diferenças na composição do conteúdo vesicular e, essa diferença é traduzida em diferenças funcionais na modulação da resposta imune do hospedeiro (OLIVEIRA *et al.*, 2010). As EVs coordenam ainda mecanismos de comunicação intercelular, aumentando a capacidade de proliferação de *C. gattii* em macrófagos (BIELSKA *et al.*, 2018). Esse padrão de proliferação é ativado através da liberação de EVs por células de alta virulência. Essas EVs atingem o fagolisossomo, onde induzem a proliferação celular das células de *C. gattii* através de mecanismo de comunicação de longa distância (BIELSKA *et al.*, 2018; COELHO e CASADEVALL, 2019; OLIVEIRA *et al.*, 2010; RODRIGUES e CASADEVALL, 2018). A transferência de EVs pode também conferir resistência a fármacos em modelos de *C. albicans* (ZARNOWSKI *et al.*, 2018).

As EVs fúngicas podem modular a resposta imune inata, resultando tanto no controle da doença quanto no progresso da infecção fúngica (HUANG *et al.*, 2012; VARGAS *et al.*, 2015). Macrófagos expostos a EVs de *Cryptococcus* mostraram aumento na produção de citocinas antinflamatórias, como IL-10 e TGF-β (CHIAPELLO *et al.*, 2004; MARIANO ANDRADE *et al.*, 2003; OLIVEIRA *et al.*, 2010).

As EVs foram indicadas, recentemente, como potenciais alternativas para o desenvolvimento de vacinas (AMBER *et al.*, 2016; COLOMBO *et al.*, 2019; NIMRICHTER *et al.*, 2016; RIZZO *et al.*, 2017). Considerando a grande diversidade de moléculas encontradas dentro das EVs, como reguladores, fatores de virulência e componentes imunogênicos, Vargas e colaboradores (2020) propuseram a utilização das EVs de *Candida albicans* como agente imunizador contra candidíase em modelo murino. Os resultados encontrados pelo grupo demonstram que a inoculação de EVs em camundongos é capaz de ativar a resposta imune dos animais induzindo a ativação de diferentes perfis de citocinas, além de diminuir a carga fúngica nos camundongos e garantir proteção aos animais imunizados contra uma infecção letal por *C. albicans*. As EVs de *C. albicans* também foram capazes de diminuir a mortalidade em modelo de *G. mellonella* (VARGAS *et al.*, 2020).

Ao contrário da maior parte dos ensaios fenotípicos que realizamos, nossos resultados revelaram que a deleção de *NOP16* teve um efeito pronunciado sobre a produção de EVs em *C. gattii*. Apesar dessas estruturas apresentarem o mesmo perfil morfológico em todas as cepas, os mutantes nos quais o gene *NOP16* foi deletado apresentaram diminuição na produção de EVs, em comparação com a cepa R265. Esse dado é aparentemente contrastante com uma produção aumentada de GXM, considerando que o polissacarídeo é exportado em EVs. Não podemos, entretanto,

descartar a possibilidade de que a relação entre GXM aumentada e EVs diminuídas reflita uma maior eficácia dos mutantes em sua capacidade de lisar vesículas para extrair o polissacarídeo, que assim ficaria disponível nos sobrenadantes em concentrações aumentadas. Todavia, a diminuição na produção das EVs poderia indicar que a deleção de *NOP16* poderia influenciar o perfil patogênico das cepas mutantes. Sendo assim, levantamos a hipótese de que a deleção de *NOP16* levaria a um fenótipo de hipovirulência. Essa hipótese também estaria de acordo com as tendências aqui observadas de maior taxa de fagocitose e ligeira redução do tamanho capsular. De fato, as cepas mutantes apresentaram virulência claramente atenuada quando comparadas a cepa parental R265. Esses resultados apontam para um papel na proteína Nop16 na virulência de *C. gattii*. Ainda que não possamos, nesse momento, definir os mecanismos que correlacionam Nop16 e a virulência desse fungo, especulamos que a falta dessa proteína afetaria a formação e/ou liberação de EVs, o que resultaria num fenótipo de virulência atenuada.

Em função dos pontos acima discutidos, é preciso esclarecer que nossos resultados ainda não nos permitem apontar o papel da proteína nucleolar Nop16 na fisiologia de *C. gattii*. Entretanto, nossos resultados nos dão fortes indícios de que a Nop16 é uma proteína importante em mecanismos relacionados tanto com a virulência quanto ao perfil de resistência da espécie a fármacos. Neste sentido, futuros estudos focados na relação entre Nop16, produção de EVs e virulência de *C. gattii* poderão trazer novos aspectos sobre o papel dessa proteína no modelo da criptococose.

7. Conclusões

1. A deleção do gene *NOP16* produziu efeitos sutis ou nulos sobre vários elementos importantes para a fisiologia de *C. gattii*, incluindo crescimento a 37 ^{o}C, produção de cápsula, arquitetura da superfície celular, ultraestrutura, e secreção de GXM.
2. A deleção do gene *NOP16* produziu efeitos importantes em elementos ligados a evolução ou controle da doença, como perfis de fagocitose, produção de EVs e sensibilidade a antifúngicos.
3. Embora os mecanismos conectando Nop16 com os elementos acima descritos ainda não sejam claros, nossos dados apontam para um papel importante dessa proteína no curso patogênico da infecção causada por *C. gattii*.

8. Referências Bibliográficas

ALBUQUERQUE, P.; NICOLA, A. M.; MAGNABOSCO, D. A. G.; DERENGOWSKI, L. D. S. *et al.* A hidden battle in the dirt: Soil amoebae interactions with *Paracoccidioides* spp. **PLoS Negl Trop Dis**, 13, n. 10, p. e0007742, Oct 2019.

AMBER, K. I.; HADI, N. R.; MUHAMMAD-BAQIR, B. M.; JAMIL, D. A. *et al.* Trimetazidine attenuates the acute inflammatory response induced by Novolimus eluting bioresorbable coronary scaffold implantation. **Int J Cardiol**, 220, p. 514-519, Oct 1 2016.

ARENDRUP, M. C.; MELETIADIS, J.; MOUTON, J. W.; GUINEA, J. *et al.* EUCAST technical note on isavuconazole breakpoints for *Aspergillus*, itraconazole breakpoints for *Candida* and updates for the antifungal susceptibility testing method documents. **Clin Microbiol Infect**, 22, n. 6, p. 571 e571-574, Jun 2016.

BIELSKA, E.; MAY, R. C. What makes *Cryptococcus gattii* a pathogen? **FEMS Yeast Res**, 16, n. 1, p. fov106, Feb 2016.

BIELSKA, E.; SISQUELLA, M. A.; ALDEIEG, M.; BIRCH, C. *et al.* Pathogen-derived extracellular vesicles mediate virulence in the fatal human pathogen *Cryptococcus* gattii. **Nat Commun**, 9, n. 1, p. 1556, Apr 19 2018.

BONVICINI, F.; GALLINELLA, G.; CRICCA, M.; VENTUROLI, S. *et al.* A new primer set improves the efficiency of competitive PCR-ELISA for the detection of B19 DNA. **J Clin Virol**, 30, n. 2, p. 134-136, Jun 2004.

BORBA, H. H. L.; STEIMBACH, L. M.; RIVEROS, B. S.; TONIN, F. S. *et al.* Cost-effectiveness of amphotericin B formulations in the treatment of systemic fungal infections. **Mycoses**, 61, n. 10, p. 754-763, Oct 2018.

BROUWER, A. E.; SIDDIQUI, A. A.; KESTER, M. I.; SIGALOFF, K. C. *et al.* Immune dysfunction in HIV-seronegative, *Cryptococcus gattii* meningitis. **J Infect**, 54, n. 3, p. e165-168, Mar 2007.

BULMER, G. S.; SANS, M. D. *Cryptococcus neoformans*. 3. Inhibition of phagocytosis. **J Bacteriol**, 95, n. 1, p. 5-8, Jan 1968.

BYRNES, E. J., 3rd; MARR, K. A. The Outbreak of *Cryptococcus gattii* in Western North America: Epidemiology and Clinical Issues. **Curr Infect Dis Rep**, 13, n. 3, p. 256-261, Jun 2011.

CAMACHO, E.; VIJ, R.; CHRISSIAN, C.; PRADOS-ROSALES, R. *et al.* The structural unit of melanin in the cell wall of the fungal pathogen *Cryptococcus neoformans*. **J Biol Chem**, 294, n. 27, p. 10471-10489, Jul 5 2019.

CAMPBELL, L. T.; FRASER, J. A.; NICHOLS, C. B.; DIETRICH, F. S. *et al.* Clinical and environmental isolates of *Cryptococcus gattii* from Australia that retain sexual fecundity. **Eukaryot Cell**, 4, n. 8, p. 1410-1419, Aug 2005.

CASADEVALL, A.; FU, M. S.; GUIMARAES, A. J.; ALBUQUERQUE, P. The 'Amoeboid Predator-Fungal Animal Virulence' Hypothesis. **J Fungi (Basel)**, 5, n. 1, Jan 21 2019.

CASADEVALL, A.; NOSANCHUK, J. D.; WILLIAMSON, P.; RODRIGUES, M. L. Vesicular transport across the fungal cell wall. **Trends Microbiol**, 17, n. 4, p. 158-162, Apr 2009.

CHATURVEDI, S.; DYAVAIAH, M.; LARSEN, R. A.; CHATURVEDI, V. *Cryptococcus gattii* in AIDS patients, southern California. **Emerg Infect Dis**, 11, n. 11, p. 1686-1692, Nov 2005.

CHAYAKULKEEREE, M.; JOHNSTON, S. A.; OEI, J. B.; LEV, S. *et al.* SEC14 is a specific requirement for secretion of phospholipase B1 and pathogenicity of *Cryptococcus neoformans*. **Mol Microbiol**, 80, n. 4, p. 1088-1101, May 2011.

CHEN, J.; GAO, X.; WANG, B.; CHEN, F. *et al.* Proteomic approach to reveal the proteins associated with encystment of the ciliate *Euplotes encysticus*. **PLoS One**, 9, n. 5, p. e97362, 2014.

CHIAPELLO, L. S.; BARONETTI, J. L.; AOKI, M. P.; GEA, S. *et al.* Immunosuppression, interleukin-10 synthesis and apoptosis are induced in rats inoculated with *Cryptococcus neoformans* glucuronoxylomannan. **Immunology**, 113, n. 3, p. 392-400, Nov 2004.

COELHO, C.; BOCCA, A. L.; CASADEVALL, A. The tools for virulence of *Cryptococcus neoformans*. **Adv Appl Microbiol**, 87, p. 1-41, 2014.

COELHO, C.; CASADEVALL, A. Cryptococcal therapies and drug targets: the old, the new and the promising. **Cell Microbiol**, 18, n. 6, p. 792-799, Jun 2016.

COELHO, C.; CASADEVALL, A. Answers to naysayers regarding microbial extracellular vesicles. **Biochem Soc Trans**, 47, n. 4, p. 1005-1012, Aug 30 2019.

COLOMBO, A. C.; RELLA, A.; NORMILE, T.; JOFFE, L. S. *et al.* *Cryptococcus neoformans* Glucuronoxylomannan and Sterylglucoside Are Required for Host Protection in an Animal Vaccination Model. **mBio**, 10, n. 2, Apr 2 2019.

COX, G. M.; MCDADE, H. C.; CHEN, S. C.; TUCKER, S. C. *et al.* Extracellular phospholipase activity is a virulence factor for *Cryptococcus neoformans*. **Mol Microbiol**, 39, n. 1, p. 166-175, Jan 2001.

DE AZAMBUJA, A. Z.; WISSMANN NETO, G.; WATTE, G.; ANTONIOLLI, L. *et al.* Cryptococcal Meningitis: A Retrospective Cohort of a Brazilian Reference Hospital in the Post-HAART Era of Universal Access. **Can J Infect Dis Med Microbiol**, 2018, p. 6512468, 2018.

DE OLIVEIRA, H. C.; JOFFE, L. S.; SIMON, K. S.; CASTELLI, R. F. *et al.* Fenbendazole Controls In Vitro Growth, Virulence Potential, and Animal Infection in the *Cryptococcus* Model. **Antimicrob Agents Chemother**, 64, n. 6, May 21 2020.

DENNING, D. W.; BROMLEY, M. J. Infectious Disease. How to bolster the antifungal pipeline. **Science**, 347, n. 6229, p. 1414-1416, Mar 27 2015.

DROMER, F.; BERNEDE-BAUDUIN, C.; GUILLEMOT, D.; LORTHOLARY, O. *et al.* Major role for amphotericin B-flucytosine combination in severe cryptococcosis. **PLoS One**, 3, n. 8, p. e2870, Aug 6 2008.

EVANS, R. J.; LI, Z.; HUGHES, W. S.; DJORDJEVIC, J. T. *et al.* Cryptococcal phospholipase B1 is required for intracellular proliferation and control of titan cell morphology during macrophage infection. **Infect Immun**, 83, n. 4, p. 1296-1304, Apr 2015.

FANG, W.; FA, Z.; LIAO, W. Epidemiology of *Cryptococcus* and cryptococcosis in China. **Fungal Genet Biol**, 78, p. 7-15, May 2015.

FARRER, R. A.; CHANG, M.; DAVIS, M. J.; VAN DORP, L. *et al.* A New Lineage of *Cryptococcus gattii* (VGV) Discovered in the Central Zambezian Miombo Woodlands. **mBio**, 10, n. 6, Nov 12 2019.

FEDER, V.; KMETZSCH, L.; STAATS, C. C.; VIDAL-FIGUEIREDO, N. *et al.* *Cryptococcus gattii* urease as a virulence factor and the relevance of enzymatic activity in cryptococcosis pathogenesis. **FEBS J**, 282, n. 8, p. 1406-1418, Apr 2015.

FELDMESSER, M.; CASADEVALL, A. Mechanism of action of antibody to capsular polysaccharide in *Cryptococcus neoformans* infection. **Front Biosci**, 3, p. d136-151, Feb 1 1998.

FELDMESSER, M.; KRESS, Y.; CASADEVALL, A. Dynamic changes in the morphology of *Cryptococcus neoformans* during murine pulmonary infection. **Microbiology**, 147, n. Pt 8, p. 2355-2365, Aug 2001.

FIRACATIVE, C.; LIZARAZO, J.; ILLNAIT-ZARAGOZI, M. T.; CASTANEDA, E. *et al.* The status of cryptococcosis in Latin America. **Mem Inst Oswaldo Cruz**, 113, n. 7, p. e170554, 2018.

FONSECA, F. L.; NIMRICHTER, L.; CORDERO, R. J.; FRASES, S. *et al.* Role for chitin and chitooligomers in the capsular architecture of *Cryptococcus neoformans.* **Eukaryot Cell**, 8, n. 10, p. 1543-1553, Oct 2009.

FU, M. S.; COELHO, C.; DE LEON-RODRIGUEZ, C. M.; ROSSI, D. C. P. *et al. Cryptococcus neoformans* urease affects the outcome of intracellular pathogenesis by modulating phagolysosomal pH. **PLoS Pathog**, 14, n. 6, p. e1007144, Jun 2018.

GACHOMO, E. W.; JIMENEZ-LOPEZ, J. C.; BAPTISTE, L. J.; KOTCHONI, S. O. GIGANTUS1 (GTS1), a member of Transducin/WD40 protein superfamily, controls seed germination, growth and biomass accumulation through ribosome-biogenesis protein interactions in *Arabidopsis thaliana*. **BMC Plant Biol**, 14, p. 37, Jan 27 2014.

GALANIS, E.; MACDOUGALL, L.; KIDD, S.; MORSHED, M. *et al.* Epidemiology of *Cryptococcus gattii*, British Columbia, Canada, 1999-2007. **Emerg Infect Dis**, 16, n. 2, p. 251-257, Feb 2010.

GARCIA-RIVERA, J.; CHANG, Y. C.; KWON-CHUNG, K. J.; CASADEVALL, A. *Cryptococcus neoformans* CAP59 (or Cap59p) is involved in the extracellular trafficking of capsular glucuronoxylomannan. **Eukaryot Cell**, 3, n. 2, p. 385-392, Apr 2004.

GONCALVES, D. S.; FERREIRA, M. D. S.; GOMES, K. X.; RODRIGUEZ-DE LA NOVAL, C. *et al.* Unravelling the interactions of the environmental host *Acanthamoeba castellanii* with fungi through the recognition by mannose-binding proteins. **Cell Microbiol**, 21, n. 10, p. e13066, Oct 2019.

HAGEN, F.; ILLNAIT-ZARAGOZI, M. T.; BARTLETT, K. H.; SWINNE, D. *et al.* In vitro antifungal susceptibilities and amplified fragment length polymorphism genotyping of a worldwide collection of 350 clinical, veterinary, and environmental *Cryptococcus gattii* isolates. **Antimicrob Agents Chemother**, 54, n. 12, p. 5139-5145, Dec 2010.

HAGEN, F.; KHAYHAN, K.; THEELEN, B.; KOLECKA, A. *et al.* Recognition of seven species in the *Cryptococcus gattii/Cryptococcus neoformans* species complex. **Fungal Genet Biol**, 78, p. 16-48, May 2015.

HARNPICHARNCHAI, P.; JAKOVLJEVIC, J.; HORSEY, E.; MILES, T. *et al.* Composition and functional characterization of yeast 66S ribosome assembly intermediates. **Mol Cell**, 8, n. 3, p. 505-515, Sep 2001.

HERKERT, P. F.; AMATUZZI, R. F.; ALVES, L. R.; RODRIGUES, M. L. Extracellular Vesicles as Vehicles for the Delivery of Biologically Active Fungal Molecules. **Curr Protein Pept Sci**, 20, n. 10, p. 1027-1036, 2019.

HORSEY, E. W.; JAKOVLJEVIC, J.; MILES, T. D.; HARNPICHARNCHAI, P. *et al.* Role of the yeast Rrp1 protein in the dynamics of pre-ribosome maturation. **RNA**, 10, n. 5, p. 813-827, May 2004.

HUANG, S. H.; WU, C. H.; CHANG, Y. C.; KWON-CHUNG, K. J. *et al. Cryptococcus neoformans*-derived microvesicles enhance the pathogenesis of fungal brain infection. **PLoS One**, 7, n. 11, p. e48570, 2012.

IANIRI, G.; IDNURM, A. Essential gene discovery in the basidiomycete *Cryptococcus neoformans* for antifungal drug target prioritization. **mBio**, 6, n. 2, Mar 31 2015.

JANBON, G. *Cryptococcus neoformans* capsule biosynthesis and regulation. **FEMS Yeast Res**, 4, n. 8, p. 765-771, Sep 2004.

JOFFE, L. S.; SCHNEIDER, R.; LOPES, W.; AZEVEDO, R. *et al.* The Anti-helminthic Compound Mebendazole Has Multiple Antifungal Effects against *Cryptococcus neoformans*. **Front Microbiol**, 8, p. 535, 2017.

JUNG, E. H.; MEYERS, D. J.; BOSCH, J.; CASADEVALL, A. Novel Antifungal Compounds Discovered in Medicines for Malaria Venture's Malaria Box. **mSphere**, 3, n. 2, Mar-Apr 2018.

KIDD, S. E.; CHOW, Y.; MAK, S.; BACH, P. J. *et al.* Characterization of environmental sources of the human and animal pathogen *Cryptococcus gattii* in British Columbia, Canada, and the Pacific Northwest of the United States. **Appl Environ Microbiol**, 73, n. 5, p. 1433-1443, Mar 2007.

KIDD, S. E.; HAGEN, F.; TSCHARKE, R. L.; HUYNH, M. *et al.* A rare genotype of *Cryptococcus gattii* caused the cryptococcosis outbreak on Vancouver Island (British Columbia, Canada). **Proc Natl Acad Sci U S A**, 101, n. 49, p. 17258-17263, Dec 7 2004.

KNOKE, M.; SCHWESINGER, G. One hundred years ago: the history of cryptococcosis in Greifswald. Medical mycology in the nineteenth century. **Mycoses**, 37, n. 7-8, p. 229-233, Jul-Aug 1994.

KUNDEL, D. W.; STROMQUIST, E.; GREENE, A. L.; ZHDANKIN, O. *et al.* Molecular characterizations of Nop16 in murine mammary tumors with varying levels of c-Myc. **Transgenic Res**, 21, n. 2, p. 393-406, Apr 2012.

KWON-CHUNG, K. J.; BENNETT, J. E.; WICKES, B. L.; MEYER, W. *et al.* The Case for Adopting the "Species Complex" Nomenclature for the Etiologic Agents of Cryptococcosis. **mSphere**, 2, n. 1, Jan-Feb 2017.

LEE, K. T.; HONG, J.; LEE, D. G.; LEE, M. *et al.* Fungal kinases and transcription factors regulating brain infection in *Cryptococcus neoformans*. **Nat Commun**, 11, n. 1, p. 1521, Mar 23 2020.

LEVITZ, S. M. The ecology of *Cryptococcus neoformans* and the epidemiology of cryptococcosis. **Rev Infect Dis**, 13, n. 6, p. 1163-1169, Nov-Dec 1991.

LITTMAN, M. L.; BOROK, R. Relation of the pigeon to cryptococcosis: natural carrier state, heat resistance and survival of *Cryptococcus neoformans*. **Mycopathol Mycol Appl**, 35, n. 3, p. 329-345, Oct 14 1968.

LOCKHART, S. R.; IQBAL, N.; HARRIS, J. R.; GROSSMAN, N. T. *et al. Cryptococcus gattii* in the United States: genotypic diversity of human and veterinary isolates. **PLoS One**, 8, n. 9, p. e74737, 2013.

MALLIARIS, S. D.; STEENBERGEN, J. N.; CASADEVALL, A. *Cryptococcus neoformans* var. *gattii* can exploit *Acanthamoeba castellanii* for growth. **Med Mycol**, 42, n. 2, p. 149-158, Apr 2004.

MARIANO ANDRADE, R.; MONTEIRO ALMEIDA, G.; ALEXANDRE DOSREIS, G.; ALVES MELO BENTO, C. Glucuronoxylomannan of *Cryptococcus neoformans* exacerbates in vitro yeast cell growth by interleukin 10-dependent inhibition of CD4+ T lymphocyte responses. **Cell Immunol**, 222, n. 2, p. 116-125, Apr 2003.

MAY, R. C.; STONE, N. R.; WIESNER, D. L.; BICANIC, T. *et al. Cryptococcus*: from environmental saprophyte to global pathogen. **Nat Rev Microbiol**, 14, n. 2, p. 106-117, Feb 2016.

MAYER, F. L.; KRONSTAD, J. W. Discovery of a Novel Antifungal Agent in the Pathogen Box. **mSphere**, 2, n. 2, Mar-Apr 2017.

MAZIARZ, E. K.; PERFECT, J. R. Cryptococcosis. **Infect Dis Clin North Am**, 30, n. 1, p. 179-206, Mar 2016.

MEDNICK, A. J.; NOSANCHUK, J. D.; CASADEVALL, A. Melanization of *Cryptococcus neoformans* affects lung inflammatory responses during cryptococcal infection. **Infect Immun**, 73, n. 4, p. 2012-2019, Apr 2005.

MURTHY, J. M.; SUNDARAM, C. Fungal infections of the central nervous system. **Handb Clin Neurol**, 121, p. 1383-1401, 2014.

MYLONAKIS, E.; MORENO, R.; EL KHOURY, J. B.; IDNURM, A. *et al. Galleria mellonella* as a model system to study *Cryptococcus neoformans* pathogenesis. **Infect Immun**, 73, n. 7, p. 3842-3850, Jul 2005.

NIMRICHTER, L.; DE SOUZA, M. M.; DEL POETA, M.; NOSANCHUK, J. D. *et al.* Extracellular Vesicle-Associated Transitory Cell Wall Components and Their Impact on the Interaction of Fungi with Host Cells. **Front Microbiol**, 7, p. 1034, 2016.

NOSANCHUK, J. D.; RUDOLPH, J.; ROSAS, A. L.; CASADEVALL, A. Evidence that *Cryptococcus neoformans* is melanized in pigeon excreta: implications for pathogenesis. **Infect Immun**, 67, n. 10, p. 5477-5479, Oct 1999.

NYAZIKA, T. K.; TATUENE, J. K.; KENFAK-FOGUENA, A.; VERWEIJ, P. E. *et al.* Epidemiology and aetiologies of cryptococcal meningitis in Africa, 1950-2017: protocol for a systematic review. **BMJ Open**, 8, n. 7, p. e020654, Jul 30 2018.

OLIVEIRA, D. L.; FREIRE-DE-LIMA, C. G.; NOSANCHUK, J. D.; CASADEVALL, A. *et al.* Extracellular vesicles from *Cryptococcus neoformans* modulate macrophage functions. **Infect Immun**, 78, n. 4, p. 1601-1609, Apr 2010.

OLSZEWSKI, M. A.; NOVERR, M. C.; CHEN, G. H.; TOEWS, G. B. *et al.* Urease expression by *Cryptococcus neoformans* promotes microvascular sequestration, thereby enhancing central nervous system invasion. **Am J Pathol**, 164, n. 5, p. 1761-1771, May 2004.

OSTERHOLZER, J. J.; SURANA, R.; MILAM, J. E.; MONTANO, G. T. *et al.* Cryptococcal urease promotes the accumulation of immature dendritic cells and a non-protective T2 immune response within the lung. **Am J Pathol**, 174, n. 3, p. 932-943, Mar 2009.

OSTERMANN, H.; SOLANO, C.; JARQUE, I.; GARCIA-VIDAL, C. *et al.* Cost analysis of voriconazole versus liposomal amphotericin B for primary therapy of invasive aspergillosis among patients with haematological disorders in Germany and Spain. **BMC Pharmacol Toxicol**, 15, p. 52, Sep 24 2014.

PARK, B. J.; WANNEMUEHLER, K. A.; MARSTON, B. J.; GOVENDER, N. *et al.* Estimation of the current global burden of cryptococcal meningitis among persons living with HIV/AIDS. **AIDS**, 23, n. 4, p. 525-530, Feb 20 2009.

PERFECT, J. R. The antifungal pipeline: a reality check. **Nat Rev Drug Discov**, 16, n. 9, p. 603-616, Sep 2017.

PERFECT, J. R.; DISMUKES, W. E.; DROMER, F.; GOLDMAN, D. L. *et al.* Clinical practice guidelines for the management of cryptococcal disease: 2010 update by the infectious diseases society of america. **Clin Infect Dis**, 50, n. 3, p. 291-322, Feb 1 2010.

PIANALTO, K. M.; ALSPAUGH, J. A. New Horizons in Antifungal Therapy. **J Fungi (Basel)**, 2, n. 4, Oct 2 2016.

PIERINI, L. M.; DOERING, T. L. Spatial and temporal sequence of capsule construction in *Cryptococcus neoformans*. **Mol Microbiol**, 41, n. 1, p. 105-115, Jul 2001.

PRATTE, D.; SINGH, U.; MURAT, G.; KRESSLER, D. Mak5 and Ebp2 act together on early pre-60S particles and their reduced functionality bypasses the requirement for the essential pre-60S factor Nsa1. **PLoS One**, 8, n. 12, p. e82741, 2013.

RAJASINGHAM, R.; SMITH, R. M.; PARK, B. J.; JARVIS, J. N. *et al.* Global burden of disease of HIV-associated cryptococcal meningitis: an updated analysis. **Lancet Infect Dis**, 17, n. 8, p. 873-881, Aug 2017.

RAMAN SHARMA, R. Fungal infections of the nervous system: current perspective and controversies in management. **Int J Surg**, 8, n. 8, p. 591-601, 2010.

RAUCHWAY, A. C.; HUSAIN, S.; SELHORST, J. B. Neurologic presentations of fungal infections. **Neurol Clin**, 28, n. 1, p. 293-309, Feb 2010.

REIS, F. C. G.; BORGES, B. S.; JOZEFOWICZ, L. J.; SENA, B. A. G. *et al.* A Novel Protocol for the Isolation of Fungal Extracellular Vesicles Reveals the Participation of a Putative Scramblase in Polysaccharide Export and Capsule Construction in *Cryptococcus gattii*. **mSphere**, 4, n. 2, Mar 20 2019.

RIZZO, J.; COLOMBO, A. C.; ZAMITH-MIRANDA, D.; SILVA, V. K. A. *et al.* The putative flippase Apt1 is required for intracellular membrane architecture and biosynthesis of polysaccharide and lipids in *Cryptococcus neoformans*. **Biochim Biophys Acta Mol Cell Res**, 1865, n. 3, p. 532-541, Mar 2018.

RIZZO, J.; NIMRICHTER, L.; RODRIGUES, M. L. What is new? Recent Knowledge on Fungal Extracellular Vesicles. **Curr Fungal Infections Report**, 11, p. 141-147, 2017.

RODRIGUES, M. L. Funding and Innovation in Diseases of Neglected Populations: The Paradox of Cryptococcal Meningitis. **PLoS Negl Trop Dis**, 10, n. 3, p. e0004429, Mar 2016.

RODRIGUES, M. L.; ALBUQUERQUE, P. C. Searching for a change: The need for increased support for public health and research on fungal diseases. **PLoS Negl Trop Dis**, 12, n. 6, p. e0006479, Jun 2018.

RODRIGUES, M. L.; ALVIANO, C. S.; TRAVASSOS, L. R. Pathogenicity of *Cryptococcus neoformans*: virulence factors and immunological mechanisms. **Microbes Infect**, 1, n. 4, p. 293-301, Apr 1999.

RODRIGUES, M. L.; CASADEVALL, A. A two-way road: novel roles for fungal extracellular vesicles. **Mol Microbiol**, 110, n. 1, p. 11-15, Oct 2018.

RODRIGUES, M. L.; NAKAYASU, E. S.; OLIVEIRA, D. L.; NIMRICHTER, L. *et al.* Extracellular vesicles produced by *Cryptococcus neoformans* contain protein components associated with virulence. **Eukaryot Cell**, 7, n. 1, p. 58-67, Jan 2008.

RODRIGUES, M. L.; NIMRICHTER, L.; OLIVEIRA, D. L.; FRASES, S. *et al.* Vesicular polysaccharide export in *Cryptococcus neoformans* is a eukaryotic solution to the problem of fungal trans-cell wall transport. **Eukaryot Cell**, 6, n. 1, p. 48-59, Jan 2007.

ROSAS, A. L.; MACGILL, R. S.; NOSANCHUK, J. D.; KOZEL, T. R. *et al.* Activation of the alternative complement pathway by fungal melanins. **Clin Diagn Lab Immunol**, 9, n. 1, p. 144-148, Jan 2002.

ROSSI, S. A.; DE OLIVEIRA, H. C.; AGREDA-MELLON, D.; LUCIO, J. *et al.* Identification of Off-Patent Drugs That Show Synergism with Amphotericin B or That Present Antifungal Action against *Cryptococcus neoformans* and *Candida* spp. **Antimicrob Agents Chemother**, 64, n. 4, Mar 24 2020.

SAMANTARAY, S.; CORREIA, J. N.; GARELNABI, M.; VOELZ, K. *et al.* Novel cell-based in vitro screen to identify small-molecule inhibitors against intracellular replication of *Cryptococcus neoformans* in macrophages. **Int J Antimicrob Agents**, 48, n. 1, p. 69-77, Jul 2016.

SCHNEIDER, C. A.; RASBAND, W. S.; ELICEIRI, K. W. NIH Image to ImageJ: 25 years of image analysis. **Nat Methods**, 9, n. 7, p. 671-675, Jul 2012.

SHI, M.; LI, S. S.; ZHENG, C.; JONES, G. J. *et al.* Real-time imaging of trapping and urease-dependent transmigration of *Cryptococcus neoformans* in mouse brain. **J Clin Invest**, 120, n. 5, p. 1683-1693, May 2010.

SILVA, V. K. A.; MAY, R. C.; RODRIGUES, M. L. Pyrifenox, an ergosterol inhibitor, differentially affects *Cryptococcus neoformans* and *Cryptococcus gattii*. **Med Mycol**, Jan 8 2020.

SINGH, A.; PANTING, R. J.; VARMA, A.; SAIJO, T. *et al.* Factors required for activation of urease as a virulence determinant in *Cryptococcus neoformans*. **mBio**, 4, n. 3, p. e00220-00213, May 7 2013.

SLOAN, D. J.; PARRIS, V. Cryptococcal meningitis: epidemiology and therapeutic options. **Clin Epidemiol**, 6, p. 169-182, 2014.

SOUZA, J. A. M.; BALTAZAR, L. M.; CARREGAL, V. M.; GOUVEIA-EUFRASIO, L. *et al.* Characterization of *Aspergillus fumigatus* Extracellular Vesicles and Their Effects on Macrophages and Neutrophils Functions. **Front Microbiol**, 10, p. 2008, 2019.

STEENBERGEN, J. N.; CASADEVALL, A. The origin and maintenance of virulence for the human pathogenic fungus *Cryptococcus neoformans*. **Microbes Infect**, 5, n. 7, p. 667-675, Jun 2003.

STEENBERGEN, J. N.; SHUMAN, H. A.; CASADEVALL, A. *Cryptococcus neoformans* interactions with amoebae suggest an explanation for its virulence and intracellular pathogenic strategy in macrophages. **Proc Natl Acad Sci U S A**, 98, n. 26, p. 15245-15250, Dec 18 2001.

TRILLES, L.; LAZERA MDOS, S.; WANKE, B.; OLIVEIRA, R. V. *et al.* Regional pattern of the molecular types of *Cryptococcus neoformans* and *Cryptococcus gattii* in Brazil. **Mem Inst Oswaldo Cruz**, 103, n. 5, p. 455-462, Aug 2008.

VARGAS, G.; HONORATO, L.; GUIMARAES, A. J.; RODRIGUES, M. L. *et al.* Protective effect of fungal extracellular vesicles against murine candidiasis. **Cell Microbiol**, p. e13238, Jun 18 2020.

VARGAS, G.; ROCHA, J. D.; OLIVEIRA, D. L.; ALBUQUERQUE, P. C. *et al.* Compositional and immunobiological analyses of extracellular vesicles released by *Candida albicans*. **Cell Microbiol**, 17, n. 3, p. 389-407, Mar 2015.

VOELZ, K.; JOHNSTON, S. A.; RUTHERFORD, J. C.; MAY, R. C. Automated analysis of cryptococcal macrophage parasitism using GFP-tagged cryptococci. **PLoS One**, 5, n. 12, p. e15968, Dec 31 2010.

YONEDA, A.; DOERING, T. L. A eukaryotic capsular polysaccharide is synthesized intracellularly and secreted via exocytosis. **Mol Biol Cell**, 17, n. 12, p. 5131-5140, Dec 2006.

YOON, Y. J.; KIM, O. Y.; GHO, Y. S. Extracellular vesicles as emerging intercellular communicasomes. **BMB Rep**, 47, n. 10, p. 531-539, Oct 2014.

ZARAGOZA, O. Basic principles of the virulence of *Cryptococcus*. **Virulence**, 10, n. 1, p. 490-501, Dec 2019.

ZARAGOZA, O.; CASADEVALL, A. Experimental modulation of capsule size in *Cryptococcus neoformans*. **Biol Proced Online**, 6, p. 10-15, 2004.

ZARAGOZA, O.; GARCIA-RODAS, R.; NOSANCHUK, J. D.; CUENCA-ESTRELLA, M. *et al.* Fungal cell gigantism during mammalian infection. **PLoS Pathog**, 6, n. 6, p. e1000945, Jun 17 2010.

ZARNOWSKI, R.; SANCHEZ, H.; COVELLI, A. S.; DOMINGUEZ, E. *et al. Candida albicans* biofilm-induced vesicles confer drug resistance through matrix biogenesis. **PLoS Biol**, 16, n. 10, p. e2006872, Oct 2018.

ZAVALA, S.; BADDLEY, J. W. Cryptococcosis. **Semin Respir Crit Care Med**, 41, n. 1, p. 69-79, Feb 2020.

ZHANG, C.; YIN, C.; WANG, L.; ZHANG, S. *et al.* HSPC111 governs breast cancer growth by regulating ribosomal biogenesis. **Mol Cancer Res**, 12, n. 4, p. 583-594, Apr 2014.

9. Produção científica durante o período da dissertação

Anexo I. Haroldo C. de Oliveira, Rafael F. Castelli, Diogo Kuczera, Taiane N. Souza, Caroline M. Marcos, Liliana Scorzoni, Leonardo Nimrichter, Marcio L. Rodrigues. (2020). Fungal Infections of the Central Nervous System, **Reference Module in Life Sciences**, Elsevier. https://doi.org/10.1016/B978-0-12-809633-8.21019-4.

Anexo II. de Oliveira, H. C., Joffe, L. S., Simon, K. S., Castelli, R. F., Reis, F., Bryan, A. M., Borges, B. S., Medeiros, L., Bocca, A. L., Del Poeta, M., & Rodrigues, M. L. (2020) Fenbendazole Controls *In Vitro* Growth, Virulence Potential, and Animal Infection in the *Cryptococcus* Model. Antimicrobial **Agents and Chemotherapy**, 64(6). https://doi.org/10.1128/AAC.00286-20.

Fungal Infections of the Central Nervous System

Haroldo C de Oliveira, Rafael F Castelli, and Diogo Kuczera, Carlos Chagas Institute, Curitiba, Brazil
Taiane N Souza, Federal University of Rio de Janeiro, Rio de Janeiro, Brazil
Caroline M Marcos, São Paulo State University, Araraquara, Brazil
Liliana Scorzoni, São Paulo State University, São José dos Campos, Brazil
Leonardo Nimrichter, Federal University of Rio de Janeiro, Rio de Janeiro, Brazil
Marcio L Rodrigues, Carlos Chagas Institute, Curitiba, Brazil and Federal University of Rio de Janeiro, Rio de Janeiro, Brazil

© 2020 Elsevier Inc. All rights reserved.

Central Nervous System Fungal Infections

Over the last few decades, cases of life-threatening fungal infections of the central nervous system (CNS) have significantly increased. Specifically, immunocompromised populations, the number of which has expanded in recent years, suffer from high mortality rates due to these infections (Murthy and Sundaram, 2014). The expansion of the immunocompromised population is due to increase in advanced transplant procedures, the use of immunosuppressive therapies, and the pandemic spread of HIV (Raman Sharma, 2010). The increased prevalence of these infections challenges physicians and researchers across the globe to develop accurate and rapid diagnostics associated with effective management strategies (Panackal and Williamson, 2015; Raman Sharma, 2010). In fact, research on fungal brain infections has produced impressive publication records over the last 20 years (**Fig. 1**).

Pathogenic fungi comprise approximately 300 species among highly diverse fungi, of which an estimated 1.5 million species are found living as saprophytic organisms that colonize distinct environmental niches, including some in animals and human hosts. Among the species able to colonize and cause disease in mammalian hosts, only approximately 10%–15% are able to colonize the CNS, where they cause severe infection (Murthy and Sundaram, 2014; Goralska *et al.*, 2018).

Upon exposure to fungi, immunocompetent individuals are generally able to defend against and avoid infection, having effective clearance. However, an immunocompromised host who is not able to fight the infection develops disease that generally begins in the lungs and skin and can be disseminated elsewhere in the organism, including the CNS, through hematogenous spread (Murthy and Sundaram, 2014; Black and Baden, 2007; Rauchway *et al.*, 2010).

Brain colonization is not an easy task for fungal pathogens, since the CNS is surrounded by a relatively impermeable blood–brain barrier (BBB). This barrier makes the CNS an immunologically privileged site, where few immunological cells, mainly activated T-lymphocytes, are able to penetrate. However, in immunocompromised hosts, the BBB permeability is increased, which facilitates fungal penetration into the CNS (Raman Sharma, 2010).

Fig. 1 Genus-based distribution of documents resulting from research on fungal brain infections from 1998 to 2018. Google Scholar (https://scholar.google.com.br) searches combining each fungal genus with the term "brain" indicated *Candida*, *Aspergillus*, *Cryptococcus*, *Fusarium*, *Pneumocystis*, *Histoplasma*, *Rhizopus*, *Blastomyces*, *Mucor* and *Coccidioides* as the top 10 fungal genera producing research documents. In combination, these 10 genera produced more than 200,000 research documents.

 doi:10.1016/B978-0-12-809633-8.21019-4

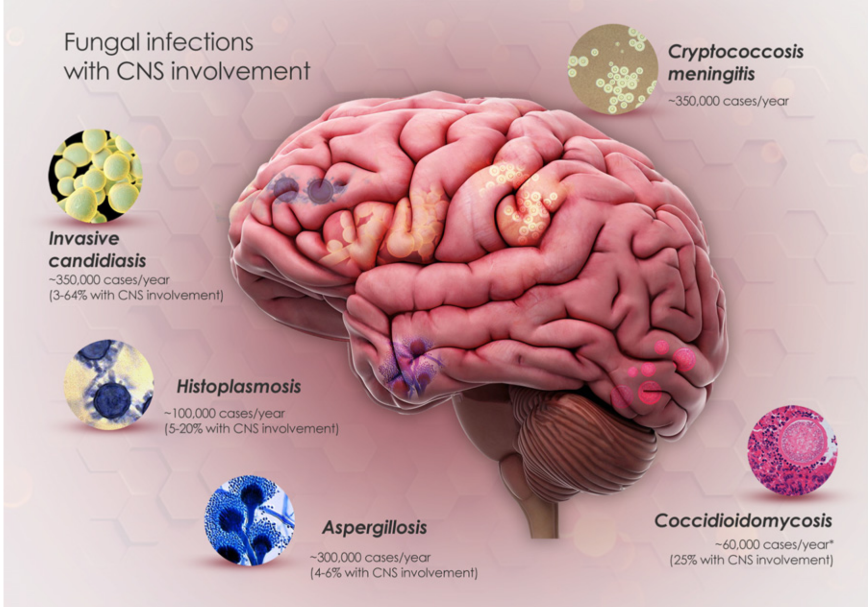

Fig. 2 Brain diseases caused by fungi and their incidence in humans. Data was collected from Goralska, K., Blaszkowska, J., Dzikowiec, M., 2018. Neuroinfections caused by fungi. Infection 46, 443–459 and the Global action Fund for Fungal Infections (GAFFI, https://www.gaffi.org). Asterisks indicate epidemiological data available in the US only. Image credit: Wagner Nagib (Instituto Carlos Chagas, Fiocruz).

Although the host's immunological status has an important role in brain colonization, fungi have also evolved strategies to modulate and evade the host immune system. Fig. 2 presents an overview of the most common fungi that causes CNS infections, represented by yeasts (*Cryptococcus* spp. and *Candida* spp.), filamentous (*Aspergillus* spp.) and dimorphic (*Histoplasma capsulatum* and *Coccidioides* spp.) species, together with the number of cases of each type of mycosis that is diagnosed per year and the frequency with which these mycoses can disseminate to brain tissue to cause lethal CNS diseases.

Candida species are known for their capacity to cause an invasive disease that can affect the CNS. Invasive candidiasis presents with a high incidence rate of CNS involvement (Panackal and Williamson, 2015), and has a mortality of 10%–70%, which is increased to 90% for patients in which the CNS is involved (Goralska *et al.*, 2018; McCarthy *et al.*, 2017; Pana *et al.*, 2017). The most common manifestation of *Candida* spp. CNS infection is meningitis, which mostly affects newborns and neurosurgical and immunocompromised patients (Panackal and Williamson, 2015; Murthy and Sundaram, 2014); however, it can occasionally affect healthy patients (Borha *et al.*, 2009).

Aspergillosis can also affect the brain and is associated with mortality rates of more than 90% (Baddley *et al.*, 2010; Deigendesch *et al.*, 2017). In addition to its ability to cause meningitis, the most common CNS infection by *Aspergillus* affects intra-axial brain structures (Deigendesch *et al.*, 2017). Immunocompromised patients are the individuals most commonly affected by invasive aspergillosis, with bone marrow transplantation, hematological diseases, AIDS, pulmonary diseases, chronic granulomatous disease, and solid organ transplantation among the most common risk factors (Ruhnke *et al.*, 2007; Singh and Paterson, 2005; Potluri *et al.*, 2014).

Coccidioidomycosis is an endemic mycosis caused by the dimorphic fungi *Coccidioides immitis* and *C. posadasii* that, in addition to being commonly asymptomatic, can evolve to a disease that is disseminated with CNS involvement, leading to meningitis, which is the most serious form of the disease (Galgiani *et al.*, 2005; Johnson *et al.*, 2018). Although able to affect immunocompetent individuals, *Coccidioides* meningitis development depends, to some extent, on the immunological status of the patients, with immunocompromised patients being the most susceptible (Brown *et al.*, 2013; Twarog and Thompson, 2015; Jackson *et al.*, 2019).

Histoplasma capsulatum is the etiological agent of another endemic mycosis, histoplasmosis. In addition to being rare, the dissemination of *Histoplasma* to the CNS generally occurs in patients with AIDS and other immunosuppression disorders, leading to severe cases of meningitis (Riddell and Wheat, 2019) that are associated with high morbidity and mortality rates (Wheat *et al.*, 2018); however, immunocompetent patients can be affected (Schestatsky *et al.*, 2006). In addition to meningitis, CNS histoplasmosis causes parenchymal mass lesions in the brains or spinal cord, stroke due to cerebral emboli and diffuse encephalitis (Saccente, 2008; Wheat *et al.*, 1990).

The main species responsible for fungal meningitis worldwide is *Cryptococcus neoformans* (Srikanta *et al.*, 2014). In cryptococcal infections, meningitis is the clinical manifestation that has the greatest effect on patients. Even when properly treated, in most cases, this meningitis cannot be ameliorated, and the mortality is approximately 70%, depending to the condition of the patient's immune system and the geographical location (Rajasingham *et al.*, 2017).

On the basis of the highest indices of mortality deriving from brain infection, in this essay, we mostly address the mechanisms used by *Cryptococcus* to disseminate in the body and invade the CNS and discuss some virulence factors associated with the infection of the CNS, elucidating interesting studies that have helped to unravel the fascinating predilection of this fungus for the CNS.

The *Cryptococcus* Genus

The *Cryptococcus* genus includes two important species, *C. gattii* and *C. neoformans*, that infect humans, causing cryptococcosis, an important systemic mycosis with high rates of morbidity and mortality worldwide (Maziarz and Perfect, 2016; Zaragoza, 2019).

Cryptococcus neoformans and *C. gattii* are spherical yeast with buds that each have a polysaccharide capsule that can vary in size among distinct strains (Voelz *et al.*, 2010; Rodrigues *et al.*, 1999; Negroni, 2012). Under the capsule, a rigid and dynamic cell wall consists of pigments, proteins, and polysaccharides that determine cell shape, interaction with other matrix cells, osmotic control, and other important biological processes, such as permeability (Rodrigues *et al.*, 2007, 2008). In nature, these species inhabit different niches. *C. neoformans* can be found in the soil and bird excreta, while *C. gattii* is more likely to be found in eucalyptus trees (Mitchell and Perfect, 1995), as shown in **Fig. 3**.

Both *Cryptococcus* species are etiological agents of cryptococcosis, a systemic worldwide mycosis able to affect both human and animal individuals (Rodrigues *et al.*, 1999) and to affect both healthy and immunocompromised individuals (Bandalizadeh *et al.*, 2019), as shown in **Fig. 3**. *C. neoformans* is the major causative agent of cryptococcosis, infecting mainly immunocompromised individuals (Voelz *et al.*, 2010; Rodrigues *et al.*, 1999), displaying a predilection for infecting the CNS, leading to the most severe manifestation of cryptococcosis, cryptococcal meningitis (Rodrigues *et al.*, 2007; May *et al.*, 2016; Bielska and May, 2016). In immunocompetent individuals, *C. gattii* shows the ability to establish cryptococcal infection with a predilection for infecting the lungs, showing elevated pathogenicity that is difficult to treat and is associated with high mortality rates (Brouwer *et al.*, 2007; Voelz *et al.*, 2010; Bielska and May, 2016).

Cryptococcosis starts with the inhalation of *Cryptococcus* spores or small, desiccated and less-encapsulated yeast cells spread in the environment. These are the infectious propagules of an ideal size for alveolar deposition and interaction with resident macrophages. In this first contact with the host, the host defenses will determine the development of the infection (Bielska and May, 2016; Gottfredsson and Perfect, 2000; Rodrigues *et al.*, 1999; Velagapudi *et al.*, 2009).

To evade host defenses and cause systemic mycosis, in addition to producing different virulence factors, *Cryptococci* undergo substantial morphological changes that drive their interaction with hosts (Rodrigues *et al.*, 1999, 2008). Morphological changes are common among fungi; however, *Cryptococcus* morphological changes are unique, as they permit the fungi to significantly increase its size by increasing its capsule, its body or both, becoming so-called titan cells (cells with bodies larger than 15 μm, excluding the capsule) (Zaragoza and Nielsen, 2013). Titan cells are polyploid cells with a thickened cell wall and a dense capsule, and they are important virulence factors because they impair phagocytosis and induce the polarization of the host immune response to promote successful infection (Zaragoza *et al.*, 2008; García-Rodas *et al.*, 2018; Zaragoza *et al.*, 2009).

Cryptococcus interactions with the host are critically influenced by polysaccharides that are produced and mounted into a network composed mainly of glucuronoxylomannan (GXM), glucuronoxylomannogalactan (GXMGal), and mannoproteins that form a capsule surrounding the cell (Rodrigues *et al.*, 1999; Bielska and May, 2016; Rodrigues *et al.*, 2015; Larocque-de-Freitas *et al.*, 2018). The capsule is a distinctive feature of cryptococcal cells that protect the fungus against host immunological defenses

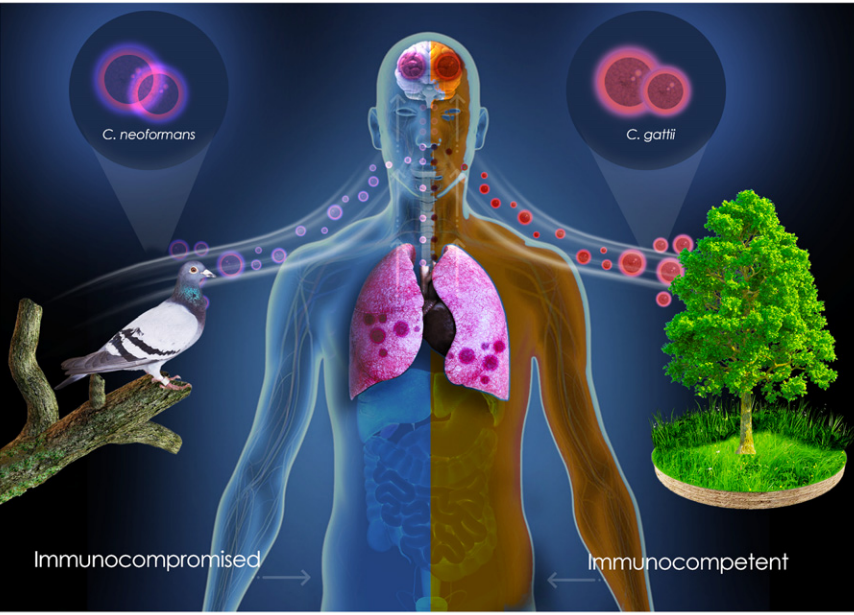

Fig. 3 Transmission of cryptococcal propagules from environmental niches to the human host. *C. neoformans* preferentially affects immunocompromised hosts, while *C. gattii* is an efficient causer of human disease in immunocompetent individuals. For details about the environmental niches of each species, see text. Image credit: Wagner Nagib (Instituto Carlos Chagas, Fiocruz).

during infection (Zaragoza *et al.*, 2006). The *Cryptococcus* capsule can be visualized by microscopy, and **Fig. 4** shows different techniques to visualize this structure, such as India-ink staining, immunofluorescence, and electron microscopy.

Capsule components are synthesized in the cytoplasm and released to the extracellular space by extracellular vesicles (EVs) (Bielska and May, 2016). These particles are efficient carriers of molecules, such as lipids, pigments, polysaccharides, proteins,

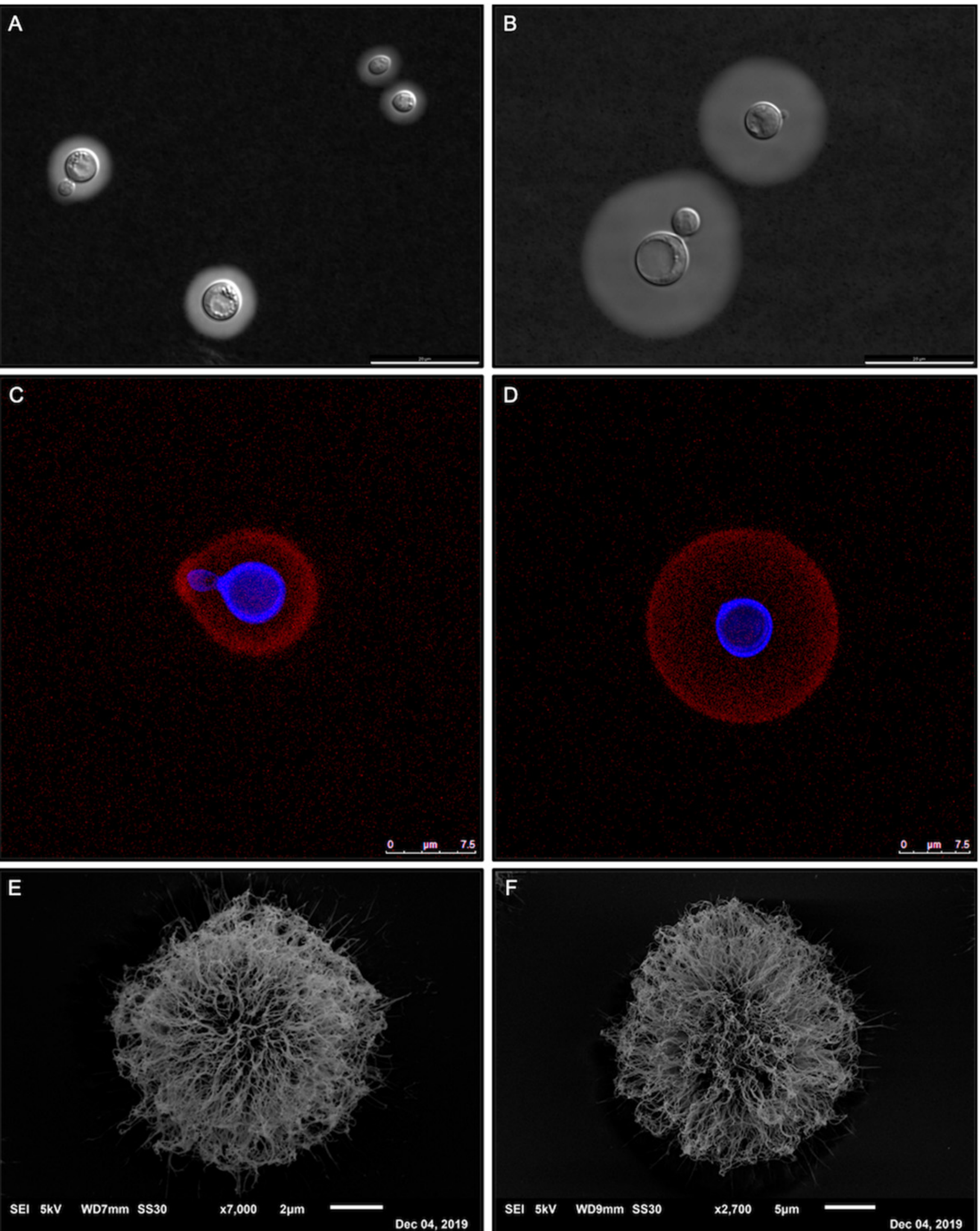

Fig. 4 Microscopic examination of the cryptococcal capsule. Panels A, C and E illustrate *C. neoformans* cells, while panels B, D and F illustrate *C. gattii*. Capsular structures can be evidenced by counterstaining with India ink (A–B), immunofluorescence (C–D, where the blue fluorescence denotes the cell wall after staining with calcofluor-white and the red fluorescence represents the capsule after antibody staining) and scanning electron microscopy (E–F).

toxins, nucleic acids, and other virulence factors, to the extracellular environment (Herkert *et al.*, 2019; Coelho and Casadevall, 2019). EV size and cargo may also affect the fungi–host interactions by delivering toxins to the host and affecting antimicrobial resistance (Coelho and Casadevall, 2019; Herkert *et al.*, 2019).

In addition to their morphological changes, other important virulence factors must be considered, such as melanin deposition into the cell wall, lipids, phospholipase, urease, and laccase, in addition to the ability to grow at mammalian temperatures (Rodrigues *et al.*, 1999, 2007; Bielska and May, 2016; Janbon, 2004). Altogether, these factors result in a great ability to manipulate the host immune system and cause life-threatening CNS infection both in immunocompetent and immunocompromised individuals, making it an important worldwide health and economic problem.

Cryptococcosis Epidemiology

Epidemiological data show that the majority of cryptococcal disease cases occur among immunocompromised individuals (Nyazika *et al.*, 2018), with HIV infection presenting as the main risk factor and accounting for 95% of the cases in middle- and low-income countries and 80% of the cases in high-income countries. Individuals taking immunosuppressive drugs constitute most of the remaining cases, although immunocompetent patients can also be affected in some settings (Sloan and Parris, 2014; de Azambuja *et al.*, 2018). Given the differences in HIV endemic status and geographic and ethnic factors, cryptococcosis numbers can vary greatly between different countries and regions, ranging from 6.6 cases per million in Australia to 15.6 per 100,000 in the Gauteng Province of South Africa (Fang *et al.*, 2015).

At the peak of the HIV pandemic, more than 600,000 deaths were estimated to have occurred globally as a result of cryptococcosis (Park *et al.*, 2009). France reported a fivefold increase in cryptococcosis from 1985 to 1993, while the number of cases in patients not infected with HIV remained stable. Of the 517 reported cases in New York City in 1991, 96% were related to HIV (Sloan and Parris, 2014). Although this number was greatly reduced as access to effective antiretroviral therapy expanded in developed countries, cryptococcosis continued to have a great impact on immunocompromised individuals, mainly in sub-Saharan Africa and low- and medium-income countries of middle Southeast Asia (Nissapatorn, 2008) and Latin America (Leimann and Koifman, 2008), where mortality rates could be as high as 70% (Leimann and Koifman, 2008).

C. gattii was previously prevalent in subtropical and tropical regions, spreading to temperate zones and affecting the Vancouver Island, British Columbia (218 cases during 1999–2007) (Galanis *et al.*, 2010), and the northwestern US states of Washington and Oregon (96 cases reported to the CDC between December 2004 and July 2011) (Harris *et al.*, 2011). Evidence suggests that the outbreak is expanding along the US West Coast (Applen Clancey *et al.*, 2019). Data from studies conducted in Australia, Papua New Guinea, British Columbia, Canada, and the US Pacific Northwest point to a mortality rate ranging from 13 to 33%, depending on differences in treatment, time of follow-up and patient characteristics (see "Relevant Websites section").

In addition to outbreaks in previously unaffected regions, another important fact to consider is the epidemiological change currently observed in medium- and high-income countries, attributed to the effectiveness of HIV diagnosis and treatment, skewing cryptococcosis susceptibility data and highlighting other susceptible populations. For example, between 1992 and 2007, in Atlanta and Houston in the United States, diabetes was found to be the most common underlying condition associated with cryptococcal infection. In Ottawa, Canada, data from 2005 to 2017 revealed that the most common underlying condition associated with cryptococcosis was hematological malignancies and, considering the fatality rates, solid organ transplantation was also considered an important risk factor (Patel *et al.*, 2019).

Cryptococcosis represents approximately 8% of the invasive fungal infection cases among solid organ transplantation recipients, being the third most common fungal infection in these patients, with an overall incidence ranging from 0.2% to 5%. Among the types of organs transplanted, the lung is associated with an increased risk of cryptococcosis (Baddley *et al.*, 2019). In patients with malignancies, lymphomas were the most common predisposing conditions (66%), followed by leukemias (29%) and myelomas (4%) (Schmalzle *et al.*, 2016).

Sex also seems to have had a role in the epidemiology of cryptococcosis. Curiously, men are affected by cryptococcosis more frequently than women with the disparity present both in HIV^{+} (~8 M:2F) and HIV^{-} (~3 M:1F) subjects. In addition to being male as a predisposing risk factor, men affected by cryptococcosis also have more severe symptoms and poorer outcomes (Guess *et al.*, 2018). Although the mechanisms involved in this trend have not been completely elucidated, it seems that hormones may play a role in influencing both the immune response and *Cryptococcus* virulence (McClelland *et al.*, 2013).

With respect to CNS infection, cryptococcal meningitis (CM) is the most common cause of adult meningitis in large parts of the world with high rates of HIV infection. Cryptococcosis is considered, after tuberculosis, the most common cause of illness in people living with HIV/AIDS, being responsible for 15% of the AIDS-related deaths globally. Approximately 200,000 cases are estimated to occur worldwide every year (see "Relevant Websites section"), culminating in 181,000 deaths, of which 73% occur in sub-Saharan Africa (Rajasingham *et al.*, 2017). The management of CM is complicated by the fact that, in several locations, one-half of the patients present with a medical history of antiretroviral therapy (ART) combined with persistently low CD4+ T cell counts due to loss of follow-up, treatment non-adherence or development of resistance to therapy (Williamson *et al.*, 2017).

Although globally associated with HIV cases in developed countries, the prevalence of CM is also increasing in populations not infected with HIV, such as solid organ transplantation recipients, patients with rheumatic diseases, and those receiving immunosuppressive therapies (Beardsley *et al.*, 2019).

Regarding the CM 1-year mortality rate worldwide, the numbers generally reflect country income level. In low-income patients, mortality ranges from 70% for patients in care to 100% for patients not in care. In the medium income category, mortality is

approximately 40% and 60% of all in-care and not-in-care patients, respectively; specifically, in Europe, it is 30 and 45%, and in North America, it is 20% and 30% (de Azambuja *et al.*, 2018; Rajasingham *et al.*, 2017).

Cryptococcus "Travels" to the Brain

Cryptococcus can disseminate and reach the CNS due a specific tropism for this site (Santiago-Tirado *et al.*, 2017). The CNS environment confers an immune privilege condition to the fungi that is related to the lack of a robust inflammatory response against antigenic changes (Santiago-Tirado and Doering, 2017; Vestweber, 2015). The first step required to reach and invade the CNS is to interact with endothelial cells and then pass through the BBB that protects the host against invaders or toxic compounds (Weiss *et al.*, 2009; Kim, 2008).

The structure of the BBB is composed of an endothelial cell layer with tight junctions and microcapillary blood vessels, representing the interface between the peripheral circulation and CNS. The BBB is highly selective for drug and microorganism permeation due to the action of efflux transporters, restrictive passive diffusion, absence of gaps and paracellular permeation (Daneman and Prat, 2015). To reach the CNS, *Cryptococcus* uses three routes, known to occur concomitantly: (1) inside infected phagocytes and possibly neutrophils (Trojan horse model) (Santangelo *et al.*, 2004; Shi *et al.*, 2010; Charlier *et al.*, 2009), (2) penetration between the cell barriers with or without disruption of the BBB endothelial cell tight junctions (paracellular model), and (3) crossing through the microvasculature as free fungi (transcellular model). **Fig. 5** illustrates each mechanism.

Trojan Horse Model

In the Trojan horse mechanism, *Cryptococcus* parasitizes phagocytes and survives within them, using these cells as vehicles to reach the brain (Zaragoza, 2019; Casadevall, 2010). Evidence that *Cryptococcus* can disseminate to the CNS through Trojan horse mechanisms was obtained from macrophage depletion studies in which the results showed a reduction in BBB invasion (Cheng *et al.*, 2009). Additionally, several studies have pointed to the occurrence of this phenomenon in vivo. First, monocyte depletion in mice before *Cryptococcus* infection resulted in a reduction in disease severity and in fungal burden (Charlier *et al.*, 2009). Second, the transfer of macrophages and monocytes from mice infected with *Cryptococcus* to healthy animals caused cerebral cryptococcosis. Finally, intravenous infection of mice with macrophages infected with ingested cryptococcal cells led to cryptococcal meningoencephalitis (Santangelo *et al.*, 2004; Charlier *et al.*, 2005). Indeed, Santiago-Tirado *et al.* (2017) demonstrated that cryptococcal cells inside phagocytes cross the BBB. Once in the brain, *Cryptococcus* can be expelled from the phagocytes through a mechanism called vomocytosis, a nonlytic process that represents the end of the Trojan horse route (Taylor-Smith and May, 2016), spreading the cells to the CNS.

Paracellular Model

This route of brain infection involves crossing the BBB through intercellular spaces with or without tight junction damage. Olszewski *et al.* (2004) demonstrated that *C. neoformans* had the ability to cross the BBB, showing fungal colocalization in

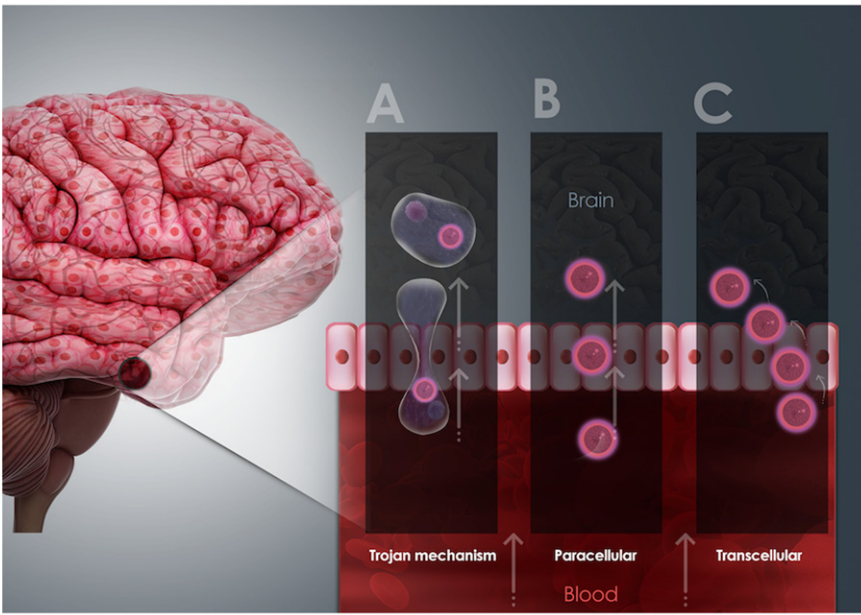

Fig. 5 Brain invasion by cryptococci. The three major mechanisms illustrating how cryptococci leave the blood to cross the endothelial layer and colonize the brain tissue are illustrated. For details, see related text. Image credit: Wagner Nagib (Instituto Carlos Chagas, Fiocruz).

capillaries and damaged endothelial cells. The same paracellular entry was verified by Charlier *et al.* (2005). Additionally, differences related to the capsule and size of the yeast could be involved in the damage to the endothelium. During infection, *Cryptococcus* induces host cell cytoskeleton changes; fungal adhesion promotes the dephosphorylation of cofilin and occludin, two proteins involved in cytoskeleton integrity, resulting in actin rearrangement and alterations in tight junction integrity that can facilitate the paracellular route of entry into the CNS (Chen *et al.*, 2003). Another possible route of paracellular entry by *Cryptococcus* relates to its ability to subvert host plasminogen by converting it into plasmin, a serine protease with proteolytic activity that can promote disruptions to the host membrane and extracellular matrix, thus weakening tight junctions and facilitating fungal invasion of the CNS (Stie *et al.*, 2009; Stie and Fox, 2012).

Transcellular Model

CNS invasion by transcytosis involves the endocytosis processes and requires that cryptococci adhere to endothelial cells before entering into brain tissue. Chang *et al.* (2004) demonstrated that, during the interaction of *Cryptococcus* with human brain microvascular endothelial cells (HBMECs) and after fungal adhesion to host cells, endothelial cells form microvillus-like projections that engulf the yeast cell; additionally, they verified the presence of free yeast inside the brain parenchyma near the capillaries, demonstrating the transcellular passage of *Cryptococcus* through the BBB. Charlier *et al.* (2005) reported the presence of yeast at cortical capillaries without the involvement of the choroid plexus at early stages after *Cryptococcus* infection and detected the damage to endothelial layers (Charlier *et al.*, 2005); in addition, the yeast crossed the HBMECs without affecting HBMEC integrity.

The association of hyaluronic acid (HA), produced by *Cryptococcus*, with CD44, the receptor in lipid rafts of endothelial cells, was described as important to the entry of the fungus at HBMEC membrane rafts since it can induce protein kinase alpha (PKc-α), which contributes to host cytoskeleton reorganization and phagocytosis (Chang *et al.*, 2006; Jong *et al.*, 2008).

CD44, an HBMEC cell surface protein, has been in fact identified as a *C. neoformans* receptor. The association of (HA), with CD44 increased the presence of this molecule in lipid rafts of HBMEC during fungal engagement. This recruitment generated docking sites for a subsequent yeast engulfment. The association of *C. neoformans* with HBMEC was followed by the activation of protein kinase alpha (PKc-α), which contributed to host cytoskeleton reorganization and phagocytosis (Chang *et al.*, 2006; Jong *et al.*, 2008). Indeed, the interaction of *Cryptococcus* with HBMECs triggered the activation of other host signaling proteins relevant to cytoskeleton rearrangement, impacting fungal transmigration. Among the host proteins activated, Rho GTPases can phosphorylate other host proteins, such as FAK, PKCα and ezrin (Kim *et al.*, 2012), promoting cytoskeleton remodeling tight junctions modulation. Another signaling pathway that likely contributes to cryptococcal transmigration is that involving the EPH-EphrinA1 (EphA2) tyrosine kinase receptor, which, when activated via CD44, triggers changes in membrane permeability, promoting the weakening of tight junctions through the activity of Rho, Rac and Cdc42. Inhibition of EphA2 resulted in the prevention of transmigration; in contrast, endothelial cell treatment with an EphA2 agonist, a ligand of EphA2, resulted in enhanced *C. neoformans* transmigration (Aaron *et al.*, 2018).

Cryptococcus "Passport" to Brain Travel

Both fungal and host factors have been identified to be involved in CNS invasion. Some virulence factors are described as being important to *Cryptococcus* infection and are shared by both pathogenic species, such as phospholipase B1 (Plb1) and laccase, which are related to fungal egress at the initial site of infection (lungs) and dissemination into the CNS (Noverr *et al.*, 2004; Santangelo *et al.*, 2004), and Plb1 and urease in the crossing of the blood–brain barrier (Santangelo *et al.*, 2004; Shi *et al.*, 2010).

Inositol

Cryptococcus CNS predilection is not yet fully understood. However, some evidence points to inositol involvement. Inositol is a carbocyclic sugar that is found at higher levels in the brain, where it acts as an osmolyte. *Cryptococcus* has also developed ways to acquire inositol, using it as a carbon source, thus influencing brain infection. The availability of inositol to fungal cells can be influenced by the induction of *Cryptococcus* alterations in the tight junctions between endothelial cells, which leads to an increase in inositol permeability and increasing levels of inositol that enhance *Cryptococcus* transmigration in a species-specific way; inositol does not influence the transmigration of *C. albicans* (Liu *et al.*, 2013).

Inositol acquisition occurs through a specific system comprised of the transporter gene (*ITR*) family, mainly the Itr1a and Itr3c transporters. Mutations in these transporters led to a significant reduction (50%) in BBB transmigration in vitro when compared to the wild-type strain. In vivo, defects in inositol acquisition correlated with reduced fungal burden and lesions in the brain (Liu *et al.*, 2013). Exposure of *Cryptococcus* to inositol leads to an increase in the expression of a hyaluronic acid synthase that can associate with CD44 in endothelial cell membrane lipid rafts to enhance the invasive potential of *Cryptococcus* (Jong *et al.*, 2012; Liu *et al.*, 2013). The inhibition of inositol transporters reduced the inositol uptake and impaired the crossing of *Cryptococcus* through the HBMEC monolayer (Liu *et al.*, 2013). Finally, strains lacking ITR1a and ITR3c inositol transporters evoked a more

pronounced protective immune response and had reduced levels of GXM secretion in the presence of inositol as carbon source (Liu *et al.*, 2014).

Urease

Urease is a metalloenzyme evenly distributed in the human body, including in the CNS, responsible for catalyzing the hydrolysis of urea into carbon dioxide and ammonia, the latter of which can be protonated to form ammonium, resulting in an increase in pH with consequences to pathogen-host interaction (Rutherford, 2014).

Urease improves the ability of *Cryptococcus* to invade the CNS. Mice infected with a mutant strain lacking urease showed a reduced brain fungal burden when compared to the load in the wild type mice (Olszewski *et al.*, 2004). Urease can directly affect the *Cryptococcus*–host BBB interaction. The ammonia generated due to urea hydrolysis can elicit both direct toxic effects in endothelial cells, promoting BBB disruption ("opening" the endothelial cell junctions) and resulting in increased permeability to cells, which facilitates brain invasion (Stamatovic *et al.*, 2008) and the induction of adhesion molecules at the endothelial surface (Olszewski *et al.*, 2004).

Fu *et al.* (2018) infected mice with macrophages containing urease-positive and urease-negative strains and compared the fungal burden in the lungs and brain. Differences were observed only in fungal recovery from the brain with a reduced number of viable urease-negative strains. Knowing that *Cryptococcus* can cross the BBB through the Trojan horse mechanism or transcytosis of endothelial cells, the authors suggested that cryptococcal urease enabled the fungus to persist in the phagocytes and thus be transported to the brain, where it is likely released through the induction of nonlytic exocytosis.

Phospholipase B1

Phospholipase B (PLB1) facilitates *C. neoformans* adhesion to host cells, replication, and survival within macrophages (Ganendren *et al.*, 2006; Santangelo *et al.*, 2004; Noverr *et al.*, 2003). Because of its hydrolytic activity on ester linkages in glycerophospholipids found abundantly in the host cell membrane and in pulmonary surfactants (Djordjevic, 2010), PLB1 contributes to the invasion and dissemination processes of fungus (Cox *et al.*, 2001; Noverr *et al.*, 2003) by breaking down host membranes and contributing to fungi escape from phagolysosomes (Wright *et al.*, 2007).

Rearrangement of host cell actin is related to the internalization process for several pathogens (Munoz-Duarte *et al.*, 2016; Mendes-Giannini *et al.*, 2004). During *Cryptococcus* transmigration to the brain, remodeling of the host endothelial cell cytoskeleton occurs, with fingerlike projections (microvilli) of actin surrounding intracellular yeast (Maruvada *et al.*, 2012) without altering host cell integrity (Chang *et al.*, 2004). *Cryptococcus* PLB1 participates in the activation of an important molecule involved in actin cytoskeleton dynamics, Rac1, which belongs to the small Rho GTPase family (Sepp and Auld, 2003; Noverr *et al.*, 2003). *Cryptococcus* mutant strains lacking PLB1 showed lower Rac1 activation levels in endothelial cells, leading to a significant reduction in *Cryptococcus* transmigration and fungal burden in the brain (Noverr *et al.*, 2003).

Laccase

The functions of laccase in *C. neoformans* include protection against macrophage antifungal activity through the production of melanin, iron oxidation products, and prostaglandin E2 (PGE2) (Liu *et al.*, 1999a; Eisenman *et al.*, 2007). Laccase can oxidize catecholamine substrates (dopamine, norepinephrine, and epinephrine) to generate melanin during infection (Liu *et al.*, 1999b), and melanin has the potential to alter host cell defense (Montine *et al.*, 1997). Melanins are polyphenolic and/or polyindolic pigments that can be produced by several pathogens and are frequently related to the pathogenicity (Lee *et al.*, 2019). When comparing melanized and nonmelanized yeast strains, several studies have concluded that melanin can protect the fungus against oxidant agents, microbicidal peptides, phagocytosis, and killing by macrophages and that melanin confers particular resistance to antifungals (Wang *et al.*, 1995; Liu *et al.*, 1999a; Wang and Casadevall, 1994; Jacobson and Tinnell, 1993), acting as a free radical scavenger (Porebska-Budny *et al.*, 1992). The presence of fungal melanin in vivo was first detected in tissues from patients with AIDS and cryptococcal meningoencephalitis (Nosanchuk *et al.*, 2000). The ability of the fungus to produce melanin from catecholamines was associated with the neurotropism of *Cryptococcus* (Polacheck *et al.*, 1982) Qiu *et al.* (2012). A mutant strain lacking laccase was unable to disseminate from the lungs to the CNS, leading to a nonprotective polarization of the host immune response.

Metalloprotease 1 (Mrp1)

Mrp1 belongs to the M36 peptidase class. It is upregulated during CNS infection and secreted by *C. neoformans* during the infectious process (Steen *et al.*, 2003; Vu *et al.*, 2014). Mutant strains lacking Mrp1 had a decreased ability to adhere to endothelial cells and to transmigrate through the host BBB (Vu *et al.*, 2014). In addition, in mice infected with a mutant yeast strain lacking Mrp1 the brain fungal burden was significantly reduced, suggesting the involvement of Mpr1 in the BBB transmigration process (Vu *et al.*, 2014). Interestingly, Na Pombejra *et al.* (2017) showed that *Cryptococcus* Mrp1 expressed in *Saccharomyces cerevisiae* led to nonpathogenic fungi crossing the BBB model in vitro without any damage to tight junctions. They also found that *Cryptococcus*

Mrp1 interacts with several endothelial cell surface proteins, most of which were related to membrane and cytoskeleton rearrangement.

Antifungal Alternatives for Treating Cryptococcal Meningitis

The treatment of fungal infections continues to be a challenge. The limited antifungal arsenal is related to the similarity between fungal and human cells, leading to serious toxicity and difficulty in the search for new targets (Perfect, 2017). Another obstacles for mycosis treatment are the high cost, narrow spectrum of action and low bioavailability of the currently available antifungals (Denning and Bromley, 2015). Currently, the available antifungal drugs are classified into four classes: (1) inhibitors of membrane ergosterol biosynthesis (azoles, triazoles, and allylamine); (2) compounds affecting membrane stability (polyenes); (3) inhibitors of cell wall and β-glucan synthesis (echinocandins); and (4) anti-metabolite action (5-fluorocytosine, 5-FC).

The recommended treatment regimen for cryptococcosis in HIV patients is composed of three steps: induction therapy, consisting of the combination of amphotericin B (AmB) and 5-FC for 2 weeks; next, this treatment set is consolidated with fluconazole (8 weeks); and finally, maintenance therapy consists of fluconazole (FLZ) (until the immunodeficiency is reverted). Alternatives to this treatment regimen are also described in **Fig. 6** (Perfect *et al.*, 2010).

AmB is a fungicidal compound belonging to the polyene class, and its mechanism of action is the formation of pores in the fungus cell membrane causing the loss of ions and sugars and, as a consequence, osmotic imbalance; however, it has been proposed that the mechanism of action involves the production of reactive oxygen species and immune response modulation (Walsh *et al.*, 2008; Sangalli-Leite *et al.*, 2011; Mesa-Arango *et al.*, 2012; Perfect, 2017). *Cryptococcus* resistance to AmB is rare (Kelly *et al.*, 1994; Nolte *et al.*, 1997); however, this antifungal agent has high toxic effects, especially nephrotoxicity (de Souza *et al.*, 2016).

5-Fluorocytosine (5-FC) inhibits nucleic acid (DNA and RNA) synthesis by incorporating 5-FC metabolites, which have a molecular structure analogous to pyrimidines (Odds *et al.*, 2003; Perfect, 2017). 5-FC treatment is recommended during CM in combination with AmB. The use of this combination decreases the risk of CM relapse and promotes a faster clearance of *Cryptococcus* spp. from the cerebrospinal fluid compared to AmB alone (Day *et al.*, 2013).

Belonging to the triazole class, fluconazole (FLZ) has as mechanism of action that involves the inhibition of the 14-alpha demethylase enzyme (encoded by the *ERG11* gene), which is critical for converting lanosterol to ergosterol (Perfect, 2017). Different studies reported the resistance of *Cryptococcus*. spp. to FLZ, with efflux pumps and *ERG11* gene mutations responsible for this phenotype. In special cases, such as intolerance to FLZ, other triazoles and itraconazole can be used during consolidation therapy; however, these alternative antifungal agents have poor aqueous solubility and poor oral bioavailability, which means that their levels must be monitored in the serum (Perfect *et al.*, 2010; Kale and Johnson, 2005).

Cryptococcus spp. cause meningitis mainly in HIV-infected individuals in an advanced stage (CD4 cell count < 200 cells/mm^3), and the introduction of antiretroviral therapy (ART) was an important milestone for the reduced mortality incidence rate of this mycosis in

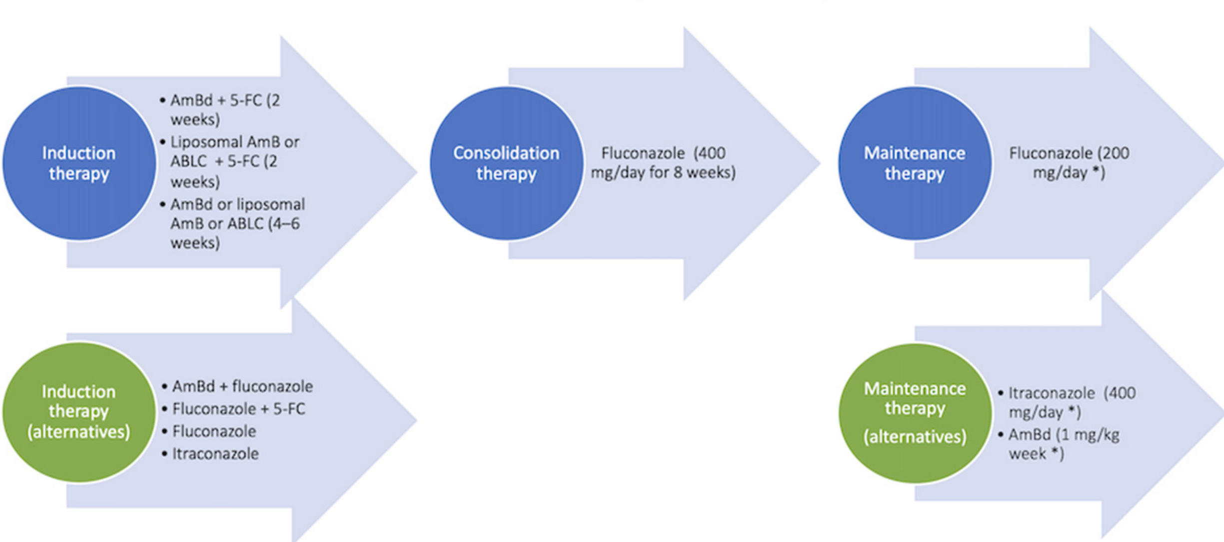

Fig. 6 Therapeutic protocols for fighting cryptococcal disease. AmBd, deoxycholate amphotericin B; 5-FC, fluorocytosine; ABLC, amphotericin B lipid complex.

developed countries (Mirza *et al.*, 2003; Antinori *et al.*, 2009). However, in limited-resource counties where late HIV diagnosis and limited access to treatment is prevalent, the number of deaths caused by cryptococcal meningitis are still alarming (Rajasingham *et al.*, 2017). Moreover, recommended induction treatment (AmB plus 5-FC) is not available in most African clinical centers, and FLZ is often the only drug available (Roemer and Krysan, 2014).

With the unavailability of the induction treatment in resource-limited settings, only monotherapy intervention can be performed, and the use of FLZ at 400 mg/kg as monotherapy is related to inefficacy (Lightowler *et al.*, 2010). However, good outcomes have been described for FLZ ranging from 800 to 2000 mg/daily (Milefchik *et al.*, 2008). To control residual infection, high-dose FLZ (800 mg/day) was also described as an option during consolidation therapy and has been recommended as an alternative by the World Health Organization HIV management guidelines (after short-course induction with amphotericin for 5–7 days) (Murphy *et al.*, 2018). A recent study demonstrated that the use of high fluconazole doses can kill a susceptible population of yeast but can also cause emerging fungal resistance, which is associated with the development of aneuploidy (Hope *et al.*, 2019).

Aiming for treatment optimization, a review of clinical trials reported the evidence of effectiveness treatment for *Cryptococcus* meningitis by comparing the following antifungal regimens: FLZ to FLZ with 5-FC; AmB to AmB with 5-FC; AmB given alone to AmB given with 5-FC and FLZ alone; high to standard dose AmB with 5-FC; and AmB to liposomal AmB; however, no evidence was found to consider one treatment superior to any other (Sloan *et al.*, 2008). Recently, in a meta-analysis study that investigated 13 trials with a total of 2426 participants and compared 21 antifungal therapy interventions (July 2014 to July 2018), the authors concluded that the combination of AmB deoxycholate and 5-FC therapy for one week is a promising treatment alternative for the treatment of cryptococcal meningitis in HIV patients in limited-resource conditions. Moreover, the combination of 5FC and FLZ for two weeks, administered orally, may be an alternative for AmB deoxycholate or when intravenous therapy is unavailable (Tenforde *et al.*, 2018).

CM also affects HIV-negative immunocompromised patients (e.g., solid organ transplantation). In these cases, the treatment regimen is similar to the recommended regimen for HIV-infected individuals. Moreover, important considerations, such as the immunocompromised state, antifungal response, presence of neurological complications, therapy cost and toxicity, should be taken into account (Henao-Martinez *et al.*, 2018). An alternative treatment for CM in patients not infected with HIV but with refractory infection or intolerance to other antifungal drugs is therapy with fluconazole 800 mg/day; however, the data on this therapeutic regimen are scarce, and this treatment needs further investigation (Zhao *et al.*, 2018).

Alternatives to CM treatment also have been studied. The antidepressant sertraline (selective serotonin reuptake inhibitor) is one example. The in vitro and in vivo antifungal activity and synergistic activity of sertraline with other antifungals have been described (Trevino-Rangel Rde *et al.*, 2016; Rossato *et al.*, 2016; Zhai *et al.*, 2012). However, a phase 3 clinical trial did not find benefit for the use of sertraline as a therapeutic component, and this trial was terminated (Rhein *et al.*, 2019). Other treatment strategies include use of natural product derivatives (Li *et al.*, 2019a,b), administration of vaccines (Hester *et al.*, 2019) and extracorporeal filtration of yeast from cerebrospinal fluid to reduce the fungal burden (neurapheresis therapy) (Smilnak *et al.*, 2018).

References

Aaron, P.A., Jamklang, M., Uhrig, J.P., Gelli, A., 2018. The blood-brain barrier internalises *Cryptococcus neoformans* via the EphA2-tyrosine kinase receptor. Cell. Microbiol. 20.

Antinori, S., Ridolfo, A., Fasan, M., *et al.*, 2009. AIDS-associated cryptococcosis: A comparison of epidemiology, clinical features and outcome in the pre- and post-HAART eras. Experience of a single centre in Italy. HIV Med. Jan; 10 (1), 6–11. doi:10.1111/j.1468-1293.2008.00645.x. PMID: 19125961.

Applen Clancey, S., Ciccone, E.J., Coelho, M.A., *et al.*, 2019. *Cryptococcus deuterogattii* VGIIa infection associated with travel to the Pacific Northwest outbreak region in an anti-granulocyte-macrophage colony-stimulating factor autoantibody-positive patient in the United States. mBio 10.

Baddley, J.W., Andes, D.R., Marr, K.A., *et al.*, 2010. Factors associated with mortality in transplant patients with invasive aspergillosis. Clin. Infect. Dis. 50, 1559–1567.

Baddley, J.W., Forrest, G.N., AST Infectious Diseases Community of Practice, 2019. Cryptococcosis in solid organ transplantation – Guidelines from the American Society of Transplantation Infectious Diseases Community of Practice. Clin. Transplant. 33, e13543.

Bandalizadeh, Z., Shokohi, T., Badali, H., *et al.*, 2019. Molecular epidemiology and antifungal susceptibility profiles of clinical *Cryptococcus neoformans/Cryptococcus gattii* species complex. J. Med. Microbiol. 69 (1), 72–81.

Beardsley, J., Sorrell, T.C., Chen, S.C., 2019. Central nervous system Cryptococcal infections in non-HIV infected patients. J. Fungi 5.

Bielska, E., May, R.C., 2016. What makes *Cryptococcus gattii* a pathogen? FEMS Yeast Res. 16, fov106.

Black, K.E., Baden, L.R., 2007. Fungal infections of the CNS: Treatment strategies for the immunocompromised patient. CNS Drugs 21, 293–318.

Borha, A., Parienti, J.J., Emery, E., *et al.*, 2009. *Candida Albicans* cerebral granuloma in an immunocompetent patient. A case report]. Neurochirurgie 55, 57–62.

Brouwer, A.E., Siddiqui, A.A., Kester, M.I., *et al.*, 2007. Immune dysfunction in HIV-seronegative, *Cryptococcus gattii* meningitis. J. Infect. 54, e165–e168.

Brown, J., Benedict, K., Park, B.J., Thompson III, G.R., 2013. Coccidioidomycosis: Epidemiology. Clin Epidemiol. 5, 185–197.

Casadevall, A., 2010. Cryptococci at the brain gate: Break and enter or use a Trojan horse? J Clin Investig. 120, 1389–1392.

Chang, Y.C., Stins, M.F., Mccaffery, M.J., *et al.*, 2004. Cryptococcal yeast cells invade the central nervous system via transcellular penetration of the blood-brain barrier. Infect. Immun. 72, 4985–4995.

Chang, Y.C., Jong, A., Huang, S., Zerfas, P., Kwon-Chung, K.J., 2006. CPS1, a homolog of the *Streptococcus pneumoniae* type 3 polysaccharide synthase gene, is important for the pathobiology of *Cryptococcus neoformans*. Infect. Immun. 74, 3930–3938.

Charlier, C., Chretien, F., Baudrimont, M., *et al.*, 2005. Capsule structure changes associated with *Cryptococcus neoformans* crossing of the blood-brain barrier. Am. J. Pathol. 166, 421–432.

Charlier, C., Nielsen, K., Daou, S., *et al.*, 2009. Evidence of a role for monocytes in dissemination and brain invasion by *Cryptococcus neoformans*. Infect. Immun. 77, 120–127.

Chen, S.H., Stins, M.F., Huang, S.H., *et al.*, 2003. *Cryptococcus neoformans* induces alterations in the cytoskeleton of human brain microvascular endothelial cells. J. Med. Microbiol. 52, 961–970.

Cheng, P.Y., Sham, A., Kronstad, J.W., 2009. *Cryptococcus gattii* isolates from the British Columbia cryptococcosis outbreak induce less protective inflammation in a murine model of infection than *Cryptococcus neoformans*. Infect. Immun. 77, 4284–4294.

Coelho, C., Casadevall, A., 2019. Answers to naysayers regarding microbial extracellular vesicles. Biochem. Soc. Trans. 47, 1005–1012.
Cox, G.M., Mcdade, H.C., Chen, S.C., *et al*., 2001. Extracellular phospholipase activity is a virulence factor for *Cryptococcus neoformans*. Mol. Microbiol. 39, 166–175.
Daneman, R., Prat, A., 2015. The blood-brain barrier. Cold Spring Harb Perspect. Biol. 7, a020412.
Day, J.N., Chau, T.T.H., Wolbers, M., *et al*., 2013. Combination antifungal therapy for cryptococcal meningitis. N. Engl. J. Med. 368, 1291–1302.
de Azambuja, A.Z., Wissmann Neto, G., Watte, G., Antoniolli, L., Goldani, L.Z., 2018. Cryptococcal meningitis: A retrospective cohort of a Brazilian reference hospital in the Post-HAART era of universal access. Can. J. Infect. Dis. Med. Microbiol. 2018, 6512468.
De Souza, M.C., Santos, A.G., Reis, A.M., 2016. Adverse drug reactions in patients receiving systemic antifungal therapy at a high-complexity hospital. J. Clin. Pharmacol. 56, 1507–1515.
Deigendesch, N., Costa Nunez, J., Stenzel, W., 2017. Parasitic and fungal infections. Handb. Clin. Neurol. 145, 245–262.
Denning, D.W., Bromley, M.J., 2015. Infectious disease. How to bolster the antifungal pipeline. Science 347, 1414–1416.
Djordjevic, J.T., 2010. Role of phospholipases in fungal fitness, pathogenicity, and drug development – Lessons from *Cryptococcus neoformans*. Front. Microbiol. 1, 125.
Eisenman, H.C., Mues, M., Weber, S.E., *et al*., 2007. *Cryptococcus neoformans* laccase catalyses melanin synthesis from both D- and L-DOPA. Microbiology 153, 3954–3962.
Fang, W., Fa, Z., Liao, W., 2015. Epidemiology of *Cryptococcus* and cryptococcosis in China. Fungal Genet. Biol. 78, 7–15.
Fu, M.S., Coelho, C., de Leon-Rodriguez, C.M., *et al*., 2018. *Cryptococcus neoformans* urease affects the outcome of intracellular pathogenesis by modulating phagolysosomal pH. PLOS Pathog. 14, e1007144.
Galanis, E., Macdougall, L., Kidd, S., Morshed, M., 2010. British Columbia *Cryptococcus gattii* Working Group. Epidemiology of *Cryptococcus gattii*, British Columbia, Canada, 1999–2007. Emerg. Infect. Dis. 16, 251–257.
Galgiani, J.N., Ampel, N.M., Blair, J.E., *et al*., 2005. Coccidioidomycosis. Clin. Infect. Dis. 41, 1217–1223.
Ganendren, R., Carter, E., Sorrell, T., Widmer, F., Wright, L., 2006. Phospholipase B activity enhances adhesion of *Cryptococcus neoformans* to a human lung epithelial cell line. Microbes Infect. 8, 1006–1015.
García-Rodas, R., De Oliveira, H.C., Trevijano-Contador, N., Zaragoza, O., 2018. Cryptococcal titan cells: When yeast cells are all grown up. Curr. Top. Microbiol. Immunol. 101–120.
Goralska, K., Blaszkowska, J., Dzikowiec, M., 2018. Neuroinfections caused by fungi. Infection 46, 443–459.
Gottfredsson, M., Perfect, J.R., 2000. Fungal meningitis. Semin. Neurol. 20, 307–322.
Guess, T.E., Rosen, J.A., Mcclelland, E.E., 2018. An overview of sex bias in *C. neoformans* infections. J. Fungi 4.
Harris, J.R., Lockhart, S.R., Debess, E., *et al*., 2011. *Cryptococcus gattii* in the United States: Clinical aspects of infection with an emerging pathogen. Clin. Infect. Dis. 53, 1188–1195.
Henao-Martinez, A.F., Chastain, D.B., Franco-Paredes, C., 2018. Treatment of cryptococcosis in non-HIV immunocompromised patients. Curr. Opin. Infect. Dis. 31, 278–285.
Herkert, P.F., Amatuzzi, R.F., Alves, L.R., Rodrigues, M.L., 2019. Extracellular vesicles as vehicles for the delivery of biologically active fungal molecules. Curr. Protein Pept. Sci. 20, 1027–1036.
Hester, M.M., Lee, C.K., Abraham, A., *et al*., 2019. Protection of mice against experimental cryptococcosis using glucan particle-based vaccines containing novel recombinant antigens. Vaccine. 38 (3), 620–626.
Hope, W., Stone, N.R.H., Johnson, A., *et al*., 2019. Fluconazole monotherapy is a suboptimal option for initial treatment of cryptococcalmeningitis because of emergence of resistance. mBio 10, e0257-19.
Jackson, N.R., Blair, J.E., Ampel, N.M., 2019. Central nervous system infections due to coccidioidomycosis. J Fungi 5.
Jacobson, E.S., Tinnell, S.B., 1993. Antioxidant function of fungal melanin. J. Bacteriol. 175, 7102–7104.
Janbon, G., 2004. *Cryptococcus neoformans* capsule biosynthesis and regulation. FEMS Yeast Res. 4, 765–771.
Johnson, R., Ho, J., Fowler, P., Heidari, A., 2018. Coccidioidal meningitis: A review on diagnosis, treatment, and management of complications. Curr. Neurol. Neurosci. Rep. 18, 19.
Jong, A., Wu, C.H., Shackleford, G.M., *et al*., 2008. Involvement of human CD44 during *Cryptococcus neoformans* infection of brain microvascular endothelial cells. Cell. Microbiol. 10, 1313–1326.
Jong, A., Wu, C.H., Gonzales-Gomez, I., *et al*., 2012. Hyaluronic acid receptor CD44 deficiency is associated with decreased *Cryptococcus neoformans* brain infection. J. Biol. Chem. 287, 15298–15306.
Kale, P., Johnson, L.B., 2005. Second-generation azole antifungal agents. Drugs Today 41, 91–105.
Kelly, S.L., Lamb, D.C., Taylor, M., *et al*., 1994. Resistance to amphotericin B associated with defective sterol delta 8–>7 isomerase in a *Cryptococcus neoformans* strain from an AIDS patient. FEMS Microbiol. Lett. 122, 39–42.
Kim, J.C., Crary, B., Chang, Y.C., Kwon-Chung, K.J., Kim, K.J., 2012. *Cryptococcus neoformans* activates RhoGTPase proteins followed by protein kinase C, focal adhesion kinase, and ezrin to promote traversal across the blood-brain barrier. J. Biol. Chem. 287, 36147–36157.
Kim, K.S., 2008. Mechanisms of microbial traversal of the blood-brain barrier. Nat. Rev. Microbiol. 6, 625–634.
Larocque-de-Freitas, I.F., Rocha, J.D.B., Nunes, M.P., *et al*., 2018. Involvement of the capsular GalXM-induced IL-17 cytokine in the control of *Cryptococcus neoformans* infection. Sci. Rep. 8, 16378.
Lee, D., Jang, E.H., Lee, M., *et al*., 2019. Unraveling melanin biosynthesis and signaling networks in *Cryptococcus neoformans*. mBio 10.
Leimann, B.C., Koifman, R.J., 2008. Cryptococcal meningitis in Rio de Janeiro state, Brazil, 1994–2004. Cad. Saude Publica 24, 2582–2592.
Li, Z., Liu, N., Tu, J., *et al*., 2019a. Discovery of simplified sampangine derivatives with potent antifungal activities against cryptococcal meningitis. ACS Infect. Dis. 5, 1376–1384.
Li, Z., Liu, N., Tu, J., *et al*., 2019b. Discovery of novel simplified isoxazole derivatives of sampangine as potent anti-cryptococcal agents. Bioorg. Med. Chem. 27, 832–840.
Lightowler, J.V., Cooke, G.S., Mutevedzi, P., *et al*., 2010. Treatment of cryptococcal meningitis in KwaZulu-Natal, South Africa. PLOS One 5, e8630.
Liu, L., Tewari, R.P., Williamson, P.R., 1999a. Laccase protects *Cryptococcus neoformans* from antifungal activity of alveolar macrophages. Infect. Immun. 67, 6034–6039.
Liu, L., Wakamatsu, K., Ito, S., Williamson, P.R., 1999b. Catecholamine oxidative products, but not melanin, are produced by *Cryptococcus neoformans* during neuropathogenesis in mice. Infect. Immun. 67, 108–112.
Liu, T.B., Kim, J.C., Wang, Y., *et al*., 2013. Brain inositol is a novel stimulator for promoting *Cryptococcus* penetration of the blood-brain barrier. PLOS Pathog. 9, e1003247.
Liu, T.B., Subbian, S., Pan, W., *et al*., 2014. *Cryptococcus* inositol utilization modulates the host protective immune response during brain infection. Cell Commun. Signal. 12, 51.
Maruvada, R., Zhu, L., Pearce, D., *et al*., 2012. *Cryptococcus neoformans* phospholipase B1 activates host cell Rac1 for traversal across the blood-brain barrier. Cell. Microbiol. 14, 1544–1553.
May, R.C., Stone, N.R., Wiesner, D.L., Bicanic, T., Nielsen, K., 2016. *Cryptococcus*: From environmental saprophyte to global pathogen. Nat. Rev. Microbiol. 14, 106–117.
Maziarz, E.K., Perfect, J.R., 2016. Cryptococcosis. Infect. Dis. Clin. North Am. 30, 179–206.
McCarthy, M.W., Kalasauskas, D., Petraitis, V., Petraitiene, R., Walsh, T.J., 2017. Fungal infections of the central nervous system in children. J. Pediatr. Infect. Dis. Soc. 6, e123–e133.
McClelland, E.E., Hobbs, L.M., Rivera, J., *et al*., 2013. The role of host gender in the pathogenesis of *Cryptococcus neoformans* infections. PLOS One 8, e63632.
Mendes-Giannini, M.J., Hanna, S.A., Da Silva, J.L., *et al*., 2004. Invasion of epithelial mammalian cells by *Paracoccidioides brasiliensis* leads to cytoskeletal rearrangement and apoptosis of the host cell. Microbes Infect. 6, 882–891.
Mesa-Arango, A.C., Scorzoni, L., Zaragoza, O., 2012. It only takes one to do many jobs: Amphotericin B as antifungal and immunomodulatory drug. Front. Microbiol. 3, 286.

Milefchik, E., Leal, M.A., Haubrich, R., *et al*., 2008. Fluconazole alone or combined with flucytosine for the treatment of AIDS-associated cryptococcal meningitis. Med. Mycol. 46, 393–395.
Mirza, S.A., Phelan, M., Rimland, D., *et al*. 2003. The changing epidemiology of cryptococcosis: An update from population-based active surveillance in 2 large metropolitan areas, 1992–2000. Clin Infect Dis. 2003 Mar 15, 36 (6), 789–94. doi:10.1086/368091. Epub 2003 Feb 27. PMID: 12627365.
Mitchell, T.G., Perfect, J.R., 1995. Cryptococcosis in the era of AIDS – 100 years after the discovery of *Cryptococcus neoformans*. Clin. Microbiol. Rev. 8, 515–548.
Montine, T.J., Picklo, M.J., Amarnath, V., Whetsell Jr., W.O., Graham, D.G., 1997. Neurotoxicity of endogenous cysteinylcatechols. Exp. Neurol. 148, 26–33.
Munoz-Duarte, A.R., Castrejon-Jimenez, N.S., Baltierra-Uribe, S.L., *et al*., 2016. *Candida glabrata* survives and replicates in human osteoblasts. Pathog. Dis. 74, ftw030.
Murphy, R.A., Hatlen, T.J., Moosa, M.S., 2018. High-dose fluconazole consolidation therapy for Cryptococcal meningitis in Sub-Saharan Africa: Much to gain, little to lose. AIDS Res. Hum. Retrovir. 34, 399–403.
Murthy, J.M., Sundaram, C., 2014. Fungal infections of the central nervous system. Handb. Clin. Neurol. 121, 1383–1401.
Na Pombejra, S., Salemi, M., Phinney, B.S., Gelli, A., 2017. The Metalloprotease, Mpr1, Engages AnnexinA2 to promote the transcytosis of fungal cells across the blood-brain barrier. Front. Cell. Infect. Microbiol. 7, 296.
Negroni, R., 2012. Cryptococcosis. Clin. Dermatol. 30, 599–609.
Nissapatorn, V., 2008. Lessons learned about opportunistic infections in southeast Asia. Southeast Asian J. Trop. Med. Public Health 39, 625–641.
Nolte, F.S., Parkinson, T., Falconer, D.J., *et al*., 1997. Isolation and characterization of fluconazole- and amphotericin B-resistant *Candida albicans* from blood of two patients with leukemia. Antimicrob. Agents Chemother. 41, 196–199.
Nosanchuk, J.D., Rosas, A.L., Lee, S.C., Casadevall, A., 2000. Melanisation of *Cryptococcus neoformans* in human brain tissue. Lancet 355, 2049–2050.
Noverr, M.C., Cox, G.M., Perfect, J.R., Huffnagle, G.B., 2003. Role of PLB1 in pulmonary inflammation and cryptococcal eicosanoid production. Infect. Immun. 71, 1538–1547.
Noverr, M.C., Williamson, P.R., Fajardo, R.S., Huffnagle, G.B., 2004. CNLAC1 is required for extrapulmonary dissemination of *Cryptococcus neoformans* but not pulmonary persistence. Infect. Immun. 72, 1693–1699.
Nyazika, T.K., Tatuene, J.K., Kenfak-Foguena, A., *et al*., 2018. Epidemiology and aetiologies of cryptococcal meningitis in Africa, 1950–2017: Protocol for a systematic review. BMJ Open 8, e020654.
Odds, F.C., Brown, A.J., Gow, N.A., 2003. Antifungal agents: Mechanisms of action. Trends Microbiol. 11, 272–279.
Olszewski, M.A., Noverr, M.C., Chen, G.H., *et al*., 2004. Urease expression by *Cryptococcus neoformans* promotes microvascular sequestration, thereby enhancing central nervous system invasion. Am. J. Pathol. 164, 1761–1771.
Pana, Z.D., Roilides, E., Warris, A., Groll, A.H., Zaoutis, T., 2017. Epidemiology of invasive fungal disease in children. J. Pediatr. Infect. Dis. Soc. 6, S3–S11.
Panackal, A.A., Williamson, P.R., 2015. Fungal infections of the central nervous system. Continuum 21, 1662–1678.
Park, B.J., Wannemuehler, K.A., Marston, B.J., *et al*., 2009. Estimation of the current global burden of cryptococcal meningitis among persons living with HIV/AIDS. AIDS 23, 525–530.
Patel, V., Desjardins, M., Cowan, J., 2019. Shift in epidemiology of cryptococcal infections in Ottawa with high mortality in non-HIV immunocompromised patients. J. Fungi 5.
Perfect, J.R., 2017. The antifungal pipeline: A reality check. Nat. Rev. Drug Discov. 16, 603–616.
Perfect, J.R., Dismukes, W.E., Dromer, F., *et al*., 2010. Clinical practice guidelines for the management of cryptococcal disease: 2010 update by the infectious diseases society of america. Clin. Infect. Dis. 50, 291–322.
Polacheck, I., Hearing, V.J., Kwon-Chung, K.J., 1982. Biochemical studies of phenoloxidase and utilization of catecholamines in *Cryptococcus neoformans*. J. Bacteriol. 150, 1212–1220.
Porebska-Budny, M., Sakina, N.L., Stepien, K.B., Dontsov, A.E., Wilczok, T., 1992. Antioxidative activity of synthetic melanins. Cardiolipin liposome model. Biochim. Biophys. Acta 1116, 11–16.
Potluri, K., Holt, D., Hou, S., 2014. Neurologic complications in renal transplantation. Handb. Clin. Neurol. 121, 1245–1255.
Qiu, Y., Davis, M.J., Dayrit, J.K., *et al*., 2012. Immune modulation mediated by cryptococcal laccase promotes pulmonary growth and brain dissemination of virulent *Cryptococcus neoformans* in mice. PLOS One 7, e47853.
Rajasingham, R., Smith, R.M., Park, B.J., *et al*., 2017. Global burden of disease of HIV-associated cryptococcal meningitis: an updated analysis. Lancet Infect. Dis. 17, 873–881.
Raman Sharma, R., 2010. Fungal infections of the nervous system: Current perspective and controversies in management. Int. J. Surg. 8, 591–601.
Rauchway, A.C., Husain, S., Selhorst, J.B., 2010. Neurologic presentations of fungal infections. Neurol. Clin. 28, 293–309.
Rhein, J., Huppler Hullsiek, K., Tugume, L., *et al*., 2019. Adjunctive sertraline for HIV-associated cryptococcal meningitis: A randomised, placebo-controlled, double-blind phase 3 trial. Lancet Infect. Dis. 19, 843–851.
Riddell, J.T., Wheat, L.J., 2019. Central nervous system infection with Histoplasma capsulatum. J. Fungi 5.
Rodrigues, J., Fonseca, F.L., Schneider, R.O., *et al*., 2015. Pathogenic diversity amongst serotype C VGIII and VGIV *Cryptococcus gattii* isolates. Sci. Rep. 5, 11717.
Rodrigues, M.L., Alviano, C.S., Travassos, L.R., 1999. Pathogenicity of *Cryptococcus neoformans*: Virulence factors and immunological mechanisms. Microbes Infect. 1, 293–301.
Rodrigues, M.L., Nimrichter, L., Oliveira, D.L., *et al*., 2007. Vesicular polysaccharide export in *Cryptococcus neoformans* is a eukaryotic solution to the problem of fungal trans-cell wall transport. Eukaryot. Cell 6, 48–59.
Rodrigues, M.L., Nakayasu, E.S., Oliveira, D.L., *et al*., 2008. Extracellular vesicles produced by *Cryptococcus neoformans* contain protein components associated with virulence. Eukaryot. Cell 7, 58–67.
Roemer, T., Krysan, D.J., 2014. Antifungal drug development: Challenges, unmet clinical needs, and new approaches. Cold Spring Harb. Perspect. Med. 4.
Rossato, L., Loreto, E.S., Zanette, R.A., *et al*., 2016. In vitro synergistic effects of chlorpromazine and sertraline in combination with amphotericin B against *Cryptococcus neoformans* var. *grubii*. Folia Microbiol. 61, 399–403.
Ruhnke, M., Kofla, G., Otto, K., Schwartz, S., 2007. CNS aspergillosis: Recognition, diagnosis and management. CNS Drugs 21, 659–676.
Rutherford, J.C., 2014. The emerging role of urease as a general microbial virulence factor. PLOS Pathog. 10, e1004062.
Saccente, M., 2008. Central nervous system histoplasmosis. Curr. Treat. Options Neurol. 10, 161–167.
Sangalli-Leite, F., Scorzoni, L., Cecilia Mesa-Arango, A., *et al*., 2011. Amphotericin B mediates killing in *Cryptococcus neoformans* through the induction of a strong oxidative burst. Microbes Infect. 13, 457–467.
Santangelo, R., Zoellner, H., Sorrell, T., *et al*., 2004. Role of extracellular phospholipases and mononuclear phagocytes in dissemination of cryptococcosis in a murine model. Infect. Immun. 72, 2229–2239.
Santiago-Tirado, F.H., Doering, T.L., 2017. False friends: Phagocytes as Trojan horses in microbial brain infections. PLOS Pathog. 13, e1006680.
Santiago-Tirado, F.H., Onken, M.D., Cooper, J.A., Klein, R.S., Doering, T.L., 2017. Trojan Horse transit contributes to blood-brain barrier crossing of a eukaryotic pathogen. mBio 8.
Schestatsky, P., Chedid, M.F., Amaral, O.B., *et al*., 2006. Isolated central nervous system histoplasmosis in immunocompetent hosts: A series of 11 cases. Scand. J. Infect. Dis. 38, 43–48.
Schmalzle, S.A., Buchwald, U.K., Gilliam, B.L., Riedel, D.J., 2016. *Cryptococcus neoformans* infection in malignancy. Mycoses 59, 542–552.
Sepp, K.J., Auld, V.J., 2003. RhoA and Rac1 GTPases mediate the dynamic rearrangement of actin in peripheral glia. Development 130, 1825–1835.
Shi, M., Li, S.S., Zheng, C., *et al*., 2010. Real-time imaging of trapping and urease-dependent transmigration of *Cryptococcus neoformans* in mouse brain. J. Clin. Investig. 120, 1683–1693.
Singh, N., Paterson, D.L., 2005. Aspergillus infections in transplant recipients. Clin. Microbiol. Rev. 18, 44–69.

Sloan, D., Dlamini, S., Paul, N., Dedicoat, M., 2008. Treatment of acute cryptococcal meningitis in HIV infected adults, with anemphasis on resource-limited settings. Cochrane Database Sys. Rev 8, (4): CD005647. doi:10.1002/14651858.CD005647. pub2. Update in: Cochrane Database Syst Rev. 2018 Jul 25, 7: CD005647. PMID: 18843697.
Sloan, D.J., Parris, V., 2014. Cryptococcal meningitis: Epidemiology and therapeutic options. Clin. Epidemiol. 6, 169–182.
Smilnak, G.J., Charalambous, L.T., Cutshaw, D., *et al*., 2018. Novel treatment of cryptococcal meningitis via neurapheresis therapy. J. Infect. Dis. 218, 1147–1154.
Srikanta, D., Santiago-Tirado, F.H., Doering, T.L., 2014. *Cryptococcus neoformans*: Historical curiosity to modern pathogen. Yeast 31, 47–60.
Stamatovic, S.M., Keep, R.F., Andjelkovic, A.V., 2008. Brain endothelial cell-cell junctions: How to "open" the blood brain barrier. Curr. Neuropharmacol. 6, 179–192.
Steen, B.R., Zuyderduyn, S., Toffaletti, D.L., *et al*., 2003. *Cryptococcus neoformans* gene expression during experimental cryptococcal meningitis. Eukaryot. Cell 2, 1336–1349.
Stie, J., Fox, D., 2012. Induction of brain microvascular endothelial cell urokinase expression by *Cryptococcus neoformans* facilitates blood-brain barrier invasion. PLOS One 7, e49402.
Stie, J., Bruni, G., Fox, D., 2009. Surface-associated plasminogen binding of *Cryptococcus neoformans* promotes extracellular matrix invasion. PLOS One 4, e5780.
Taylor-Smith, L.M., May, R.C., . New weapons in the *Cryptococcus* infection toolkit. Curr. Opin. Microbiol. 34, 67–74.
Tenforde, M.W., Shapiro, A.E., Rouse, B., *et al*., 2018. Treatment for HIV-associated cryptococcal meningitis. Cochrane Database Syst. Rev. 7.
Trevino-Rangel Rde, J., Villanueva-Lozano, H., Hernandez-Rodriguez, P., *et al*., 2016. Activity of sertraline against *Cryptococcus neoformans*: In vitro and in vivo assays. Med. Mycol. 54, 280–286.
Twarog, M., Thompson 3rd, G.R., 2015. Coccidioidomycosis: Recent Updates. Semin. Respir. Crit. Care Med. 36, 746–755.
Velagapudi, R., Hsueh, Y.P., Geunes-Boyer, S., Wright, J.R., Heitman, J., 2009. Spores as infectious propagules of *Cryptococcus neoformans*. Infect. Immun. 77, 4345–4355.
Vestweber, D., 2015. How leukocytes cross the vascular endothelium. Nat. Rev. Immunol. 15, 692–704.
Voelz, K., Johnston, S.A., Rutherford, J.C., May, R.C., 2010. Automated analysis of cryptococcal macrophage parasitism using GFP-tagged cryptococci. PLOS One 5, e15968.
Vu, K., Tham, R., Uhrig, J.P., *et al*., 2014. Invasion of the central nervous system by *Cryptococcus neoformans* requires a secreted fungal metalloprotease. MBio 5, e01101-14.
Walsh, T.J., Anaissie, E.J., Denning, D.W., *et al*., 2008. Treatment of aspergillosis: Clinical practice guidelines of the Infectious Diseases Society of America. Clin. Infect. Dis. 46, 327–360.
Wang, Y., Casadevall, A., 1994. Susceptibility of melanized and nonmelanized *Cryptococcus neoformans* to nitrogen- and oxygen-derived oxidants. Infect. Immun. 62, 3004–3007.
Wang, Y., Aisen, P., Casadevall, A., 1995. *Cryptococcus neoformans* melanin and virulence: Mechanism of action. Infect. Immun. 63, 3131–3136.
Weiss, N., Miller, F., Cazaubon, S., Couraud, P.O., 2009. The blood-brain barrier in brain homeostasis and neurological diseases. Biochim. Biophys. Acta 1788, 842–857.
Wheat, J., Myint, T., Guo, Y., *et al*., 2018. Central nervous system histoplasmosis: multicenter retrospective study on clinical features, diagnostic approach and outcome of treatment. Medicine 97, e0245.
Wheat, L.J., Batteiger, B.E., Sathapatayavongs, B., 1990. *Histoplasma capsulatum* infections of the central nervous system. A clinical review. Medicine 69, 244–260.
Williamson, P.R., Jarvis, J.N., Panackal, A.A., *et al*., 2017. Cryptococcal meningitis: Epidemiology, immunology, diagnosis and therapy. Nat. Rev. Neurol. 13, 13–24.
Wright, L.C., Santangelo, R.M., Ganendren, R., *et al*., 2007. Cryptococcal lipid metabolism: phospholipase B1 is implicated in transcellular metabolism of macrophage-derived lipids. Eukaryot. Cell 6, 37–47.
Zaragoza, O., 2019. Basic principles of the virulence of *Cryptococcus*. Virulence 10, 490–501.
Zaragoza, O., Nielsen, K., 2013. Titan cells in *Cryptococcus neoformans*: Cells with a giant impact. Curr. Opin. Microbiol. 16, 409–413.
Zaragoza, O., Chrisman, C.J., Castelli, M.V., *et al*., 2008. Capsule enlargement in *Cryptococcus neoformans* confers resistance to oxidative stress suggesting a mechanism for intracellular survival. Cell. Microbiol. 10, 2043–2057.
Zaragoza, O., Rodrigues, M.L., De Jesus, M., *et al*., 2009. The capsule of the fungal pathogen *Cryptococcus neoformans*. Adv. Appl. Microbiol. 68, 133–216.
Zaragoza, O., Telzak, A., Bryan, R.A., Dadachova, E., Casadevall, A., 2006. The polysaccharide capsule of the pathogenic fungus *Cryptococcus neoformans* enlarges by distal growth and is rearranged during budding. Mol. Microbiol. 59, 67–83.
Zhai, B., Wu, C., Wang, L., Sachs, M.S., Lin, X., 2012. The antidepressant sertraline provides a promising therapeutic option for neurotropic cryptococcal infections. Antimicrob. Agents Chemother. 56, 3758–3766.
Zhao, H.Z., Wang, R.Y., Wang, X., *et al*., 2018. High dose fluconazole in salvage therapy for HIV-uninfected cryptococcal meningitis. BMC Infect. Dis. 18, 643.

Further Reading

Alanio, A., Vernel-Pauillac, F., Sturny-Leclere, A., Dromer, F., 2015. *Cryptococcus neoformans* host adaptation: Toward biological evidence of dormancy. mBio 6.
Feder, V., Kmetzsch, L., Staats, C.C., *et al*., 2015. *Cryptococcus gattii* urease as a virulence factor and the relevance of enzymatic activity in cryptococcosis pathogenesis. FEBS J. 282, 1406–1418.
Lang, R., Stokes, W., Lemaire, J., Johnson, A., Conly, J., 2019. A case report of *Coccidioides posadasii* meningoencephalitis in an immunocompetent host. BMC Infect. Dis. 19, 722.
Levitz, S.M., Harrison, T.S., Tabuni, A., Liu, X., 1997. Chloroquine induces human mononuclear phagocytes to inhibit and kill *Cryptococcus neoformans* by a mechanism independent of iron deprivation. J. Clin. Investig. 100, 1640–1646.
Levitz, S.M., Nong, S.H., Seetoo, K.F., *et al*., 1999. *Cryptococcus neoformans* resides in an acidic phagolysosome of human macrophages. Infect. Immun. 67, 885–890.
Mada, P., Nowack, B., Cady, B., Chandranesan, A.S.J., 2017. Disseminated cryptococcosis in an immunocompetent patient. BMJ Case Rep. 2017.
May, R.C., Casadevall, A., 2018. In fungal intracellular pathogenesis, form determines fate. mBio 9.
Nicola, A.M., Robertson, E.J., Albuquerque, P., Derengowski Lda, S., Casadevall, A., 2011. Nonlytic exocytosis of *Cryptococcus neoformans* from macrophages occurs in vivo and is influenced by phagosomal pH. mBio 2.
Schwartz, J.T., Allen, L.A., 2006. Role of urease in megasome formation and *Helicobacter pylori* survival in macrophages. J. Leukoc. Biol. 79, 1214–1225.

Relevant Websites

https://www.cdc.gov/fungal/diseases/cryptococcosis-gattii/statistics.html
C. gattii Infection Statistics.
https://www.cdc.gov/fungal/diseases/cryptococcosis-neoformans/statistics.html
C. neoformans Infection Statistics.

EXPERIMENTAL THERAPEUTICS

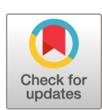

Fenbendazole Controls *In Vitro* Growth, Virulence Potential, and Animal Infection in the *Cryptococcus* Model

Haroldo C. de Oliveira,[a] Luna S. Joffe,[b] Karina S. Simon,[c] Rafael F. Castelli,[a] Flavia C. G. Reis,[a,d] Arielle M. Bryan,[b] Beatriz S. Borges,[a] Lia C. Soares Medeiros,[a] Anamelia L. Bocca,[c] Maurizio Del Poeta,[b,e,f] Marcio L. Rodrigues[a,g]

[a]Instituto Carlos Chagas, Fundação Oswaldo Cruz (Fiocruz), Curitiba, Brazil
[b]Department of Microbiology and Immunology, Stony Brook University, Stony Brook, New York, USA
[c]Departamento de Biologia Celular, Universidade de Brasília, Brasília, Brazil
[d]Centro de Desenvolvimento Tecnológico em Saúde (CDTS), Fundação Oswaldo Cruz, Rio de Janeiro, Brazil
[e]Veterans Affairs Medical Center, Northport, New York, USA
[f]Division of Infectious Diseases, Stony Brook University, Stony Brook, New York, USA
[g]Instituto de Microbiologia Paulo de Góes (IMPG), Universidade Federal do Rio de Janeiro, Rio de Janeiro, Brazil

Haroldo C. de Oliveira and Luna S. Joffe contributed equally to this work. Author order was determined on the basis of the future steps of the antifungal project in the Rodrigues laboratory.

ABSTRACT The human diseases caused by the fungal pathogens *Cryptococcus neoformans* and *Cryptococcus gattii* are associated with high indices of mortality and toxic and/or cost-prohibitive therapeutic protocols. The need for affordable antifungals to combat cryptococcal disease is unquestionable. Previous studies suggested benzimidazoles as promising anticryptococcal agents combining low cost and high antifungal efficacy, but their therapeutic potential has not been demonstrated so far. In this study, we investigated the antifungal potential of fenbendazole, the most effective anticryptococcal benzimidazole. Fenbendazole was inhibitory against 17 different isolates of *C. neoformans* and *C. gattii* at a low concentration. The mechanism of anticryptococcal activity of fenbendazole involved microtubule disorganization, as previously described for human parasites. In combination with fenbendazole, the concentrations of the standard antifungal amphotericin B required to control cryptococcal growth were lower than those required when this antifungal was used alone. Fenbendazole was not toxic to mammalian cells. During macrophage infection, the anticryptococcal effects of fenbendazole included inhibition of intracellular proliferation rates and reduced phagocytic escape through vomocytosis. Fenbendazole deeply affected the cryptococcal capsule. In a mouse model of cryptococcosis, the efficacy of fenbendazole to control animal mortality was similar to that observed for amphotericin B. These results indicate that fenbendazole is a promising candidate for the future development of an efficient and affordable therapeutic tool to combat cryptococcosis.

KEYWORDS *Cryptococcus*, antifungal, fenbendazole

Cryptococcosis caused by *Cryptococcus neoformans* and *Cryptococcus gattii* kills almost 200,000 humans each year (1). The disease, which is devastating in sub-Saharan Africa, significantly affects other regions of the globe, including Asia, Oceania, Europe, and the Americas (2–4). The World Health Organization (WHO) recently recommended three therapeutic phases for treating cryptococcal meningitis, including an induction therapy with amphotericin B plus flucytosine (week 1) followed by fluconazole (week 2), a consolidation phase with fluconazole (weeks 3 to 10) and maintenance therapy of up to 12 months also with fluconazole (5, 6). However, amphotericin B and flucytosine are not available in many countries (7). In addition, the effective treatment

Citation de Oliveira HC, Joffe LS, Simon KS, Castelli RF, Reis FCG, Bryan AM, Borges BS, Medeiros LCS, Bocca AL, Del Poeta M, Rodrigues ML. 2020. Fenbendazole controls *in vitro* growth, virulence potential, and animal infection in the *Cryptococcus* model. Antimicrob Agents Chemother 64:e00286-20. https://doi.org/10.1128/AAC.00286-20.

Copyright © 2020 American Society for Microbiology. All Rights Reserved.

Address correspondence to Marcio L. Rodrigues, marcio.rodrigues@fiocruz.br.

Received 13 February 2020
Returned for modification 18 March 2020
Accepted 29 March 2020
Accepted manuscript posted online 6 April 2020
Published 21 May 2020

Downloaded from http://aac.asm.org/ on May 21, 2020 by guest

of human cryptococcosis is cost prohibitive in most of the regions that are severely affected by *C. neoformans* and *C. gattii* (8). In Brazil, the therapeutic costs of lipid formulations of amphotericin B can exceed $100,000 per patient (9). In summary, novel therapeutic protocols for treating the diseases caused by *C. neoformans* and *C. gattii* are urgent. However, the development of novel drugs is time-consuming, highly expensive, and commonly unsuccessful (10, 11). In this context, drug repurposing has emerged as a promising alternative for the development of novel therapies against neglected pathogens, including fungi (12–14).

Benzimidazoles are anthelmintic compounds that were introduced in clinical practice nearly 60 years ago (15). *C. neoformans* and *C. gattii* are sensitive to benzimidazoles *in vitro* (16–18). Flubendazole is inhibitory against all pathogenic *Cryptococcus* species, including isolates that are resistant to fluconazole (14). In mice, orally administered flubendazole resulted in a reduction in fungal burden in comparison with controls, but in the rabbit model, there were no quantifiable drug concentrations or antifungal activity in the cerebrospinal fluid or brain (19). Mebendazole, another member of the family of benzimidazoles, also showed antifungal activity against *C. neoformans*, including phagocytized yeast cells and cryptococcal biofilms (20).

The anticryptococcal effects of other benzimidazoles have been superficially examined. In comparison to other benzimidazoles, fenbendazole was the most efficient compound showing *in vitro* fungicidal activity (20), but mechanistic approaches and *in vivo* activity of this compound were not evaluated. Fenbendazole has been licensed worldwide for the treatment and control of helminth infections in food-producing and non-food-producing animals for more than 30 years, and its safety is well established. According to the European Medicines Agency (21), fenbendazole had negligible acute toxicity in single-dose animal studies, and no points of concern relevant for the safety of fenbendazole in humans could be identified, although the effects of multiple doses are still not known. No treatment-related effects were observed in the offspring of dogs, pigs, sheep, and cattle administered fenbendazole at various times during gestation. Finally, the compound was not genotoxic, and no evidence of carcinogenicity was found (21, 22).

Based on the anticryptococcal effects of fenbendazole (20) and negligible toxicity to humans and animals (21, 22), we evaluated the therapeutic potential of this benzimidazole against pathogenic cryptococci. Our results demonstrated that fenbendazole was inhibitory against several strains of *C. neoformans* and *C. gattii*. The mechanism of antifungal activity of fenbendazole involved the functionality of microtubules. Fenbendazole had low toxicity to mammalian cells alone or in combination with amphotericin B, and its antifungal effects included inhibition of virulence determinants and reduced proliferation of *Cryptococcus* inside macrophages. Finally, fenbendazole was highly effective in a mouse model of cryptococcosis. These results support the use of fenbendazole as a prototype for the development of novel pharmaceutical preparations for treating cryptococcosis.

RESULTS

Fenbendazole affects several isolates of *Cryptococcus* and has low toxicity to mammalian cells. We first determined the MIC of fenbendazole against strains H99 and R265, the standard isolates of *C. neoformans* and *C. gattii*, respectively. A similar MIC of 0.012 μg/ml was found for both strains (Fig. 1A). We tested 12 additional isolates of *C. neoformans* and 3 other isolates of *C. gattii*, and the same MIC of 0.012 μg/ml was found for all of them, despite their differential susceptibility to fluconazole and amphotericin B (Table 1). At the MIC, fenbendazole exerted fungicidal effects, as concluded from the highly reduced detection of CFU of *C. neoformans* and *C. gattii* after exposure to the drug (Fig. 1B). In a toxicity model using mammalian macrophages, the concentration of fenbendazole required to kill 50% of the cell population (LD_{50}) corresponded to 3.072, generating a selectivity index (LD_{50}/MIC) of 256. This result confirmed the low toxicity of fenbendazole.

Downloaded from http://aac.asm.org/ on May 21, 2020 by guest

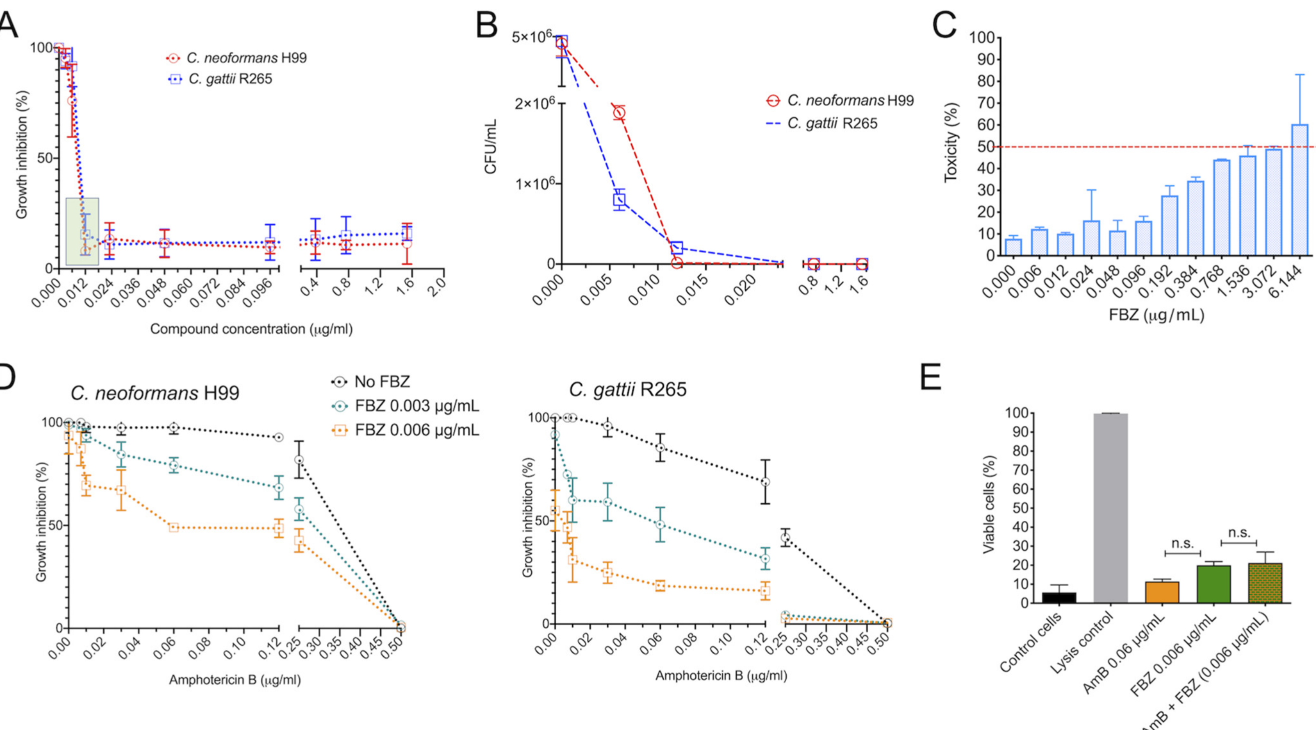

FIG 1 Antifungal effect and toxicity of fenbendazole (FBZ). (A) Determination of the MIC of fenbendazole against *C. neoformans* (strain H99) and *C. gattii* (strain R265). Both strains were sensitive to a MIC of 0.012 µg/ml (boxed area). (B) FBZ is fungicidal, as concluded from its ability to drastically reduce the numbers of CFU of *C. neoformans* H99 and *C. gattii* R265 at the MIC. (C) Dose-dependent profile of toxicity of fenbendazole against RAW 264.7 macrophages. The dotted line represents the 50% cutoff of cellular viability. (D) Antifungal effects of subinhibitory doses of fenbendazole (0.003 and 0.006 µg/ml) in combination with variable concentrations of amphotericin B (AmB) against *C. neoformans* H99 and *C. gattii* R265. In both cases, the presence of fenbendazole results in decreased concentrations of amphotericin B required for growth inhibition. (E) Analysis of the potential of fenbendazole and amphotericin B alone or in combination to kill RAW 264.7 macrophages. Control cells consisted of mammalian cultures treated with vehicle (DMSO) alone. Lysis control consisted of cells treated with 1× lysis solution (provided by the manufacturer). No significant (n.s.) differences were found between the antifungal preparations.

Fenbendazole potentiated the antifungal activity of amphotericin B, as inferred from the results obtained from the checkerboard assay. When used alone, amphotericin B produced a MIC of 0.5 µg/ml against both *C. neoformans* (H99 strain) and *C. gattii* (R265 strain). However, when tested in combination with 0.006 µg/ml fenbendazole, the amphotericin B MIC was decreased 8-fold (0.06 µg/ml). Indeed, dose-response analyses efficiently illustrate that the anticryptococcal effects of amphotericin B are boosted by different concentrations of fenbendazole, especially against *C. gattii* R265 (Fig. 1D). Analysis of the toxic effects of the compounds in combination or alone revealed that all systems had low and similar toxicity to mammalian macrophages (Fig. 1E).

The fractional inhibitory concentration index (FICI) corresponded to 0.62 for *C. neoformans* H99 and 0.49 for *C. gattii* R265. These data suggested that the combination was synergistic only in the *C. gattii* R265 isolate. However, considering that fenbendazole and amphotericin B belong to different molecular classes with distinct cellular targets, we also evaluated our synergism data using the SynergyFinder tool (https://synergyfinder.fimm.fi) applying the Bliss independence model, which is based on stochastic processes in which two drugs elicit their effects independently (23). With this method, scores of less than −10 indicate that the interaction between two drugs is antagonistic. Scores from −10 to 10 suggest an additive effect, and scores larger than 10 indicate synergism. For *C. neoformans* H99, the average Bliss synergy score considering all concentrations tested corresponded to 4.755 (Fig. 2A). In *C. gattii* R265, we obtained an average score of 5.225 (Fig. 2B). However, the analysis of synergism focused on specific concentration ranges produced more promising scores. For *C. neoformans* H99, for instance, a highly synergistic score of 42.14 was calculated when amphotericin B and fenbendazole were used at 0.025 and 0.006 µg/ml, respectively. A

Downloaded from http://aac.asm.org/ on May 21, 2020 by guest

TABLE 1 Determination of MICs in different isolates of *C. neoformans* and *C. gattii* using fenbendazole (FBZ), fluconazole (FCZ), and amphotericin B as antifungals[a]

Isolate[b]	Origin	MIC (μg/ml) for:		
		FBZ	FCZ	AmB
C. neoformans H99	Clinical	0.012	2.0	0.5
C. neoformans 162	Clinical	0.012	8.0	0.5
C. neoformans 191	Clinical	0.012	8.0	0.25
C. neoformans 186	Clinical	0.012	4.0	0.25
C. neoformans 161	Clinical	0.012	4.0	0.5
C. neoformans 160	Clinical	0.012	4.0	0.5
C. neoformans 139	Clinical	0.012	4.0	0.5
C. neoformans 118	Clinical	0.012	8.0	0.25
C. neoformans 116	Clinical	0.012	8.0	0.5
C. neoformans 115	Clinical	0.012	4.0	0.5
C. neoformans 222	Clinical	0.012	2.0	0.5
C. neoformans 223	Clinical	0.012	4.0	0.5
C. neoformans 218	Clinical	0.012	2.0	0.25
C. gattii R265	Clinical	0.012	8.0	0.5
C. gattii 367	Environmental	0.012	8.0	0.25
C. gattii 368	Environmental	0.012	16.0	0.25
C. gattii 365	Environmental	0.012	4.0	0.5
C. krusei ATCC 6258[c]	Not applicable	>1.536	>64	0.25
C. parapsilosis ATCC 22019[c]	Not applicable	>1.536	1.0	0.25

[a]As determined by EUCAST, growth inhibition measurements corresponded to 50% for FLZ and 90% for AmB. FBZ inhibition rates shown in the table correspond to 90%. Identical values were obtained when 50% inhibition rates were determined for FBZ (data not shown).

[b]Strain numbers were attributed by the Collection of Pathogenic Fungi of Fiocruz. For details, see http://cfp.fiocruz.br/index.

[3]The *C. krusei* and *C. parapsilosis* isolates were used as controls of antifungal activity as preconized by EUCAST. The MIC results obtained with these isolates were at the expected range (47).

similar analysis with *C. gattii* R265 generated a score of 43.13 when amphotericin B and fenbendazole were used at 0.1250 and 0.003 μg/ml, respectively. The synergistic activity was observed in an even broader concentration interval. In the combined concentration range of 0.003 to 0.006 μg/ml of fenbendazole and 0.06 to 0.25 μg/ml of amphotericin B, Bliss scores of 20.08 and 20.56 were calculated for *C.*

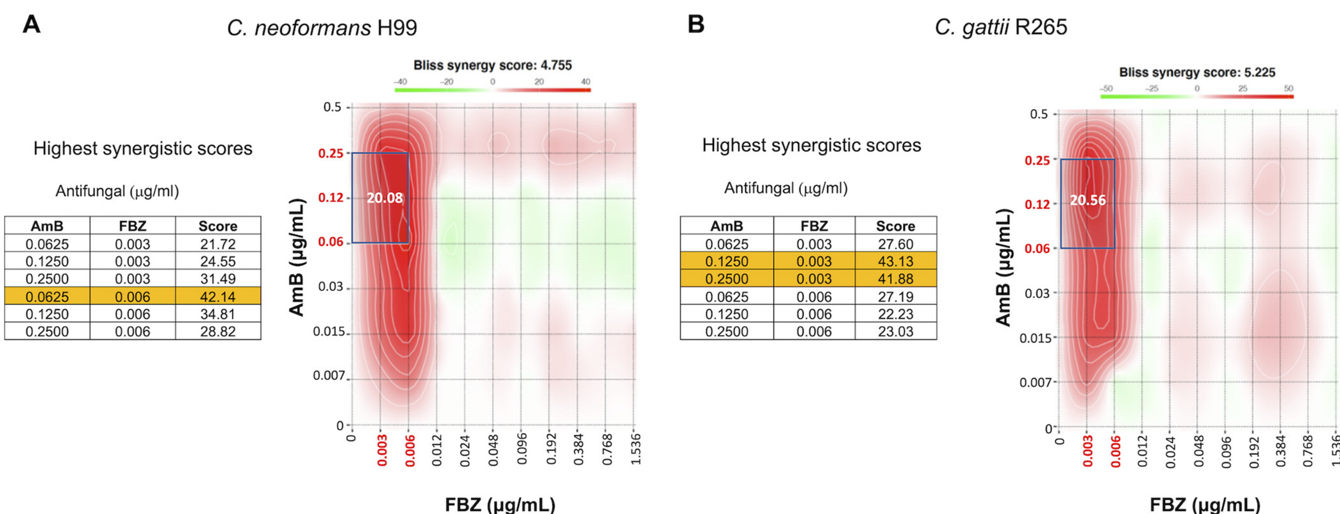

FIG 2 Synergistic antifungal activity of fenbendazole (FBZ) and amphotericin B (AmB) against *C. neoformans* H99 (A) and *C. gattii* R265 (B). The average Bliss synergy scores calculated using the full concentration range of each compound in the checkerboard assay corresponded to 4.755 and 5.225 for isolates H99 and R265, respectively. However, calculations using the antifungal concentrations producing the highest synergistic scores (left panels in A and B) generated Bliss scores of 20.08 and 20.56 for *C. neoformans* H99 and *C. gattii* R265, respectively (boxed areas in the heatmap plots). Yellow rows correspond to the highest Bliss scores obtained in our analysis. For data interpretation, please consider Bliss score values of less than −10 for antagonistic compounds, −10 to 10 for an additive effect, and larger than 10 for synergism. Calculations and graphical presentations were obtained with the SynergyFinder tool (https://synergyfinder.fimm.fi).

Downloaded from http://aac.asm.org/ on May 21, 2020 by guest

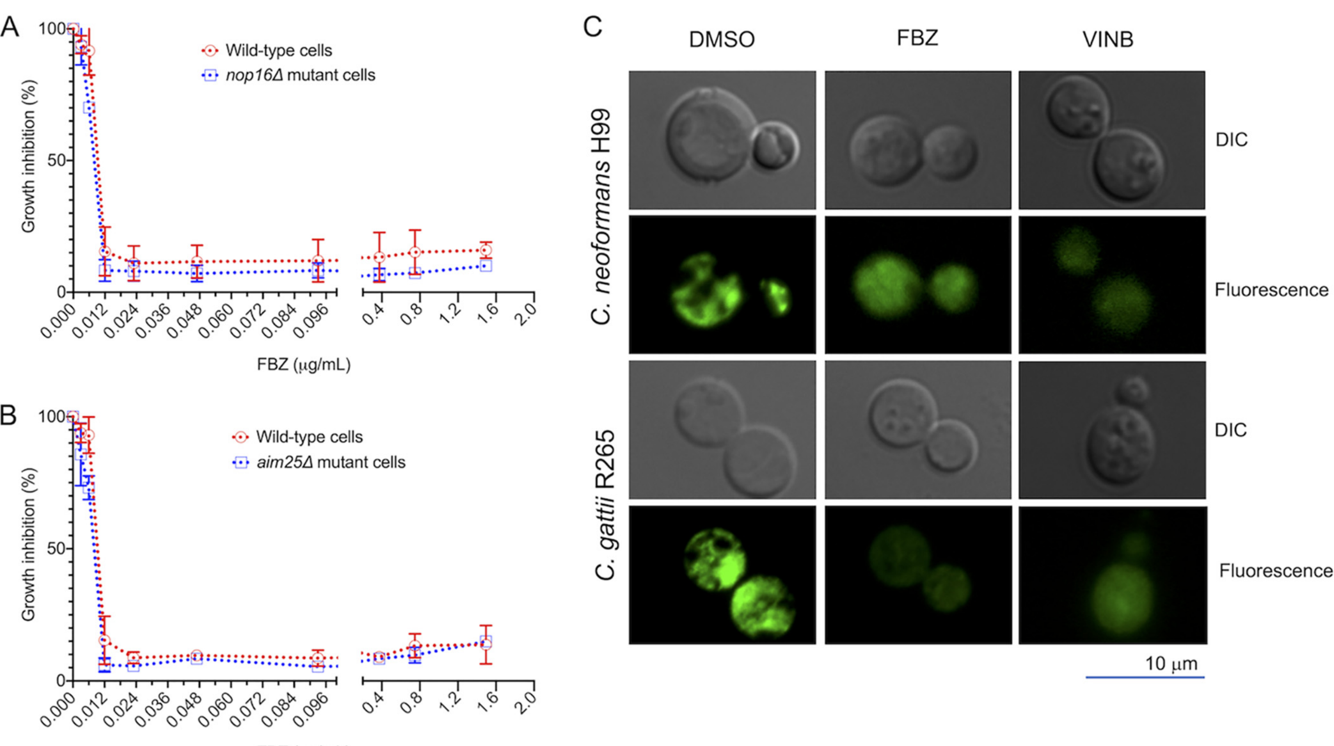

FIG 3 The antifungal effects of fenbendazole are related to microtubule disorganization. Nop16 and Aim25, which were previously suggested to be the targets of the antifungal activity of benzimidazoles in *C. gattii*, are not involved in the antifungal activity of fenbendazole (FBZ), as concluded from the similar growth rates observed for wild-type *C. gattii* (R265 strain) and mutant cells lacking *NOP16* (A) or *AIM25* (B) in the presence of variable concentrations of FBZ. A comparison between the β-tubulin staining pattern in control cells (DMSO) and FBZ-treated fungi (C) revealed that drug treatment profoundly affected microtubule distribution, with apparently more intensive effects on *C. gattii* R265. Similar staining patterns were obtained when both strains were treated with vinblastine. Fungal cells are shown under the differential interference contrast (DIC) and fluorescence modes.

neoformans H99 and *C. gattii* R265, respectively. These results indicate that fenbendazole and amphotericin B have synergistic activity against the two standard isolates of *Cryptococcus* used in our study.

Fenbendazole affects β-tubulin distribution in *C. neoformans* and *C. gattii*. We asked whether the mechanism of anticryptococcal activity of fenbendazole was similar to what was previously described for *C. gattii* (20) or if it was related to its well-characterized anthelmintic effect (15, 24, 25). Mutant strains of *C. gattii* lacking expression of the Aim25 scramblase or the nucleolar protein Nop16 were resistant to mebendazole (20), suggesting that these proteins are potential targets for the antifungal activity of benzimidazoles. To investigate the mechanism of action of fenbendazole, we first evaluated its antifungal activity against mutant strains of *C. gattii* lacking the *AIM25* or *NOP16* genes and observed that both strains and wild-type cells were similarly sensitive to this benzimidazole (Fig. 3A and B). This result suggested that, in contrast to mebendazole, Aim25 and Nop16 are not required for the antifungal activity of fenbendazole. We then asked whether the inhibitory effect of fenbendazole against *C. neoformans* H99 and *C. gattii* R265 involves interference with the functions of β-tubulin, as is consistently described for parasites (15, 24). Staining of β-tubulin in fungal cells revealed that drug-treated fungi and untreated cryptococci had markedly different profiles of microtubule organization. Control cells showed high fluorescence intensity and a well-defined intracellular pattern of β-tubulin staining (Fig. 3C). Fluorescence detection was apparently less intense in fenbendazole-treated cells, which also manifested a markedly more disperse staining of β-tubulin. In addition, the effects of fenbendazole on β-tubulin staining were apparently more drastic in *C. gattii* R265 than in *C. neoformans* H99, as concluded from the weaker signals of β-tubulin staining in the former species. These results were similar to those obtained with the control drug

Downloaded from http://aac.asm.org/ on May 21, 2020 by guest

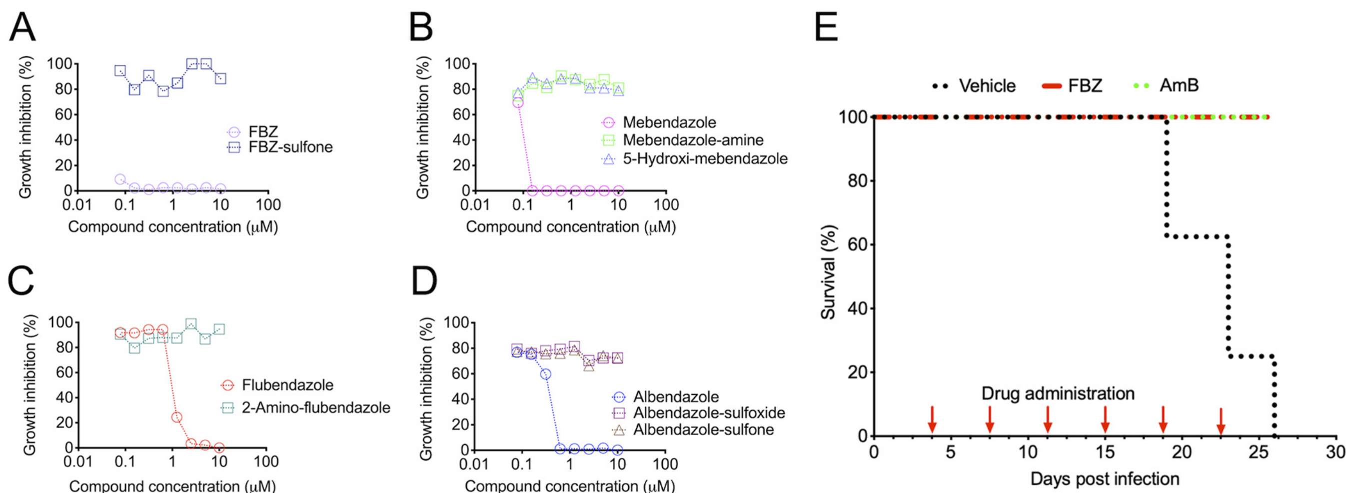

FIG 4 Analysis of the potential of fenbendazole to control animal cryptococcosis. (A to D) Antifungal effects of fenbendazole and other benzimidazoles in comparison with their liver metabolites. All benzimidazoles had clear antifungal activity, in contrast to their liver metabolites of fenbendazole (A), mebendazole (B), flubendazole (C), and albendazole (D). (E) Treatment of lethally infected mice with intranasally delivered fenbendazole or intraperitoneally administered amphotericin B (AmB). All vehicle-treated animals died 26 days postinfection. Drug-treated animals were all alive 27 days postinfection.

vinblastine, which binds tubulin and inhibits the assembly of microtubules (26), indicating that the mechanism of antifungal activity of fenbendazole against *Cryptococcus* is similar to that described for human parasites.

Intranasal administration of fenbendazole results in the control of animal cryptococcosis. The combination of low toxicity, antifungal efficacy, and a defined mechanism of action led us to test the antifungal potential of fenbendazole *in vivo*. To keep the number of animals used to a minimum, we selected the standard strain H99 of *C. neoformans* for the *in vivo* work, based on the highest prevalence of this species in human disease (3). Metabolization by host tissues is a common feature of orally administered benzimidazoles (27). Fenbendazole, specifically, is rapidly sulfoxidated by liver microsomes after oral absorption (27). Therefore, using *C. neoformans* H99, we first tested the *in vitro* antifungal activity of the sulfone derivative of fenbendazole, which showed no inhibitory potential (Fig. 4A). We performed similar tests with the liver metabolites of other benzimidazoles (mebendazole, flubendazole, and albendazole), and none of them manifested antifungal activity (Fig. 4B to D), suggesting that host metabolization is an important limitation for the antifungal activity of benzimidazoles in general. In fact, orally administered fenbendazole and mebendazole had no effects on mouse cryptococcosis (see Fig. S1 in the supplemental material). Therefore, to avoid liver metabolization and to promote an increased bioavailability of fenbendazole in its native form, we administered the drug intranasally. Under these conditions, mice lethally infected with *C. neoformans* H99 receiving intraperitoneal amphotericin B and intranasal fenbendazole had similarly high survival rates in comparison with vehicle-treated mice ($P = 0.0014$; Fig. 4E). The experiment was repeated under the same conditions, and identical results were obtained.

Fenbendazole affects the virulence potential of *Cryptococcus*. We asked whether the high efficacy of fenbendazole *in vivo* was related to neutralization of virulence determinants in addition to its antifungal effects. Capsule synthesis and intracellular proliferation rates have been consistently associated with the pathogenic potential of cryptococci (28, 29). We therefore evaluated whether fenbendazole was able to interfere with each of these biological events.

Microscopic analysis of fenbendazole-treated *C. neoformans* H99 and *C. gattii* R265 revealed clear effects on the capsular architecture, although some strain-specific particularities were observed. In all cases, fungal aggregates with reduced capsular dimensions were observed after drug treatment (Fig. 5A). Scanning electron microscopy of the H99 strain of *C. neoformans* after exposure to fenbendazole revealed shorter and

Downloaded from http://aac.asm.org/ on May 21, 2020 by guest

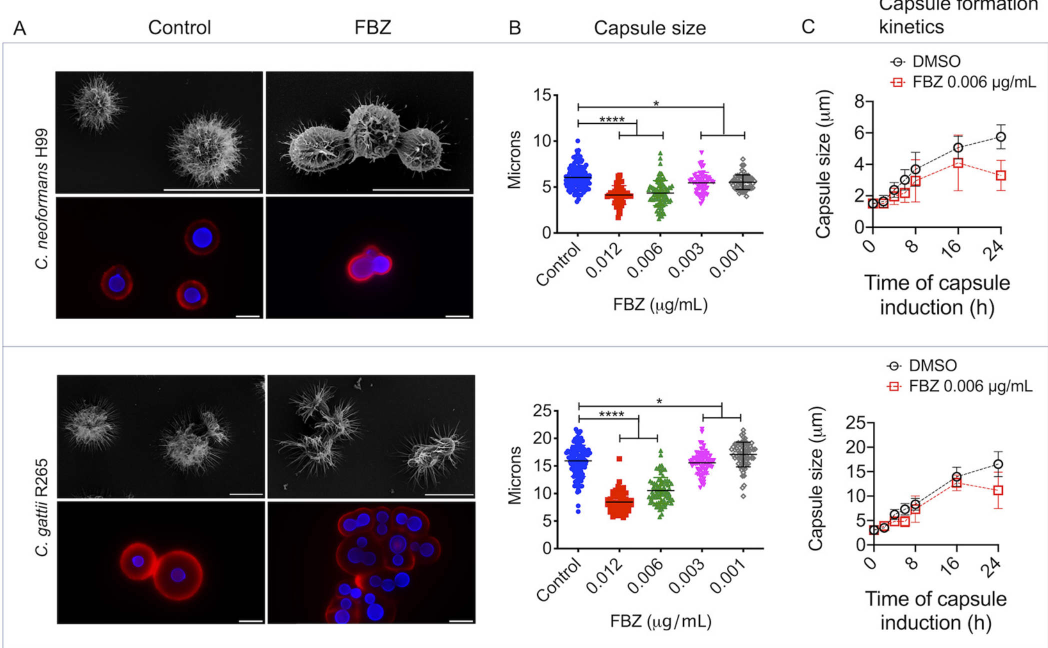

FIG 5 Fenbendazole (FBZ) affects capsule formation in *C. neoformans* and *C. gattii*. (A) Morphological analysis of vehicle (control) and drug-tread *C. neoformans* (strain H99) and *C. gattii* (strain R265). For each species, the top panels illustrate capsular alterations with scanning electron microscopy, and the bottom panels illustrate capsular morphology (red fluorescence) and cell wall staining (blue fluorescence). Scale bars, 10 μm. (B) Quantitative determination of capsular dimensions after treatment of fungal cells with vehicle alone (control) or variable concentrations of fenbendazole. *, $P < 0.05$; ****, $P < 0.0001$. (C) Kinetics of capsule formation in *C. neoformans* H99 and *C. gattii* R265 in the presence or absence of fenbendazole. The inhibitory effect on capsule formation was evident after 24 h of exposure to the drug.

scarcer capsular fibers than control cells. This perception was confirmed using immunofluorescence analysis. In *C. gattii* (strain R265), surface fibers and capsular dimensions were also reduced after exposure to fenbendazole. In both cases, a dose-dependent reduction of capsular dimensions was observed after cryptococci were treated with fenbendazole (Fig. 5B). For both *C. neoformans* H99 and *C. gattii* R265, the inhibitory effect on capsule formation was evident after 24 h of exposure to the drug, as concluded from a comparative time course analysis of capsule formation in the absence or presence of fenbendazole (Fig. 5C).

Due to the suggested link between therapeutic failure and intracellular proliferation of cryptococci (28, 30, 31), we evaluated whether fenbendazole could influence the fate of *C. neoformans* H99 and *C. gattii* R265 in infected macrophages. Initial microscopic observation suggested that fenbendazole affected the cell division frequency of both *C. neoformans* H99 and *C. gattii* R265 (Fig. 6A and B). In macrophages infected with *C. neoformans* H99 that were further treated with dimethyl sulfoxide (DMSO), intracellular division was initially observed 1 h after internalization of fungal cells, with a clear peak at 5 h postphagocytosis (Fig. 6C). In drug-treated systems, intracellular proliferation was first observed 4 h after phagocytosis, with less intense peaks at 5 and 7 h postinfection. In similar systems using *C. gattii* R265, intracellular proliferation in vehicle-treated macrophages was first observed 1 h postinfection, with more prominent peaks of replication at 5 and 7 h postinfection (Fig. 6D). In drug-treated systems, fungal intracellular proliferation was only observed after 5 h. These results were suggestive of lower intracellular proliferation rates (IPR) of phagocytized *C. neoformans* H99 and *C. gattii* R265. Since low IPR have been linked with reduced virulence (28, 30, 32), we investigated the effects of fenbendazole on this important parameter.

In both species, exposure of infected macrophages to fenbendazole resulted in reduced IPR at both inhibitory and subinhibitory concentrations (Fig. 7A and B). High IPR are related to vomocytosis, a mechanism of phagocytic escape commonly used by

Downloaded from http://aac.asm.org/ on May 21, 2020 by guest

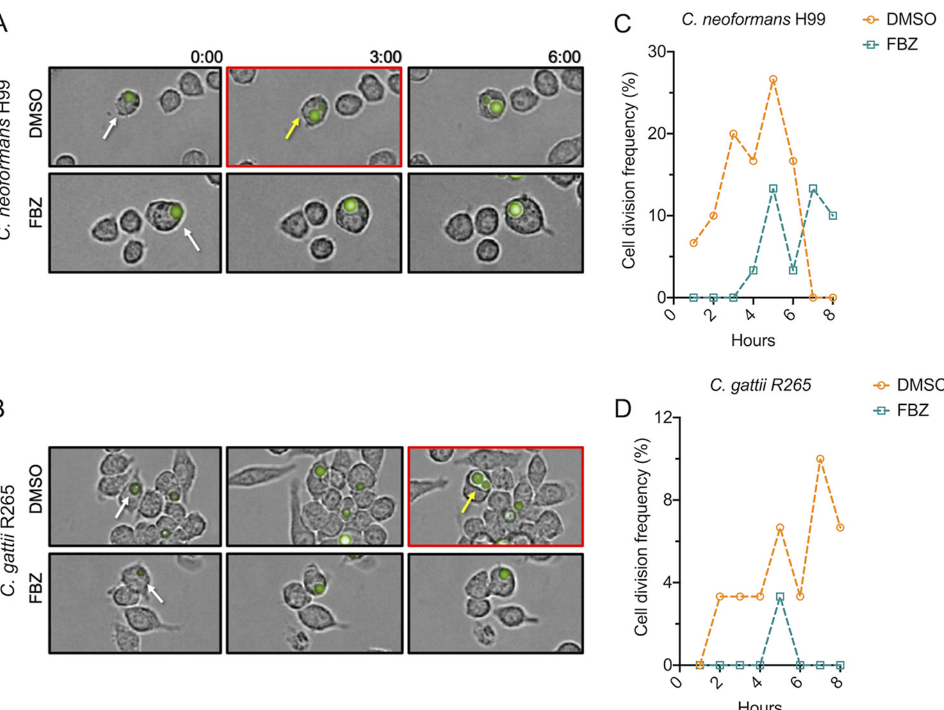

FIG 6 Time-lapse detection of budding yeast cells in macrophages infected with *C. neoformans* (strain H99) or *C. gattii* (strain R265). Video-microscopy analysis of macrophages infected with single-cell *C. neoformans* (A) or *C. gattii* (B) (white arrows) suggested that detection of yeast budding (yellow arrows) is delayed in fenbendazole (FBZ)-treated systems in comparison with vehicle (DMSO)-treated macrophages. Panels boxed in red denote the initial detection of yeast budding. This initial perception was confirmed by a quantitative analysis of intracellular budding for *C. neoformans* (C) and *C. gattii* (D).

Cryptococcus (33, 34). We therefore determined the vomocytosis levels after exposure of infected macrophages to fenbendazole. Similarly, fenbendazole reduced the rates of vomocytosis at both inhibitory and subinhibitory concentrations in macrophages infected with *C. neoformans* H99 or *C. gattii* R265 (Fig. 6C and D). Since IPR and vomocytosis are directly linked to the ability of *Cryptococcus* to survive after ingestion by phagocytic cells, we also counted viable CFU of *C. neoformans* H99 and *C. gattii* R265 after interaction with the macrophages. Once again, treatment of the mammalian cells with fenbendazole affected the growth of *C. neoformans* H99 and *C. gattii* R265. In both cases, CFU counts were reduced after treatment of infected cells with fenbendazole (Fig. 7E and F). Once again, fenbendazole promoted an increase in the antifungal efficacy of amphotericin B, as inferred from the reduced concentration of this antifungal required for the intracellular killing of *C. neoformans* H99 and *C. gattii* R265 (Fig. 7E and F).

DISCUSSION

The *in vitro* anticryptococcal activity of benzimidazoles has been consistently reported (14, 16, 19, 20). A general analysis of these reports indicated that, among all members of this drug family, fenbendazole required the lowest MIC against *C. neoformans* and *C. gattii* in comparison to other benzimidazoles (14, 16, 19, 20). In addition, a detailed study of the toxicity of fenbendazole suggested high levels of safety in humans (21, 22), which contrasts with the high toxicity of amphotericin B (35). In our study, we confirmed the efficacy of fenbendazole as an anticryptococcal agent. We tested 17 strains of *C. neoformans* and *C. gattii* and observed that they were all similarly susceptible to fenbendazole, suggesting that intrinsic resistance to this benzimidazole may not be a problem with this drug. A similar MIC of 0.012 μg/ml was found for all of them. For comparison, a recent study (19) analyzed 50 strains of *C. neoformans* according to their susceptibility to flubendazole, another member of the benzimidazole

Downloaded from http://aac.asm.org/ on May 21, 2020 by guest

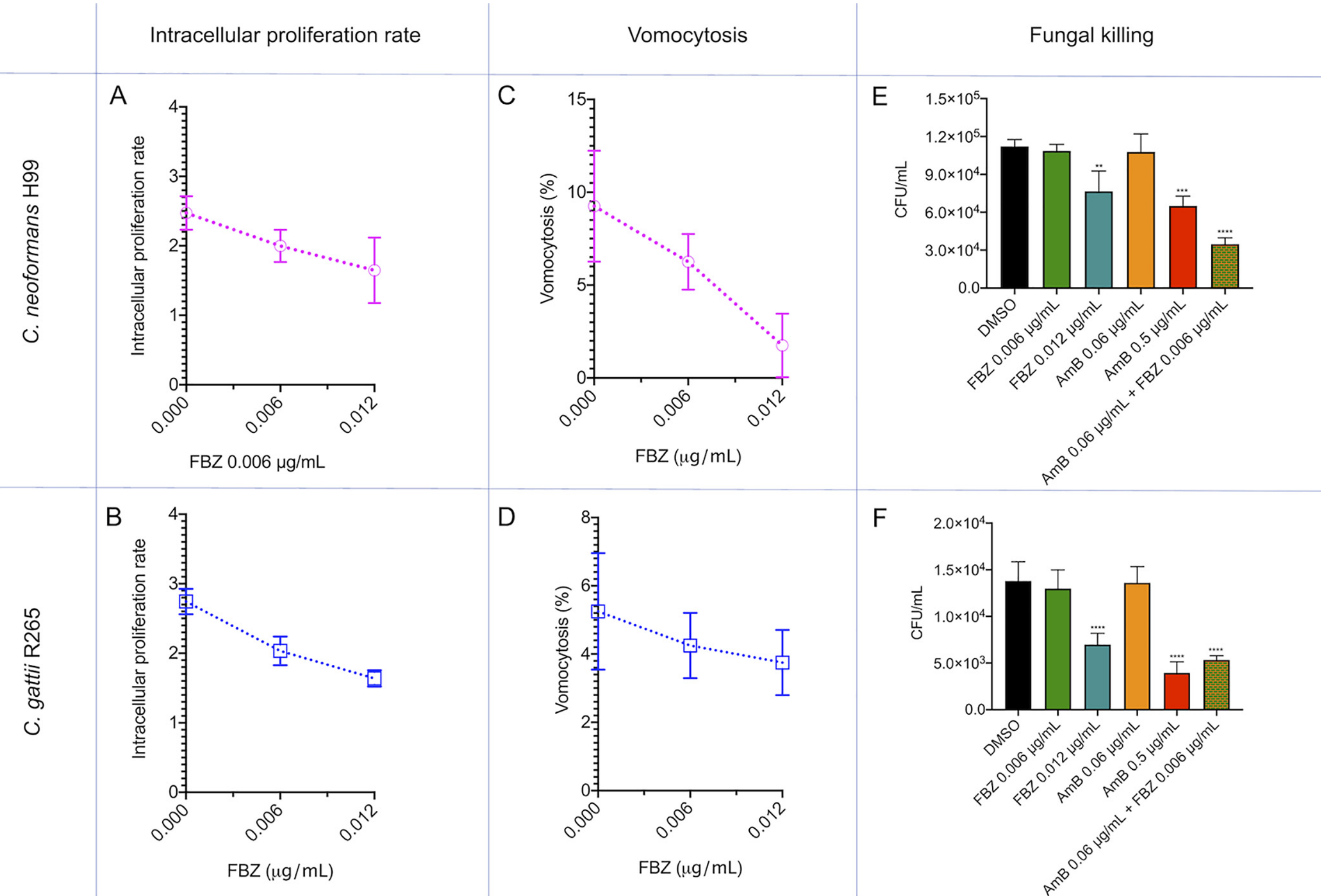

FIG 7 Effects of fenbendazole (FBZ) on the intracellular fate of *Cryptococcus*. Treatment with fenbendazole decreased the intracellular proliferation rates of *C. neoformans* (strain H99) (A) and *C. gattii* (strain R265) (B). Similar profiles of inhibitory effects were observed when vomocytosis was analyzed in macrophages infected with *C. neoformans* (C) or *C. gattii* (D). The recovery of significantly fewer fungal cells from FBZ-treated macrophages (0.012 μg/ml) indicated intracellular activity against *C. neoformans* H99 (E) and *C. gattii* R265 (F). Similar results were obtained with an antifungal concentration range of amphotericin B (AmB) or with a combination of subinhibitory doses of AmB and FBZ. **, $P = 0.01$; ***, $P = 0.001$; ****, $P < 0.0001$.

family. Using the same EUCAST methodology, MICs of 0.03 (one strain), 0.06 (19 strains), 0.125 (25 strains), and 0.25 (5 strains) μg/ml were found in this study. These values were 2.5- to 20-fold higher than the MIC found for fenbendazole in this study. The low toxicity of fenbendazole was also confirmed in our experimental model, as well as its ability to improve the antifungal activity of amphotericin B. In earlier studies, it was demonstrated that concentration of fenbendazole required to kill *Cryptococcus* was 8.5-fold lower than that of amphotericin B (16). These characteristics led us to explore the properties of fenbendazole in mechanistic and therapeutic models.

In a previous study, we used a mutant collection of *C. gattii* for determination of the cellular targets of mebendazole, another anticryptococcal benzimidazole (20). These mutants were screened for resistance phenotypes in the presence of mebendazole based on the assumption that in the absence of a cellular target required for antifungal activity, the drug would lack anticryptococcal properties. The mutants showing the highest levels of resistance to mebendazole lacked expression of Aim25, a cryptococcal scramblase (36), or Nop16, a putative nucleolar protein (20). We initially assumed that these targets were required for the activity of fenbendazole, but our current results indicate that they are not involved in the antifungal properties of this benzimidazole. In nematodes, the benzimidazoles bind to β-tubulin, leading to local unfolding of the protein and consequent abnormal conformation. This outcome results in the inhibition of the polymerization of α- and β-tubulin subunits to form microtubules, causing lethal effects in dividing cells (37). In the *C. neoformans* model, a similar mechanism was

Downloaded from http://aac.asm.org/ on May 21, 2020 by guest

attributed to flubendazole and other benzimidazoles (38). However, fenbendazole was not specifically tested in these studies. In addition, the cellular effects of benzimidazoles on the cryptococcal microtubules were not reported. In our study, treatment of both *C. neoformans* and *C. gattii* with fenbendazole led to a clear alteration in β-tubulin detection, strongly suggesting that its mechanism of action is related to that described for the nematodes and other parasites.

The benzimidazoles are extensively metabolized in mammals following oral administration. The parent compounds are generally short-lived, and metabolites predominate in plasma, tissues, and excreta (27). Fenbendazole, for instance, is rapidly metabolized by liver microsomes after oral absorption. In pigs, this benzimidazole was rapidly absorbed after oral administration, but its systemic bioavailability was low (39). The intranasal route, on the other hand, transports drugs directly to the brain from the nasal cavity along the olfactory and trigeminal nerves (40), avoiding the first-pass metabolism in the liver and gastrointestinal tract. Another advantage of the intranasal route of drug delivery is the rapid absorption of bioactive compounds. For instance, midazolam, a benzodiazepine depressant, reaches clinically effective concentrations within less than 10 min after nasal administration in humans (41). The low molecular mass of fenbendazole (299.349 g/mol) also favors brain absorption after intranasal administration (42). These findings agree with our current results showing that all animals infected with *C. neoformans* and treated with fenbendazole intranasally survived. However, our results also suggest that liver metabolization is a limitation for the oral treatment of fungal diseases with fenbendazole. In this sense, strategies for protecting drug candidates against metabolic modifications are widely available (43), and they could be applied to the use of fenbendazole as a scaffold for antifungal development. Most likely, intranasal pharmaceutical preparations of fenbendazole could be promising and safe therapeutic alternatives in the *Cryptococcus* model.

Interference with pathogenic traits in addition to primary antifungal effects were likely related to the high efficacy of fenbendazole in the control of animal cryptococcosis observed in our study. High levels of uptake of cryptococci by macrophages *in vitro* have been associated with long-term survival of human patients (44). Importantly, strains showing high uptake by macrophages were hypocapsular. The connections between phagocytic events, reduced capsules, and the outcome of human disease formed the basis of our studies on the effects of fenbendazole on capsular architecture and outcome of macrophage infection. Fenbendazole produced effects that are potentially positive to the host in all cases, since it caused a decrease in capsular density and dimensions, in addition to reducing intracellular proliferation rates and events required for phagocytic escape.

It was estimated that the cost to procure one million doses of standard benzimidazoles (500 mg each) would be approximately $20,000, including international transport (45). In comparison to the cost of treating cryptococcosis patients with lipid formulations of amphotericin B (9, 10), these numbers are extraordinarily low. In this context, our results support the development of pharmaceutical preparations of fenbendazole to be tested as alternative anticryptococcal agents. If effective in humans, fenbendazole could represent an affordable alternative for the treatment of a disease that has an extremely negative impact on the health conditions of neglected populations.

MATERIALS AND METHODS

Strains and growth conditions. *Cryptococcus neoformans* and *C. gattii* (strains H99 and R265, respectively) were used in most experiments. Of note, the reference strain R265 has been recently reclassified as *C. deuterogattii*. In this study, we kept its classification as *C. gattii*, as largely employed in the *Cryptococcus* literature. In addition, 12 isolates of *C. neoformans* (VNI genotype) and 3 isolates of *C. gattii* (VGI genotype), obtained from the Collection of Pathogenic Fungi available at the Oswaldo Cruz Foundation (Fiocruz), were tested for susceptibility to fenbendazole. For studies of mechanisms of antifungal activity, the *C. gattii* mutant strains *aim25*Δ and *nop16*Δ were also tested (20, 36). For the *in vitro* interaction assays, green fluorescence protein (GFP)-tagged *C. neoformans* and *C. gattii* were used (46). These strains, which were kindly provided by Robin May, were constructed in the H99 (*C. neoformans*) and R265 (*C. gattii*) backgrounds, respectively. All strains were maintained in Sabouraud agar

Downloaded from http://aac.asm.org/ on May 21, 2020 by guest

plates and cultivated in Sabouraud medium at 30°C for 24 h before all experiments. RAW 264.7 macrophages were used for toxicity and phagocytosis experiments. The cells were maintained in Dulbecco's modified Eagle medium (DMEM) (catalog number D5796; Sigma-Aldrich) supplemented with 10% heat-inactivated fetal bovine serum (FBS) at 37°C in a 5% CO_2 atmosphere.

Antifungal susceptibility testing. Fenbendazole was obtained from Sigma-Aldrich (catalog number F5396) in its solid form. Stock solutions were prepared in DMSO (drug vehicle). In the antifungal susceptibility tests, vehicle concentration was kept at 1%. To determine the MIC of fenbendazole, the broth microdilution method was used following the protocols established by the European Committee on Antimicrobial Susceptibility Testing (EUCAST; E.Def 7.3.1 reference method) (47). Plates to be used in the antifungal susceptibility tests contained RPMI medium supplemented with 2% glucose buffered with 165 mM 3-(*N*-morpholino)propanesulfonic acid (MOPS; pH 7.0). The medium was supplemented with fenbendazole in the concentration range of 0.003 to 1.536 μg/ml. Control systems contained the drug vehicle alone. Before inoculation in the antifungal testing plates, *C. neoformans* and *C. gattii* were grown on Sabouraud agar plates at 30°C for 48 h. A suspension of 2.5×10^5 cells/ml was prepared in distilled water, and 100 μl of this suspension was transferred to each well of 96-well plates containing 100 μl of RPMI prepared as described above. The plates were incubated at 35°C for 48 h. Growth inhibition was monitored by spectrophotometric determination of optical density at 530 nm in a Molecular Devices SpectraMax Paradigm microplate reader. The MIC was defined as the lowest concentration inhibiting 90% of cryptococcal growth. Sterility control wells were included in all plates. Similar protocols were used for determination of MICs for amphotericin B, fluconazole, and benzimidazole derivatives. As recommended by EUCAST, *Candida parapsilosis* and *Candida krusei* strains (ATCC 22019 and ATCC 6258, respectively) were used as controls for the antifungal activity of amphotericin B and fluconazole. To evaluate whether fenbendazole was fungicidal or fungistatic, the cells were incubated at the MIC under the conditions described above, washed, and plated on Sabouraud agar plates and incubated for 48 h at 30°C for determination of CFU.

Checkerboard assay. The effects of the association of fenbendazole with amphotericin B on antifungal activity were evaluated using the checkerboard assay (48). The drug concentration ranges used in this assay corresponded to 0.007 to 0.5 μg/ml for amphotericin B and 0.003 to 1.536 μg/ml for fenbendazole. Drug solutions were prepared as previously described (13). Briefly, 50 μl of each of the amphotericin B concentrations was mixed with 50 μl of each of the fenbendazole solutions in microtiter plates. The vehicle concentration was 1% in all wells. Inoculation of fungal suspensions and evaluation of fungal growth followed the EUCAST protocol described in this section. The fractional inhibitory concentration index (FICI) was calculated according to the equation ΣFICI = FICI (fenbendazole) + FICI (amphotericin B), where the FICI was the ratio of the MIC of the combination with the MIC alone (49, 50). Considering the differences in chemical nature and cellular targets of fenbendazole and amphotericin B, we also calculated the Bliss synergism scores (51) against *C. neoformans* H99 and *C. gattii* R265 using the SynergyFinder tool (https://synergyfinder.fimm.fi). In this model, the scores for antagonistic drugs are lower than –10. Additive drugs produce scores in the range of –10 to 10, and synergistic drugs produce scores larger than 10.

Cytotoxicity of fenbendazole. The cytotoxicity of fenbendazole to macrophages was determined using the Cytotox 96 nonradioactive cytotoxicity assay kit (catalog number G1780; Promega) following the manufacturer's recommendations. As recently described by our group (52), macrophages were used for cell viability assays due to their fundamental roles in the control and/or dissemination of cryptococci (32). RAW 264.7 macrophages (10^5 cells/well in DMEM supplemented with 10% FBS) were treated with 0.006 to 5.98 μg/ml fenbendazole, alone or in combination with 0.06 μg/ml amphotericin B, for 24 h at 37°C in DMEM supplemented with 10% FBS. Cytotoxicity was inferred from the determination of the levels of lactate dehydrogenase activity in the medium. Control systems included vehicle-treated cells (viability control) and macrophages lysed with the lysis solution provided by the manufacturer (death control).

Effects of fenbendazole on microtubule organization. Tubulin organization in *C. neoformans* H99 and *C. gattii* R265 was evaluated as described by Wang et al. (53) with minor modifications. Briefly, fungal cells were cultivated overnight in liquid Sabouraud medium at 30°C with shaking (200 rpm). These cultures had their optical density at 600 nm (OD_{600}) adjusted to 0.2 in fresh Sabouraud medium and then were incubated at 30°C with shaking (200 rpm) until an OD_{600} value of approximately 0.8 was reached. Samples of 1 ml of these cell suspensions were washed with PBS and resuspended in fresh Sabouraud medium supplemented with 0.12 μg/ml fenbendazole (10 times concentrated MIC value) or DMSO (0.012%). The suspensions were incubated for an additional 90 min at 30°C with shaking (200 rpm) and washed with PBS. The cells were finally suspended in 1 ml of fresh Sabouraud medium supplemented with 0.5 μl of the Tubulin Tracker green reagent (catalog number T34075; Thermo Fisher Scientific). The cells were incubated for 1 h at 37°C, washed with PBS, and fixed with 2% paraformaldehyde in PBS. Control experiments were prepared using 100 μM vinblastine (catalog number V1377; Sigma) instead of fenbendazole. Vinblastine is a tubulin-targeting alkaloid that inhibits the assembly of microtubules (54). The samples were observed under a DMi8 fluorescence microscope (Leica). Images were recorded with the LasAF software.

Effect of fenbendazole on capsular morphology. *C. neoformans* H99 and *C. gattii* R265 were grown overnight in liquid yeast extract-peptone-dextrose (YPD) medium at 30°C and washed with PBS. Yeast suspensions had their density adjusted to 5×10^4 cells/ml in a capsule induction medium (10% Sabouraud in 50 mM MOPS; pH 7.3) (55) supplemented with variable concentrations of fenbendazole. Control systems contained the vehicle alone. Capsule enlargement was induced at 37°C in a 5% CO_2 atmosphere for 0, 2, 4, 6, 8, 16, and 24 h. The cells were then washed with PBS and prepared for India

Downloaded from http://aac.asm.org/ on May 21, 2020 by guest

ink counterstaining after fixation with 4% paraformaldehyde and observation under a light microscope. Capsule dimensions were determined in digitalized images using the ImageJ software (56). The cells incubated for 24 h were also analyzed using other microscopic approaches. For immunofluorescence, the paraformaldehyde-fixed cells were initially blocked with 1% bovine serum albumin (BSA) in PBS for 1 h at 37°C, following staining of cell wall chitin with 25 μM calcofluor white (catalog number 18909; Sigma) in PBS for 30 min at 37°C. The cells were washed 3 times with PBS and incubated for 1 h at 37°C with a monoclonal antibody (MAb 18B7, donated by Arturo Casadevall) raised to capsular glucuronoxylomannan (GXM) at 10 μg/ml in a PBS solution containing 1% BSA. The cells were washed with PBS and incubated with an Alexa 546-antibody conjugate (catalog number A-11030; Invitrogen) recognizing mouse immunoglobulin G (1 h, 25°C in the dark). Washed cells were analyzed in a Leica SP5 AOBS laser confocal microscope. For scanning electron microscopy (SEM), the cells were washed with PBS and fixed with 2.5% glutaraldehyde in 0.1 M sodium cacodylate buffer (pH 7.2) for 1 h at 25°C. The cells were washed with a 0.1-M sodium cacodylate buffer (pH 7.2) containing 0.2 M sucrose and 2 mM $MgCl_2$. The cells were placed over 0.01% poly-L-lysine-coated coverslips and incubated for 30 min at 25°C. Adhered cells were then gradually dehydrated in ethanol (30, 50, and 70% for 5 min, and then 90% for 10 min, and 100% twice for 10 min). Immediately after dehydration, the cells were critical point dried (Leica EM CPD300), mounted on metallic bases, and coated with a gold layer (Leica EM ACE200). The cells were visualized in a scanning electron microscope (JEOL JSM-6010 Plus/LA) operating at 5 keV.

Intracellular antifungal activity. RAW 264.7 macrophages were suspended (5×10^5 cells/ml) in DMEM supplemented with 10% FBS, and 200 μl of this suspension was transferred to each well of 96-well plates for overnight incubation at 37°C in a 5% CO_2 atmosphere. The following day, *C. neoformans* H99 or *C. gattii* R265 (5×10^5 cells/ml) cells were opsonized by incubation for 1 h at 37°C under a 5% CO_2 atmosphere in DMEM containing 10% FBS and 5 μg/ml MAb 18B7. Macrophage cultures had their medium replaced with 200 μl of the above-described cell suspensions containing opsonized fungi and were incubated for 2 h (37°C, 5% CO_2). The cell cultures were washed 3 times with PBS to remove unattached fungal cells and were covered with 200 μl of DMEM containing 10% FBS, in addition to fenbendazole and/or amphotericin B (0.006 or 0.012 μg/ml fenbendazole; 0.06 or 0.5 μg/ml amphotericin B; 0.006 μg/ml fenbendazole combined with 0.06 μg/ml amphotericin B). Drug vehicle alone was used as a control. For determination of fungal killing, the drug-containing cell cultures were incubated for 24 h (37°C, 5% CO_2) and washed 3 times with PBS. The macrophages were then lysed with 200 μl of cold sterile water, and the resulting suspensions were plated on Sabouraud agar. The plates were incubated at 30°C for 48 h, and CFU were counted manually. For determination of intracellular proliferation and phagocytic escape of cryptococci, the plates containing infected macrophages were incubated at 37°C with 5% CO_2 for 18 h in an Operetta high-content imaging system (PerkinElmer). During this 18 h of incubation, images of each well were captured every 5 min with a 40× objective. Using the Harmony high-content imaging and analysis software (PerkinElmer), movies of each well were prepared for analysis of intracellular proliferation rates (IPR) and vomocytic escape (46). In each experimental condition, 50 cells were analyzed. The IPR were calculated as the t_{18}/t_0 ratio, where t_{18} is the number of fungal cells inside the macrophages after 18 h, and t_0 is the number of phagocyte-associated cryptococci at the beginning of the incubation. Vomocytosis was calculated as previously described (46) using 50 cells per experimental system. Three independent experiments were performed.

Animal experimentation. For intranasal administration of fenbendazole, C57BL/6 mice (8 to 12 weeks old) were used. The animals were kept with food and water *ad libitum* at the animal facility of the University of Brasília. The animals were placed in an isoflurane inhalation system (Bonther) for anesthesia and then challenged intratracheally with 25 μl of PBS containing 1×10^4 yeast cells of *C. neoformans* (H99 strain). After 3 days of infection, the animals were divided into groups of 5 individuals each. One group was treated intranasally with 20 μl of 1.25 μM fenbendazole. The other two groups were treated with PBS or amphotericin B (2 mg/kg) intraperitoneally as indicated in Fig. 3. Mice were fed *ad libitum* and monitored every day for discomfort and signs of disease. Mice showing weight loss, lethargy, tremor, or inability to reach food or water were euthanized, and survival was counted until that day. At day 30 any surviving mice were euthanized. Euthanasia was performed with CO_2 asphyxiation with 100% $FiCO_2$ for 2 min followed by cervical dislocation. The experiment was repeated under the same conditions, and identical results were found. All treatments and experimental procedures were performed after approval by the Ethics Committee on Animal Use (CEUA) of the University of Brasília (UnBDoc number 66729/2016) and according to the guidelines presented by the National Council for the Control of Animal Experimentation (CONCEA).

SUPPLEMENTAL MATERIAL

Supplemental material is available online only.

SUPPLEMENTAL FILE 1, PDF file, 0.1 MB.

ACKNOWLEDGMENTS

We thank Arturo Casadevall for donation of the 18B7 antibody and Charley Staats and Ane Garcia for the use of the *nop16*Δ and *aim25*Δ mutants. We also appreciate the donation of the fluorescent strains by Robin May. We thank the Program for Technological Development in Tools for Health-RPT-FIOCRUZ for use of the microscopy facility, RPT07C, Carlos Chagas Institute, Fiocruz-Parana. M.L.R. is currently on leave from the

Downloaded from http://aac.asm.org/ on May 21, 2020 by guest

position of associate professor at the Microbiology Institute of the Federal University of Rio de Janeiro, Brazil.

M.L.R. was supported by grants from the Brazilian Ministry of Health (grant 440015/2018-9), Conselho Nacional de Desenvolvimento Científico e Tecnológico (CNPq; grants 405520/2018-2 and 301304/2017-3), and Fiocruz (grants PROEP-ICC 442186/2019-3, VPPCB-007-FIO-18, and VPPIS-001-FIO18).

We also acknowledge support from the Instituto Nacional de Ciência e Tecnologia de Inovação em Doenças de Populações Negligenciadas (INCT-IDPN). F.C.G.R. was supported by the Coordenação de Aperfeiçoamento de Pessoal de Nível Superior (CAPES; finance code 001). This work was also supported by NIH grant AI125770 and by merit review grant I01BX002924 from the Veterans Affairs Program to M.D.P. The funders had no role in study design, data collection and analysis, decision to publish, or preparation of the manuscript. M.D.P. was a Burroughs Welcome investigator in infectious diseases.

L.S.J. initiated the project and is now a member of the Del Poeta laboratory; H.C.O. continued the project, finished the manuscript's experiments and is now in charge of the ongoing experiments in the Rodrigues laboratory.

M.D.P. is a cofounder and the chief scientific officer (CSO) of MicroRid Technologies, Inc. All other authors have no conflict of interest.

REFERENCES

1. Bongomin F, Gago S, Oladele RO, Denning DW. 2017. Global and multinational prevalence of fungal diseases-estimate precision. J Fungi (Basel) 3:E57.
2. Rajasingham R, Smith RM, Park BJ, Jarvis JN, Govender NP, Chiller TM, Denning DW, Loyse A, Boulware DR. 2017. Global burden of disease of HIV-associated cryptococcal meningitis: an updated analysis. Lancet Infect Dis 17:873–881. https://doi.org/10.1016/S1473-3099(17)30243-8.
3. Hurtado JC, Castillo P, Fernandes F, Navarro M, Lovane L, Casas I, Quinto L, Marco F, Jordao D, Ismail MR, Lorenzoni C, Martinez-Palhares AE, Ferreira L, Lacerda M, Monteiro W, Sanz A, Letang E, Marimon L, Jesri S, Cossa A, Mandomando I, Vila J, Bassat Q, Ordi J, Menendez C, Carrilho C, Martinez MJ. 2019. Mortality due to *Cryptococcus neoformans* and *Cryptococcus gattii* in low-income settings: an autopsy study. Sci Rep 9:7493. https://doi.org/10.1038/s41598-019-43941-w.
4. Alves Soares E, Lazera MDS, Wanke B, Faria Ferreira M, Carvalhaes de Oliveira RV, Oliveira AG, Coutinho ZF. 2019. Mortality by cryptococcosis in Brazil from 2000 to 2012: a descriptive epidemiological study. PLoS Negl Trop Dis 13:e0007569. https://doi.org/10.1371/journal.pntd.0007569.
5. Perfect JR, Dismukes WE, Dromer F, Goldman DL, Graybill JR, Hamill RJ, Harrison TS, Larsen RA, Lortholary O, Nguyen MH, Pappas PG, Powderly WG, Singh N, Sobel JD, Sorrell TC. 2010. Clinical practice guidelines for the management of cryptococcal disease: 2010 update by the infectious diseases society of america. Clin Infect Dis 50:291–322. https://doi.org/10.1086/649858.
6. Temfack E, Boyer-Chammard T, Lawrence D, Delliere S, Loyse A, Lanternier F, Alanio A, Lortholary O. 2019. New insights into *Cryptococcus* spp. biology and cryptococcal meningitis. Curr Neurol Neurosci Rep 19:81. https://doi.org/10.1007/s11910-019-0993-0.
7. Global Action Fund for Fungal Infections. 2020. Antifungal drug maps. GAFFI, Geneva, Switzerland. https://www.gaffi.org/antifungal-drug-maps/. Accessed 4 January 2020.
8. Chen T, ACTA Trial Team, Mwenge L, Lakhi S, Chanda D, Mwaba P, Molloy SF, Gheorghe A, Griffiths UK, Heyderman RS, Kanyama C, Kouanfack C, Mfinanga S, Chan AK, Temfack E, Kivuyo S, Hosseinipour MC, Lortholary O, Loyse A, Jaffar S, Harrison TS, Niessen LW, Team AT. 2019. Healthcare costs and life-years gained from treatments within the advancing cryptococcal meningitis treatment for Africa (ACTA) trial on cryptococcal meningitis: a comparison of antifungal induction strategies in sub-Saharan Africa. Clin Infect Dis 69:588–595. https://doi.org/10.1093/cid/ciy971.
9. Borba HHL, Steimbach LM, Riveros BS, Tonin FS, Ferreira VL, Bagatim BAQ, Balan G, Pontarolo R, Wiens A. 2018. Cost-effectiveness of amphotericin B formulations in the treatment of systemic fungal infections. Mycoses 61:754–763. https://doi.org/10.1111/myc.12801.
10. Chen J, Luo X, Qiu H, Mackey V, Sun L, Ouyang X. 2018. Drug discovery and drug marketing with the critical roles of modern administration. Am J Transl Res 10:4302–4312.
11. Mohs RC, Greig NH. 2017. Drug discovery and development: role of basic biological research. Alzheimers Dement (N Y) 3:651–657. https://doi.org/10.1016/j.trci.2017.10.005.
12. Krysan DJ. 2015. Toward improved anti-cryptococcal drugs: novel molecules and repurposed drugs. Fungal Genet Biol 78:93–98. https://doi.org/10.1016/j.fgb.2014.12.001.
13. de Oliveira HC, Monteiro MC, Rossi SA, Peman J, Ruiz-Gaitan A, Mendes-Giannini MJS, Mellado E, Zaragoza O. 2019. Identification of off-patent compounds that present antifungal activity against the emerging fungal pathogen *Candida auris*. Front Cell Infect Microbiol 9:83. https://doi.org/10.3389/fcimb.2019.00083.
14. Truong M, Monahan LG, Carter DA, Charles IG. 2018. Repurposing drugs to fast-track therapeutic agents for the treatment of cryptococcosis. PeerJ 6:e4761. https://doi.org/10.7717/peerj.4761.
15. McKellar QA, Scott EW. 1990. The benzimidazole anthelmintic agents: a review. J Vet Pharmacol Ther 13:223–247. https://doi.org/10.1111/j.1365-2885.1990.tb00773.x.
16. Cruz MC, Bartlett MS, Edlind TD. 1994. *In vitro* susceptibility of the opportunistic fungus *Cryptococcus neoformans* to anthelmintic benzimidazoles. Antimicrob Agents Chemother 38:378–380. https://doi.org/10.1128/AAC.38.2.378.
17. Del Poeta M, Schell WA, Dykstra CC, Jones S, Tidwell RR, Czarny A, Bajic M, Bajic M, Kumar A, Boykin D, Perfect JR. 1998. Structure-*in vitro* activity relationships of pentamidine analogues and dication-substituted bis-benzimidazoles as new antifungal agents. Antimicrob Agents Chemother 42:2495–2502. https://doi.org/10.1128/AAC.42.10.2495.
18. Del Poeta M, Schell WA, Dykstra CC, Jones SK, Tidwell RR, Kumar A, Boykin DW, Perfect JR. 1998. *In vitro* antifungal activities of a series of dication-substituted carbazoles, furans, and benzimidazoles. Antimicrob Agents Chemother 42:2503–2510. https://doi.org/10.1128/AAC.42.10.2503.
19. Nixon GL, McEntee L, Johnson A, Farrington N, Whalley S, Livermore J, Natal C, Washbourn G, Bibby J, Berry N, Lestner J, Truong M, Owen A, Lalloo D, Charles I, Hope W. 2018. Repurposing and reformulation of the antiparasitic agent flubendazole for treatment of cryptococcal meningoencephalitis, a neglected fungal disease. Antimicrob Agents Chemother 62:e01909-17. https://doi.org/10.1128/AAC.01909-17.
20. Joffe LS, Schneider R, Lopes W, Azevedo R, Staats CC, Kmetzsch L, Schrank A, Del Poeta M, Vainstein MH, Rodrigues ML. 2017. The Anti-helminthic compound mebendazole has multiple antifungal effects against *Cryptococcus neoformans*. Front Microbiol 8:535.
21. CVMP. 2014. CVMP assessment report for Panacur AquaSol (EMEA/V/C/002008/X/0003)—international non-proprietary name: fenbendazole.

Downloaded from http://aac.asm.org/ on May 21, 2020 by guest

(CVMP) CfMPfVU. European Medicines Agency, London, United Kingdom.
22. Villar D, Cray C, Zaias J, Altman NH. 2007. Biologic effects of fenbendazole in rats and mice: a review. J Am Assoc Lab Anim Sci 46:8–15.
23. Ianevski A, He L, Aittokallio T, Tang J. 2017. SynergyFinder: a web application for analyzing drug combination dose-response matrix data. Bioinformatics 33:2413–2415. https://doi.org/10.1093/bioinformatics/btx162.
24. Lacey E. 1988. The role of the cytoskeletal protein, tubulin, in the mode of action and mechanism of drug resistance to benzimidazoles. Int J Parasitol 18:885–936. https://doi.org/10.1016/0020-7519(88)90175-0.
25. Furtado LFV, de Paiva Bello ACP, Rabelo E. 2016. Benzimidazole resistance in helminths: from problem to diagnosis. Acta Trop 162:95–102. https://doi.org/10.1016/j.actatropica.2016.06.021.
26. Kopecka M. 2016. Microtubules and actin cytoskeleton of *Cryptococcus neoformans* as targets for anticancer agents to potentiate a novel approach for new antifungals. Chemotherapy 61:117–121. https://doi.org/10.1159/000437134.
27. Gottschall DW, Theodorides VJ, Wang R. 1990. The metabolism of benzimidazole anthelmintics. Parasitol Today 6:115–124. https://doi.org/10.1016/0169-4758(90)90228-V.
28. Johnston SA, May RC. 2013. *Cryptococcus* interactions with macrophages: evasion and manipulation of the phagosome by a fungal pathogen. Cell Microbiol 15:403–411. https://doi.org/10.1111/cmi.12067.
29. Casadevall A, Coelho C, Cordero RJB, Dragotakes Q, Jung E, Vij R, Wear MP. 2019. The capsule of *Cryptococcus neoformans*. Virulence 10:822–831. https://doi.org/10.1080/21505594.2018.1431087.
30. Bojarczuk A, Miller KA, Hotham R, Lewis A, Ogryzko NV, Kamuyango AA, Frost H, Gibson RH, Stillman E, May RC, Renshaw SA, Johnston SA. 2016. *Cryptococcus neoformans* intracellular proliferation and capsule size determines early macrophage control of infection. Sci Rep 6:21489. https://doi.org/10.1038/srep21489.
31. Alanio A, Desnos-Ollivier M, Dromer F. 2011. Dynamics of *Cryptococcus neoformans*: macrophage interactions reveal that fungal background influences outcome during cryptococcal meningoencephalitis in humans. mBio 2. https://doi.org/10.1128/mBio.00158-11.
32. Garcia-Rodas R, Zaragoza O. 2012. Catch me if you can: phagocytosis and killing avoidance by *Cryptococcus neoformans*. FEMS Immunol Med Microbiol 64:147–161. https://doi.org/10.1111/j.1574-695X.2011.00871.x.
33. Seoane PI, May RC. 2020. Vomocytosis: what we know so far. Cell Microbiol 22:e13145.
34. Alvarez M, Casadevall A. 2006. Phagosome extrusion and host-cell survival after *Cryptococcus neoformans* phagocytosis by macrophages. Curr Biol 16:2161–2165. https://doi.org/10.1016/j.cub.2006.09.061.
35. Menotti J, Alanio A, Sturny-Leclere A, Vitry S, Sauvage F, Barratt G, Bretagne S. 2017. A cell impedance-based real-time *in vitro* assay to assess the toxicity of amphotericin B formulations. Toxicol Appl Pharmacol 334:18–23. https://doi.org/10.1016/j.taap.2017.08.017.
36. Reis FCG, Borges BS, Jozefowicz LJ, Sena BAG, Garcia AWA, Medeiros LC, Martins ST, Honorato L, Schrank A, Vainstein MH, Kmetzsch L, Nimrichter L, Alves LR, Staats CC, Rodrigues ML. 2019. A novel protocol for the isolation of fungal extracellular vesicles reveals the participation of a putative scramblase in polysaccharide export and capsule construction in *Cryptococcus gattii*. mSphere 4:e00080-19. https://doi.org/10.1128/mSphere.00080-19.
37. Page SW. 2008. Antiparasitic drugs, p 584. *In* Maddison JE, Page SW, Church DB (ed), Small animal clinical pharmacology. Elsevier, Philadelphia, PA. https://doi.org/10.1016/B978-0-7020-2858-8.X5001-5.
38. Cruz MC, Edlind T. 1997. beta-Tubulin genes and the basis for benzimidazole sensitivity of the opportunistic fungus *Cryptococcus neoformans*. Microbiology 143:2003–2008. https://doi.org/10.1099/00221287-143-6-2003.
39. Petersen MB, Friis C. 2000. Pharmacokinetics of fenbendazole following intravenous and oral administration to pigs. Am J Vet Res 61:573–576. https://doi.org/10.2460/ajvr.2000.61.573.
40. Crowe TP, Greenlee MHW, Kanthasamy AG, Hsu WH. 2018. Mechanism of intranasal drug delivery directly to the brain. Life Sci 195:44–52. https://doi.org/10.1016/j.lfs.2017.12.025.
41. Haschke M, Suter K, Hofmann S, Witschi R, Frohlich J, Imanidis G, Drewe J, Briellmann TA, Dussy FE, Krahenbuhl S, Surber C. 2010. Pharmacokinetics and pharmacodynamics of nasally delivered midazolam. Br J Clin Pharmacol 69:607–616. https://doi.org/10.1111/j.1365-2125.2010.03611.x.
42. Bruinsmann FA, Richter Vaz G, de Cristo Soares Alves A, Aguirre T, Raffin Pohlmann A, Stanisçuaski Guterres S, Sonvico F. 2019. Nasal drug delivery of anticancer drugs for the treatment of glioblastoma: preclinical and clinical trials. Molecules 24:4312. https://doi.org/10.3390/molecules24234312.
43. Zhang Z, Tang W. 2018. Drug metabolism in drug discovery and development. Acta Pharm Sin B 8:721–732. https://doi.org/10.1016/j.apsb.2018.04.003.
44. Sabiiti W, Robertson E, Beale MA, Johnston SA, Brouwer AE, Loyse A, Jarvis JN, Gilbert AS, Fisher MC, Harrison TS, May RC, Bicanic T. 2014. Efficient phagocytosis and laccase activity affect the outcome of HIV-associated cryptococcosis. J Clin Invest 124:2000–2008. https://doi.org/10.1172/JCI72950.
45. Montresor A, Gabrielli AF, Diarra A, Engels D. 2010. Estimation of the cost of large-scale school deworming programmes with benzimidazoles. Trans R Soc Trop Med Hyg 104:129–132. https://doi.org/10.1016/j.trstmh.2009.10.007.
46. Voelz K, Johnston SA, Rutherford JC, May RC. 2010. Automated analysis of cryptococcal macrophage parasitism using GFP-tagged cryptococci. PLoS One 5:e15968. https://doi.org/10.1371/journal.pone.0015968.
47. Arendrup MC, Meletiadis J, Mouton JW, Guinea J, Cuenca-Estrella M, Lagrou K, Howard SJ, Subcommittee on Antifungal Susceptibility Testing of the EECfAST. 2016. EUCAST technical note on isavuconazole breakpoints for *Aspergillus*, itraconazole breakpoints for *Candida* and updates for the antifungal susceptibility testing method documents. Clin Microbiol Infect 22:571.e1-4. https://doi.org/10.1016/j.cmi.2016.01.017.
48. Rossi SA, de Oliveira HC, Agreda-Mellon D, Lucio J, Mendes-Giannini MJS, García-Cambero JP, Zaragoza O. 2020. Identification of off-patent drugs that show synergism with amphotericin B or that present antifungal action against *Cryptococcus neoformans* and *Candida* spp. Antimicrob Agents Chemother 64:e01921-19. https://doi.org/10.1128/AAC.01921-19.
49. Meletiadis J, Pournaras S, Roilides E, Walsh TJ. 2010. Defining fractional inhibitory concentration index cutoffs for additive interactions based on self-drug additive combinations, Monte Carlo simulation analysis, and *in vitro-in vivo* correlation data for antifungal drug combinations against *Aspergillus fumigatus*. Antimicrob Agents Chemother 54:602–609. https://doi.org/10.1128/AAC.00999-09.
50. Odds FC. 2003. Synergy, antagonism, and what the chequerboard puts between them. J Antimicrob Chemother 52:1–1. https://doi.org/10.1093/jac/dkg301.
51. Zhao W, Sachsenmeier K, Zhang L, Sult E, Hollingsworth RE, Yang H. 2014. A new Bliss independence model to analyze drug combination data. J Biomol Screen 19:817–821. https://doi.org/10.1177/1087057114521867.
52. Silva VKA, May RC, Rodrigues ML. 2020. Pyrifenox, an ergosterol inhibitor, differentially affects *Cryptococcus neoformans* and *Cryptococcus gattii*. Med Mycol https://doi.org/10.1093/mmy/myz132.
53. Wang LL, Lee KT, Jung KW, Lee DG, Bahn YS. 2018. The novel microtubule-associated CAP-glycine protein Cgp1 governs growth, differentiation, and virulence of *Cryptococcus neoformans*. Virulence 9:566–584. https://doi.org/10.1080/21505594.2017.1423189.
54. Gigant B, Wang C, Ravelli RB, Roussi F, Steinmetz MO, Curmi PA, Sobel A, Knossow M. 2005. Structural basis for the regulation of tubulin by vinblastine. Nature 435:519–522. https://doi.org/10.1038/nature03566.
55. Zaragoza O, Casadevall A. 2004. Experimental modulation of capsule size in *Cryptococcus neoformans*. Biol Proced Online 6:10–15. https://doi.org/10.1251/bpo68.
56. Schneider CA, Rasband WS, Eliceiri KW. 2012. NIH Image to ImageJ: 25 years of image analysis. Nat Methods 9:671–675. https://doi.org/10.1038/nmeth.2089.

Downloaded from http://aac.asm.org/ on May 21, 2020 by guest